Noise-Induced Phenomena in Collective Spinor Polariton Excitations

THÈSE N^{O} 6592 (2015)

PRÉSENTÉE LE 22 MAI 2015

À LA FACULTÉ DES SCIENCES DE BASE
LABORATOIRE D'OPTOÉLECTRONIQUE QUANTIQUE
PROGRAMME DOCTORAL EN PHOTONIQUE

ÉCOLE POLYTECHNIQUE FÉDÉRALE DE LAUSANNE

POUR L'OBTENTION DU GRADE DE DOCTEUR ÈS SCIENCES

PAR

Hadis ABBASPOUR

acceptée sur proposition du jury:

Prof. L. Thévenaz, président du jury
Prof. B. Deveaud, Dr M. Portella Oberli, directeurs de thèse
Prof. E. Giacobino, rapporteuse
Prof. M. Oestreich, rapporteur
Prof. V. Savona, rapporteur

ÉCOLE POLYTECHNIQUE
FÉDÉRALE DE LAUSANNE

Suisse
2015

Wings are a constraint that makes
it possible to fly.
— Robert Bringhurst

To my family. . .

Acknowledgements

First of all, I would like to thank professor Benoit Deveaud for total freedom, motivation, the confidence and the infinite support he provided me to examine any idea I have dreamed of. Second, I am deeply grateful to my second thesis director Dr. Marcia Portella Oberli. It has been a wonderful experience working under her supervision since she has a real charisma on providing a fantastic research mood with her students.
I warmly thank professors Elisabeth Giacobino, Vincenzo Savona, Michael Oestreich and Luc Thevenez for accepting being part of the jury of my thesis oral examination, and particularly for their careful reading of the manuscript and fruitful comments.
I would like to thank professor Savona, Hugo Flayac and Grégory Sallen for fantastic discussions and active theoretical feedbacks to our experiments. I also thank Roger Rochat, Nicolas Leiser and Francois Morier-Genoud for their invaluable technical support. A great thanks to Claire-Lyse Rouiller for all her supports and kindness.
I would like to thank my colleagues and friends from the LOEQ. I deeply thank Stephane Trebaol for passing to me all his great experimental, theoretical and communicating skills during the last four years. I am indebted to Taofiq Paraiso, Yoan Leger, Gael Nardin, Verena Kohnle, Francesco Manni and Roland Cerna for passing knowledge they provided to me during the first year. I deeply thank Daniel Oberli, Fauzia Jabeen, Gwenole Jacopin, Claudéric Ouellet-Plamondon, Naotomo Takemura, Gabriele Grosso, Rita Spano and Albert Adiyatullin for all fantastic discussions we had during journal clubs, lunch times and even coffee breaks. Last but not least, I would like to thank my best friend (rather than colleague) during the last ten years, Mehran Shahmohammadi. Of course I am deeply grateful and indebted for his companionship and consultation.
I would like also to thank my friends for providing me a lovely social environment in Lausanne. At the end I thank my father (Davoud), mother (Nahid), brother (Hosein) and my love (Mehran) for their endless love and supports.

Lausanne, 9 April 2015

Abstract

Polaritons are quasiparticles resulting from the strong coupling between photons and excitons embedded in a semiconductor microcavity. The exciton component of polaritons provides strong nonlinear interactions, while their photonic counterpart facilitates long range coherence. Moreover, polaritons carry a pseudospin that can be accessed through the polarization state of the emitted light, and brings up spinor related nonlinear effects.
This study aims at in-depth investigation of the noise related phenomena in polariton system. First, a series of experiments of polariton bistability and multistability are performed to deepen our knowledge about the effect of the biexciton creation and polariton-polariton interaction on multistable regimes in exciton polaritons. Then, using an external Gaussian noise, the polariton transition rate between two stable states of a polariton bistability is characterized. It is shown that the external noise specifications, intensity and correlation time, can efficiently modify the polariton Kramers time and residence time. We also discuss the performance of the bistable behaviour in steady state regime in terms of experimental acquisition time compared to the noise-assisted residence time.
In the next part, taking advantage of polariton bistability and spin-trigger regime, we have evidenced two different types of stochastic resonance. Intensity stochastic resonance and spinor stochastic resonance. We have shown that the synergic interplay between intensity fluctuations and external modulated signal, imprinted on the DC component of the driving field, can enhance the coherent processing of an input signal buried in noise. Moreover, we evidence that, due to the exceptional spin properties of polaritons, a noisy modulated polarized input signal can drive the switching of a fully polarized polariton population. This effect unveils an original field of stochastic resonance which we called as spinor stochastic resonance. All experimental results are well reproduced by a model based on Gross-Pitaevskii equation. At the end, the influence of nonlinear interactions on polariton intensity fluctuations and probability distribution have been investigated.

Key words: Exciton-polaritons, strong coupling regime, biexciton, bistability, multistability, spin-trigger, Gaussian noise, nonlinear oscillator, Kramers time, residence time, stochastic resonance, signal-to-noise ratio, Gross-Pitaevskii equation, second-order correlation function, Hanbury Brown and Twiss setup.

Résumé

Le polariton est une quasi-particule résultant du couplage fort entre un exciton et un photon dans une cavité semi-conductrice. Leur composante excitonique amène aux polaritons une forte interaction non-linéaire alors que la composante photonique permet une importante longueur de cohérence. De plus, les polaritons portent un pseudospin accessible à travers l'état de polarisation de la lumière émise, ce qui permet de mesurer et d'étudier les interactions non-linéaires de spin.
Les travaux présentés ont pour but d'étudier en profondeur les effets du bruit sur un système de polaritons. Premièrement, plusieurs expériences de bistabilité et de multistabilité sont réalisées sur les polaritons dans le but d'étudier et de mieux comprendre le rôle du biexciton et des interactions polariton-polariton. Ensuite, en utilisant une source externe de bruit Gaussien, les taux de transition entre les deux états stables d'une courbe de bistabilité seront caractérisés. Il sera montré que les paramètres du bruit induit, intensité et temps de corrélation, affectent les caractéristiques de ces taux de transition, temps de Kramers et temps de résidence. Nous discuterons de la stabilité du comportement bistable en régime stationnaire en comparant le temps d'acquisition expérimental avec le temps caractéristique de résidence du au bruit.
Dans la partie suivante, en utilisant la bistabilité des polaritons et le régime de spin-trigger, deux différents types de résonance stochastique seront mis en évidence : la résonance stochastique d'intensité et la résonance stochastique de spin. Nous montrerons que l'interaction synergique entre des fluctuations en intensité et une faible modulation du champ d'excitation peut permet d'augmenter le rapport signal à bruit en sortie du systéme. De plus, nous mettrons en évidence que, due aux propriétés des spins des polaritons, un signal d'entré bruité et modulé, mais polarisé peut voir son taux de polarisation augmenté pour atteindre en sortie un taux de polarisation circulaire maximum. Cet effet dévoile un champ d'investigation original grâce aux résonances stochastiques que l'on appelle la résonance stochastique de spin. Tous les résultats présentés sont bien reproduits par un modèle reposant sur l'équation de Gross-Pitaevskii. Finalement, l'influence des interactions non-linéaire, la fluctuation d'intensité et leur distribution de probabilité ont été étudiées.

Mots clefs : Exciton-polaritons, régime de couplage fort, biexciton, bistabilité, multistabilité, spin-trigger, bruit Gaussien, oscillateur non-linéaire, temps de Kramers, temps de résidence, résonance stochastique, rapport signal sur bruit, équation Gross-Pitaevskii, fonction de corrélation du deuxième ordre, montage Hanbury Brown-Twiss.

Contents

List of Figures

1 Introduction

The idea of applying electronics for emitting, sensing, transmitting and modelling light gave birth to a new category of devices, the optoelectronics. In 1962, for the first time, a direct conversion of electrical energy to coherent radiation has been observed in a GaAs p-n junction [1]. Many years later, a surface-emitting injection laser was reported [2]. The motivation behind this type of laser was to fabricate a low threshold, single mode laser array. This idea led to the design of a microcavity structure, which can be categorized by the weak coupling regime between light and excitons.

Progress in fabrication processes, allowed the crossover from the weak to strong coupling regime. The first demonstration of strong coupling regime in a GaAs based planar microcavity was done in 1992 [3]. In this case, photon and matter are strongly mixed together giving rise to a new quasi-particle called the exciton-polariton. These particles can be considered as a photon dressed with a matter excitation, which at low excitation levels satisfy Bose statistics. Due to their photonic component, a large degree of spatial coherence is maintained. In addition, the excitonic part provides strong nonlinear interactions. A polariton system is an intrinsically nonequilibrium system with properties different from other sources of Bose gas at thermodynamical equilibrium. Thanks to their unique properties, microcavity polaritons became an ideal system for both applied and fundamental research. During the last years, polaritons have been the matter of important demonstrations such as Bose-Einstein condensation (BEC) [4], superfluid effects [5, 6, 7, 8, 9], polariton based devices for signal processing [10, 11, 12], bistability [13] and polariton multistability [14] .

Multistable systems are representative of numerous physical systems, ranging from modulated Josephson junction system [15, 16], polarization multistability [17, 18] and several types of lasers [19, 20]. In many of these systems from fundamental point of view, fluctuations are important. Noise driven hopping between different states of a multistable system has long been a subject to study. In 1940, Kramers modelled a thermally activated escape rate of Brownian particles over a potential barrier [21]. Nowadays, this pioneering model contains the basics of several noise-assisted transition studies in nonlinear harmonic oscillators and bistable regimes [22, 23].

On the application point of view, fluctuations can be essential problem which should be dealt with. Nevertheless, the addition of noise in a nonlinear dynamical system can support the more regular behaviour of the system. Actually, this would be possible by reaching the stochastic resonance condition in polariton system. The half-light half-matter nature of polaritons opens the possibility to study random behaviours introduced by either their photon or exciton part bringing them as a versatile system to implement such studies. Stochastic resonance is a fascinating effect allowing one to enhance coherently the response of a nonlinear process by the addition of a noisy perturbation. Since the first experimental demonstration [24], stochastic resonance has been studied in a wide scope of fields such as chemistry [25, 26, 27], physics [20, 28, 29], and neuroscience [30].

In addition to all experimental investigations of the influence of external noise on an optical nonlinear oscillator, time-dependent intensity fluctuations of the optical field have also a great importance. In the 1950s, this effect was first investigated by Hanbury Brown and Twiss. This experimental work has central importance in the development of modern quantum optics which led to the classification of light to classic and non-classic [31].

1.1 Objective and outlines

This work aims at considering the aforementioned concerns through a complete study of the influence of noise in polariton system. To be more precise, we will study optical bistability and discriminator and polarization multistability in zero dimensional polariton system. We will define two types of bistable behaviors, optical bistability arising from nonlinear polariton-polariton interactions, and spin-trigger regime that originates mainly from biexciton formation in studied sample. The characteristic Kramers time will be studied experimentally and theoretically in optical bistability regime. These fundamental investigations give us the opportunity to demonstrate two different types of stochastic resonance: intensity stochastic resonance in optical bistability, and spinor stochastic resonance in spin-trigger regime. At the end, we present the preliminary results for intensity fluctuations in optical bistability and discriminator regimes. Therefore, the manuscript is organized as follows.

The subsequent chapter provides an introduction on microcavity polaritons. The basics of excitons as quasi-particles in a bulk semiconductor and two dimensional systems will be presented. We will discuss about exciton spinor properties and their coupling to photons. Then, two-dimensional photons in a microcavity structure with distributed-Bragg reflectors will be presented. At the end, we will discuss about the strong coupling regime in microcavity structure with embedded quantum well as nonlinear medium.

Chapter 3 presents our complete study on the effect of excitation power and polarization on optical bistability. We will discuss about the effect of nonlinear loss, due to the biexciton formation. The effect of the detuning between the laser and the zero dimensional polariton ground state on the polariton bistability will be also assessed.

We demonstrate in chapter 4, the effect of external Gaussian noise on microcavity polariton dynamics. It contains a comprehensive discussion about the effect of noise on an underdamped oscillator model. Then we will talk about the connection between the Gross-Pitaevskii equations, as a very well suited model used for describing the dynamics of the lower polariton, with a noise-driven nonlinear oscillator equation of motion. The noise-induced optical transitions between stable states and correspondingly the residence time and the Kramers time will be presented. We investigate the effect of noise on optical characteristics which can play an important role in potential device applications. All experimental results are well reproduced using Gross-Pitaevskii equation (GPE).

In chapter 5, we focus on the stochastic resonance (SR) phenomenon in different regimes. In the first part, we demonstrate the observation of intensity stochastic resonance. This study will be classified in two different regimes: SR in zero-dimensional and two-dimensional polariton bistability. In both cases, we show how the intensity noise can modify the signal-to-noise ratio in case of transmitted polariton intensity. In the second part we introduce a novel type of stochastic resonance which will be called "*spinor stochastic resonance*". We will show how taking advantage of spinor properties of polaritons can provide a noise-induced spin ordering in an ensemble of microcavity exciton-polaritons. All the experimental results are well reproduced by GPE (for the first case) and spinor GPE (for the second case) driven with a noisy input.

In chapter 6, we study the polariton intensity fluctuations through Hanbury Brown-Twiss measurement in optical bistability and also discriminator regime. We will present the super-bunching effect around the nonlinear threshold due to the polariton-polariton interactions and noise-induced polariton fluctuations.

Finally, the main outcomes of this work are summarized in chapter 7. It will further provide a brief outlook to what could be studied in the near future.

2 Microcavity polaritons

In 1958, John Hopfield noted in his pioneering paper that the fundamental optical absorption process is not a conversion of photons into excitons. In fact, the optical excitation induces an excitonic polarization that via the interaction processes can then be converted into a population. Hopfield introduced the term “polariton” for elementary excitations of exciton-photon mixed states in a bulk semiconductor [32]. Polariton luminescence was observed experimentally in different semiconductors such as CdS [33] and GaAs [34, 35]. In 1992, Weisbuch for the first time demonstrated the existence of normal-mode splitting in semiconductor quantum microcavity [3]. This work opened a novel research field of microcavity polaritons.

This chapter is organized as follows: first we introduce the exciton as a quasi-particle in semiconductor materials. Then, we explain the effect of quantization in two-dimensional structures (quantum well) on the electrical and the optical properties of excitons. In the following section the microcavity and two-dimensional photons will be discussed. This will serves as a basis for the subsequent discussion on the exciton-polaritons.

2.1 Excitons

2.1.1 Bulk excitons

In pure semiconductors, the optical properties depend on the band gap energy (E_g). For a wide energy range above the fundamental gap energy, the semiconductor absorbs the electromagnetic radiation and therefore can be excited optically. In this condition a photon promotes an electron from the valence to the conduction band and consequently a free electron hole pair is created. Figure 2. 1 **a** shows schematically the electron and the hole dispersion, and photon absorption mechanism in direct band gap semiconductors. The semiconductor absorption spectrum shows continuum states above band gap energy in addition to sharp peaks at energies lower than E_g (Fig. 2. 1 **b**). On account of the Coulomb interaction, the attraction between the electron and hole resultant the bound electron-hole pair which is called as exciton. A simplified picture of exciton state is that an electron and a hole

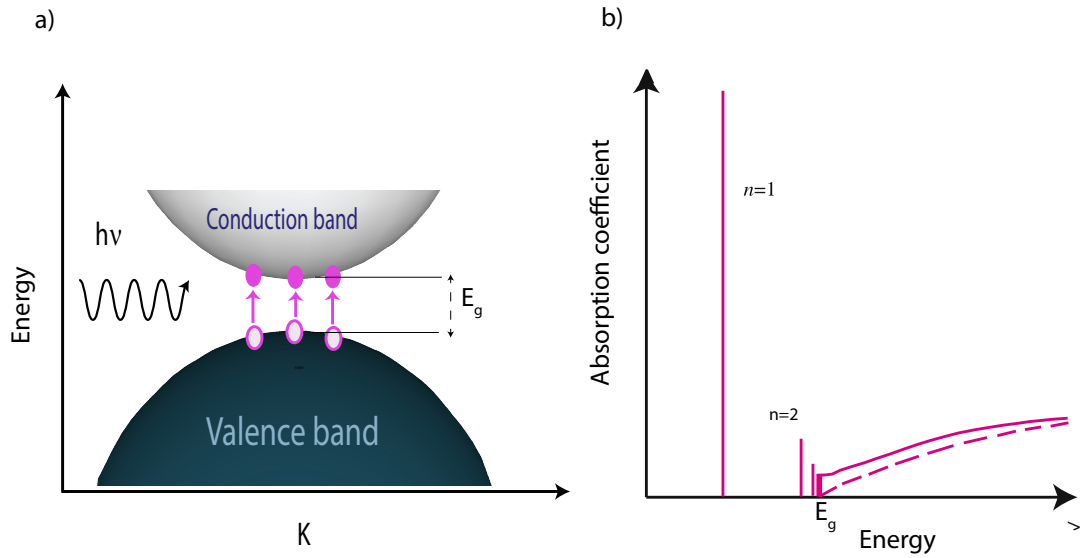

Figure 2.1: **Photon absorption in a direct band gap semiconductor. a** The attractive Coulomb interaction between electrons of conduction band and holes of valence band forms the bound electron-hole pair state. This quasiparticle is called as exciton. The hole effective mass is larger than the electron effective mass. **b** From [38]. Absorption spectra around band gap energy (E_g) of a direct-gap semiconductor with (solid line) and without (dash line) exciton effects. n represents an exciton bound state.

interacting in a dielectric medium form a hydrogen like atom. In materials like semiconductors with a strong dielectric constant and therefore small electron-hole Coulomb interactions the electron and the hole are weakly bound together. These types of excitons are known as Wannier excitons. In 1937, Wannier described the exciton effective mass (M_X) due to the motion of a hole within the valence band and an electron within the conduction band [36, 37]. The exciton can be considered as a free particle with the effective mass of:

$$M_X = m_e + m_h \tag{2.1}$$

where m_e and m_h are the effective mass of electrons and holes, respectively. As any quasi-particle system, the exciton motion can be decomposed into two parts: the motion of the center of mass of the exciton, and the relative motion of the electron and hole around the center of mass. Due to the relative motion of the electron and the hole, exciton states are both bound states and continuum states. Like hydrogen atom, the bound states are quantized with different quantum numbers and orbital angular momentums. In the continuum state, excitons can be considered as free electrons and holes where their wavefunctions are affected by Coulomb interactions. According to the calculations, the exciton wave function $\Psi(r_e, r_h)$ can be expressed in analogy to the hydrogen atom by the two-body Schrodinger equation, except for the fact that the dielectric constant (ϵ) screens the Coulomb force between electrons

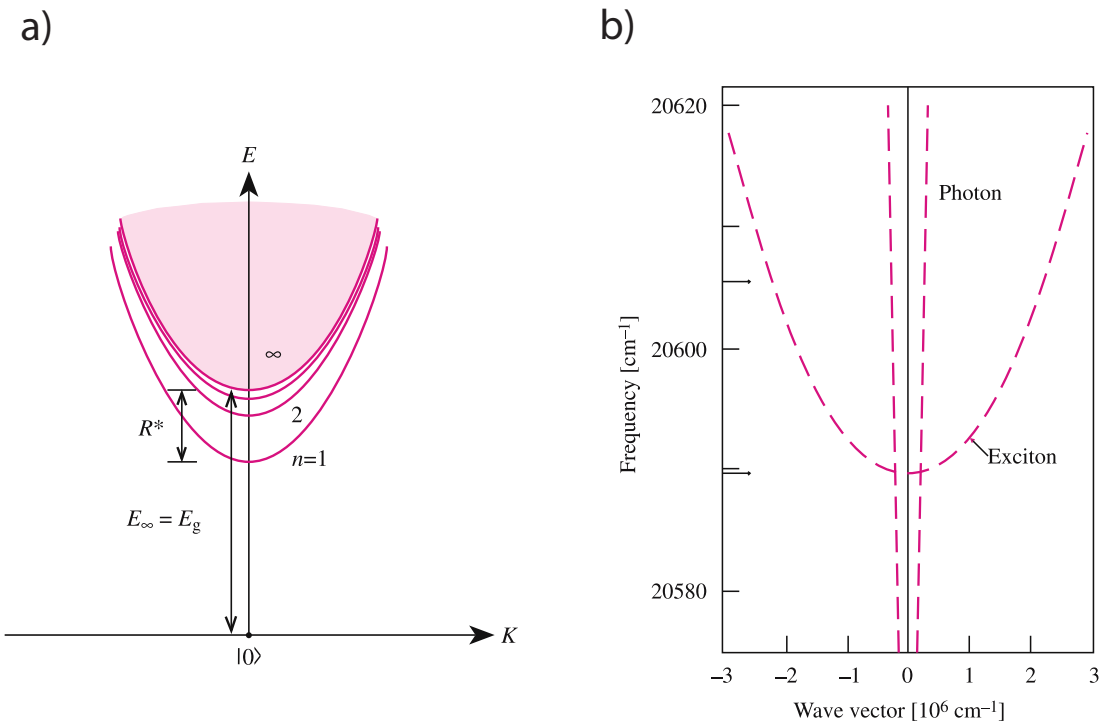

Figure 2.2: **Exciton dispersion curve. a** Illustration of the energy states of a Wannier exciton. The exciton bound states (n=1, 2, ...) and the continum states are shown. **b** Dispersion curve of a bare exciton and a bare photon for the A exciton in CdS. Because of the heavier effective mass, excitons have a much flatter dispersion curve than photons and therefore only the excitons in the light cone (with the small momentum) can interact with the light. From [38].

and holes.

$$[\frac{P_e^2}{2m_e} + \frac{P_h^2}{2m_h} - \frac{e^2}{\epsilon|r_e - r_h|}]\Psi(r_e, r_h) = (E - E_g)\Psi(r_e, r_h) \tag{2.2}$$

P_e and P_h are the electron and hole momentum operators, and $E - E_g$ represents the exciton binding energy [38]. Here $r_{e/h}$ represent the real space coordinates of the electron/hole and e the electron elementary charge. The first two terms describe the electron and hole kinetic energy. Equation 2. 2 can be solved, as in the case of the hydrogen atom, by modifying the coordinates from r_e and r_h to center-of-mass coordinate R and relative coordinate r:

$$R = \frac{m_e r_e + m_h r_h}{m_e + m_h} \tag{2.3}$$

$$r = r_e - r_h \tag{2.4}$$

Calculating the two resultant equations in new basis and in analogy to the hydrogen atom the bulk exciton dispersion can be written as follows:

$$E_X^n(K) = E_g + \frac{\hbar^2 K^2}{2M_X} - \frac{R^*}{n^2} \tag{2.5}$$

$$R^* = \frac{\mu e^4}{2\hbar^2 \epsilon^2} \tag{2.6}$$

where R^*, $\hbar$ and K are the Rydberg constant for the exciton, reduced Planck constant, and the center of mass wave vector of the exciton motion. n=1, 2,... is an integer. μ is the reduced mass of the electron-hole system $\mu^{-1} = m_e^{-1} + m_h^{-1}$. Bohr radius of semiconductor excitons is defined as

$$a_B^* = \frac{\hbar^2 \epsilon}{\mu e^2} \tag{2.7}$$

Figure 2. 2 **a** shows the energy dispersion of a Wannier exciton. The last term in Eq. 2. 5 corresponds to the exciton binding energy (E_b). The exciton binding energy in semiconductor materials is almost three orders of magnitudes smaller than hydrogen atom binding energy (13.6 eV). This difference originates from two parameters. First, the exciton reduced mass is one order of magnitude lighter that electron mass. Second, due to the change in the dielectric constant, the Bohr radius of the hydrogen atom is almost 100 times smaller than exciton Bohr radius.

2.1.2 Two-dimensional excitons

Today nanofabrication allows one to grow multiple layers of different semiconductor thin films with the widths comparable with the quantum wavelength of electrons. In the simplest superlattice structures, a semiconductor layer with small gap is sandwiched inside a large band gap semiconductor. Due to the band gap difference between the different layers a single quantum well (QW) potential is created. If the intermediate layer is thin enough, in order of few nanometers, it can provide the efficient confinement for the exciton movement. Due to the quantization along the growth direction the electron and hole state would be quantized resulting in a quantization energy (E_0) which adds up to the band gap energy of the bulk semiconductor. In fact, this quantization will effectively modify the density of states (DOS) of the charge carriers in these structures. Quantum well display a step like DOS function and the band gap energy shifts with the quantization energy (E_0) (Fig. 2. 3). The resulting QW exciton dispersion relation reads:

$$E_X^n(K_{||}) = E_g + E_0 + \frac{\hbar^2 K_{||}^2}{2M_X} - \frac{R^*}{(n-0.5)^2} \tag{2.8}$$

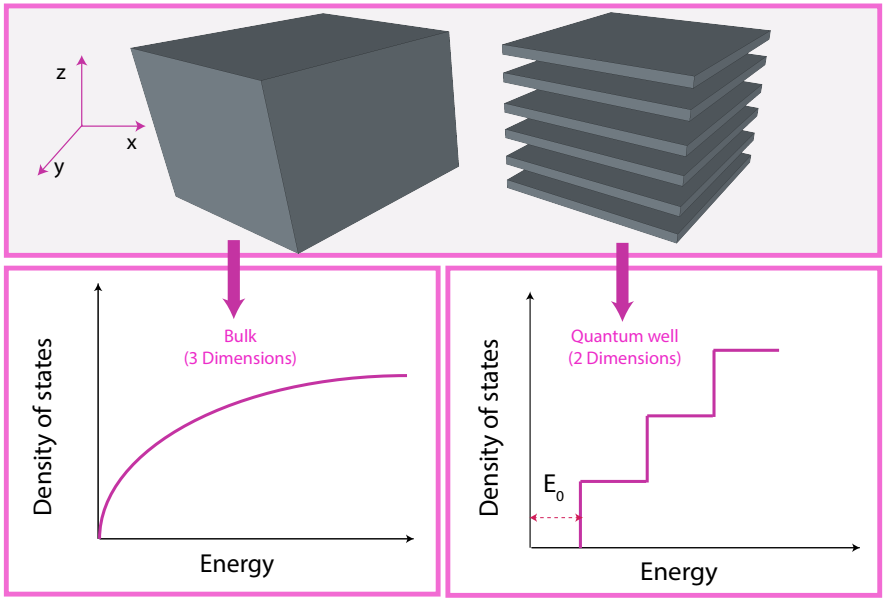

Figure 2.3: **Illustration of the density of states in bulk and quantum well as three and two dimensional semiconductor systems.** In 3D system the DOS yields a square root dependence on the energy, while in 2D system DOS changes to step like function. Due to the confinement, the band gap energy is increased by the quantization energy (E_0).

where $K_{||}$ is the two-dimensional wave vector of the center of mass exciton motion along the plane of the structure. E_g and E_0 are the bandgap and quantization energy, respectively. As we can see, the two-dimensional exciton binding energy (the last term in Eq. 2. 8) is significantly larger than for a bulk exciton (Eq. 2. 5). In two dimensional (2D) system, for the n=1 fundamental state of an exciton in an infinite well, the exciton binding energy is four times larger than for the case of bulk excitons [38].

Another feature, arising due to the confinement, is the breakdown of translational symmetry in direction of the confinement [39]. It means that the momentum conservation is only for the in-plane component of the wave vector ($K_{||}$), and the excitons can couple to a continuum of photon states with the same in-plane momentum. However the photon dispersion is much steeper than excitons (Fig. 2. 2 **b**). Due to the conservation of energy and wavevector, the coupling between exciton and photon must occur at the points where their dispersions intersect.

2.1.3 Exciton total angular momentum

The total angular momentum of an exciton is a direct combination of the valence hole and conduction electron angular momentums. The angular momentum (J) is determined by the sum of the spin (s) and the orbital momentum (L)[41, 40]. The lowest conduction band electron is a s-type orbital with the spin of s=1/2 and an orbital momentum of L=0. Therefore,

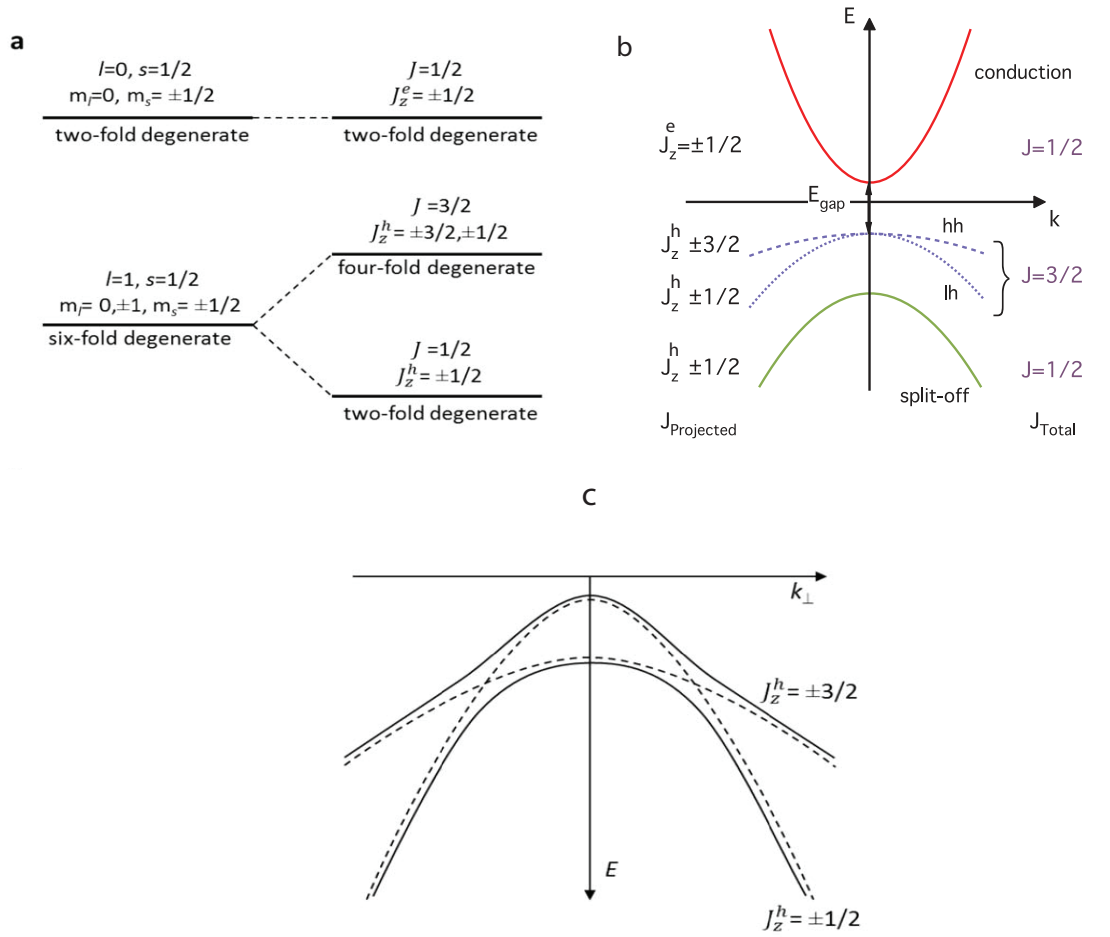

Figure 2.4: **Spin structure of excitons in zinc-blende semiconductors. a** Lowest conduction band and highest valence band at k=0 without (left) and with (right) spin-orbit coupling. Due to the coupling light and heavy hole valence band and the split-off valence band are formed. **b** Electron and hole dispersion correspond to well-defined total angular momentum in a bulk material. **c** Heavy and light hole crossed bands in a confined structure before (dashed lines) and after (solid lines) of band mixing. From[40].

conduction electrons have two possible projections along the z axis: $J_z^e = \pm\frac{1}{2}$. A valence hole is a p-type orbital with six-fold degenerate states, s=1/2 and L=1. For the case that the orbital momentum and the spin of the hole are anti-parallel, the so-called split-off band with J=1/2 is formed. For the parallel coupling between the spin and the orbital momentum, two fold degenerate valence band with J=3/2 are formed (Fig. 2. 4 **a**). The heavy hole ($J_z^h = \pm 3/2$) and light hole ($J_z^h = \pm 1/2$) bands have two different dispersions and consequently two different effective masses. In bulk zinc-blende semiconductors as GaAs the heavy and light hole states are degenerated at k=0 (Fig. 2. 4 **b**). Although the confinement along the growth axis lifts the degeneracy and push the heavy hole band to lower energies. The difference in band curvatures leads to anticrossing at the band mixing point. Due to the anti- crossing effect the heavy band

curvature is now larger than the light band curvature which is completely reverse to their bulk properties (Fig. 2. 4 **c**).

When a photon is absorbed to resonantly excite an exciton with electron and hole total angular momentum J_z^e and J_z^h, according to total angular conservation rule the light polarization J_z^{ph} would be

$$J_z^{ph} = J_z^e + J_z^h \tag{2.9}$$

where J_z^{ph} takes the value ± 1 for the right or left circular polarized photons (σ+, σ-). Exciton states with $J_z = \pm 1$ are called bright exciton states. This type of excitons can be created by absorption of a single photon and can also emit photons. Excitons with $J_z = \pm 2$ are called dark excitons, since they cannot interact with single-photon although they can be excited by two-photon processes.

We are interested mostly in the quantum well heavy hole excitons with a total angular momentum J=1. The possible spin projections of heavy hole excitons on the z axis are $J_z = \pm 1$.

2.2 Semiconductor microcavities

Technologically, photon confinement is much easier than exciton confinement, simply because the wavelength of visible photons is much greater than exciton Bohr radius. A planar Fabry-Perot resonator is the simplest structure for the confinement of the electromagnetic field. This device consists of two parallel plane mirrors separated by a dielectric layer with a well-defined thickness (L_c), the so called spacer layer. Semiconductor microcavities are Fabry-Perot resonators with a specific mirror structure called distributed Bragg reflectors (DBRs).

2.2.1 Distributed Bragg reflector (DBR)

DBRs are stacks of semiconductor layers with two different refractive indices n_1 and n_2 with $n_1 < n_2$. At each interface, because of the change in the refractive index, a part of an electromagnetic wave is transmitted while the other part is reflected. To obtain a high quality DBR at a desired wavelength (λ_{DBR}) each of the layers should feature a physical thickness equal to $\lambda_{DBR}/4n_i$. This means that the electromagnetic wave reflected from each boundary, interfere constructively, and the reflectivity (R_{DBR}) is given by [42]:

$$R_{DBR} = \frac{n_0(n_2)^{2N} - n_3(n_1)^{2N}}{n_0(n_2)^{2N} + n_3(n_1)^{2N}} \tag{2.10}$$

where n_0 and n_3 are the refractive index of the surrounding medium and of the substrate on which the mirror is grown. It is clear that for the larger number of DBR pairs (N), its reflectivity increases significantly. Due to the phase-matching condition described above, DBRs only

feature a limited reflection band which is referred to as the photonic stopband. For high N values the width of the stop band (ΔE_{DBR}) can be approximated by:

$$\Delta E_{DBR} \approx \frac{4E_{DBR}}{\pi}\left(\frac{n_2 - n_1}{n_2 + n_1}\right) \tag{2.11}$$

The DBR mirrors represent a functional solution for implementing a solid state frequency-selective mirror.

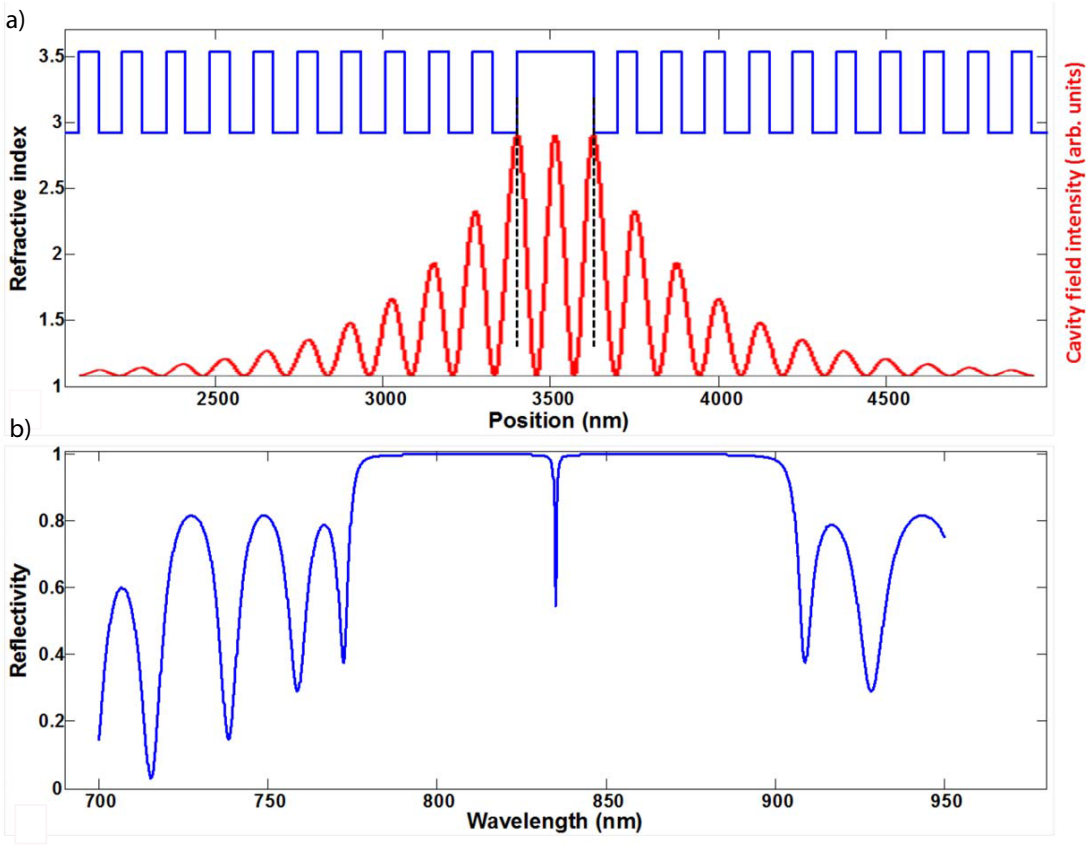

Figure 2.5: **Transfer matrix calculation of the reflectivity of GaAs/AlAs λ cavity. a** Cavity field intensity (red) and the refractive index (blue) inside the microcavity structure. **b** The cavity stop band (between 775 nm and 910 nm) and the cavity resonance (835 nm) which is centered in the stop band. The microcavity is relying on a λ spacer layer, and employing 26-pair and 20-pair DBRs on the bottom and top sides, respectively. From [8].

2.2.2 Microcavity

Microcavity denotes a structure formed in order to confine photonic mode to the order of its wavelength. The wavelength of the semiconductor microcavity mode (λ_c) is defined as

$$\lambda_c = \frac{2n_{sl}L_c}{m} \tag{2.12}$$

where m and n_{sl} represent respectively the integer mode number and the spacer layer refractive index. If λ_c belongs to the DBR stopband, a standing wave due to the multiple reflections is created inside the cavity which indicates a dip at energy ($E_c = hc/\lambda_c$) in the reflectivity spectrum [8].

Figure 2. 5 **a** shows the refractive index of the microcavity structure (blue), and the cavity field intensity (red) inside the cavity versus the growth direction position. The microcavity relying on a λ spacer layer which is a m=2 cavity, and employing 26-pair and 20-pair DBRs on the bottom and top sides, respectively. The resonator mode is determined at λ_c=835 nm. The optical field is maximized in the center of the spacer layer and at the edge of lower and upper DBRs. In the reflectivity spectrum, we observe the DBR stop band with a width of $\Delta\lambda = 135nm$ in which center (λ_c=835 nm) a clear dip appears (Fig. 2. 5 **b**). It is worth mentioning that two optical modes with m=1 (λ=1670nm) and m=3 ((λ=557nm) are out of the stopband, and are not supported by this microcavity.

The electromagnetic mode has a given linewidth (γ_c) which determines the photon lifetime in the cavity (τ_c=$(2\pi\gamma_c)^{-1}$) and also cavity quality factor:

$$Q = \frac{E_c}{\gamma_c} \tag{2.13}$$

For microcavity with high Q factor, the photon lifetime would be long and consequently the field intensity of the confined mode for a constant pump power would be higher.

2.3 Photons in two-dimensions

Inside a planar microcavity, the electromagnetic field is confined in the growth direction (**z**). Nevertheless, there is a continuum of states available in the **x** and **y** directions. This two-dimensional system for photons can be defined with an in plane wave vector ($k_{||}$=$k_x\hat{e_x}$+$k_y\hat{e_y}$). The cavity mode wave vector **k** being decomposed into two terms: **k**=$k_{||}$+k_z, the second term being a **z** component defined by the cavity spacer thickness:

$$k_z = \frac{m\pi}{L_c}\hat{e_z} \tag{2.14}$$

For small in-plane wave vectors the dispersion of the cavity mode is defined as:

$$E_C(k_{||}) \approx \frac{\hbar c}{n_{sl}} k_z + \frac{1}{2} \frac{\hbar c k_{||}^2}{n_{sl} k_z} \tag{2.15}$$

where the first term is the cavity mode energy, and the second term is related to the photon kinetic energy in-plane motion. By analogy with the typical kinetic expression the effective photon mass would be:

$$m_{ph} = \frac{\hbar k_z}{c} = \frac{\hbar n_{sl}^2}{c \lambda_{DBR}} \tag{2.16}$$

For λ_c=835 nm the photon mass of the resonator is $3.3 \times 10^{-35} kg$ which is about four orders of magnitude smaller than a free exciton mass.

2.4 Exciton-polaritons

As mentioned before, semiconductor microcavities realize a quasi-two-dimensional system for photons. Furthermore, two-dimensional excitons have higher binding energy and oscillator strength compared to 3D excitons. It means that by introducing a quantum well at the anti-node position of the microcavity standing wave, exciton photon interactions can be reversible. The strong coupling regime would occur under the resonant condition between the exciton state and the photon state at the crossing point of their respective dispersion curves. Due to the momentum conservation a QW exciton state with a well-defined transverse momentum, is coupled to a single photon mode with the same in-plane wave vector. In fact, the system undergoes a coherent evolution with multiple energy exchange events, a photon being absorbed by an exciton, which subsequently emits a photon with the same wave vector and energy. The vacuum Rabi-splitting Ω_R, corresponds to the frequency of the oscillations occurring between excitonic and photonic population in strong-coupling regime. In this regime the Rabi period must be shorter than the photon-mode decay time (photon lifetime) and the exciton scattering time (dephasing time). In such a regime, the normal perturbative approach of Fermi's golden rule breaks down. The eigenstates of the system are no more the exciton state and the photon mode, but two mixed states called lower and upper polariton (LP and UP). The intrinsic radiative lifetime in GaAs QW has been determined to be around 10 ps [43]. This short lifetime shows the effective coupling between electron and hole and eventually high oscillator strength. The polariton properties, inherited from their exciton part, give rise to the nonlinear effects which can be driven or read out through their photonic counterpart coupled in and out of the cavity.

The Hamiltonian for an interacting exciton-cavity system with in plane wave vector (k) is given by:

$$\hat{H}_K = E_X(k) \hat{a}_k^\dagger \hat{a}_k + E_C(k) \hat{b}_k^\dagger \hat{b}_k + g_0 [\hat{a}_k^\dagger \hat{b}_k + \hat{b}_k^\dagger \hat{a}_k] \tag{2.17}$$

where $E_X(k)$ and $E_C(k)$ are respectively the exciton and the cavity-photon dispersions, and $\hat{a}_k^\dagger$ and $\hat{b}_k^\dagger$ ($\hat{a}_k$, $\hat{b}_k$) are their respective creation (annihilation) operators. The last term corresponds to the light-matter interaction. Here the interaction term considered as a constant for different in-plane momentums. For a microcavity with embedded quantum well and $R_{DBR} \approx 1$, g_0 is given by:

$$g_0 = \hbar \sqrt{\frac{e^2}{2\epsilon m_0} \frac{N_{QW}}{n_{eff}^2 L_{eff}} f_X} \tag{2.18}$$

where N_{QW} is the number of QWs which are effectively coupled to the light field of the cavity mode [44]. f_X, n_{eff} and L_{eff} are exciton oscillator strength, effective refractive index and effective length of the microcavity.

With diagonalization of the Hamiltonian of Eq. 2. 17 one finds that:

$$\hat{p}_k^\dagger = F_X(k)\hat{a}_k^\dagger + F_C(k)\hat{b}_k^\dagger \tag{2.19}$$

$$\hat{q}_k^\dagger = -F_C(k)\hat{a}_k^\dagger + F_X(k)\hat{b}_k^\dagger \tag{2.20}$$

where F_X and F_C denote the exciton and the cavity Hopfield-coefficients with the unitary condition $F_X^2 + F_C^2 = 1$. The Hamiltonian of equation 2. 17 read as follows:

$$\hat{H}_k = E_{LP}(k)\hat{p}_K^\dagger \hat{p}_K + E_{UP}(k)\hat{q}_K^\dagger \hat{q}_K \tag{2.21}$$

$E_{LP}(k)$ and $E_{UP}(k)$ are two eigenenergies which depend on in-plane momentum dependent detuning:

$$\delta_k = E_C(k) - E_X(k) \tag{2.22}$$

where $E_C(k)$ and $E_X(k)$ are cavity and exciton energy respectively. The lower and upper polariton eigenenergies are given by:

$$E_{LP}(k) = \frac{1}{2}\delta_k + E_X(k) - \frac{1}{2}\sqrt{\delta_k^2 + 4g_0^2} \tag{2.23}$$

$$E_{UP}(k) = \frac{1}{2}\delta_k + E_X(k) + \frac{1}{2}\sqrt{\delta_k^2 + 4g_0^2} \tag{2.24}$$

The minimum energy distance between these two modes occurs when $\delta_k = 0$. It is referred to as the vacuum Rabi-splitting Ω_R. In the case of a zero detuning, $\Omega_R = 2g_0$.

Figure 2. 6 **a** shows the polariton mode dispersion as a function of the in-plane momentum. Because of the large effective mass of QW excitons compared to the cavity photons, exciton

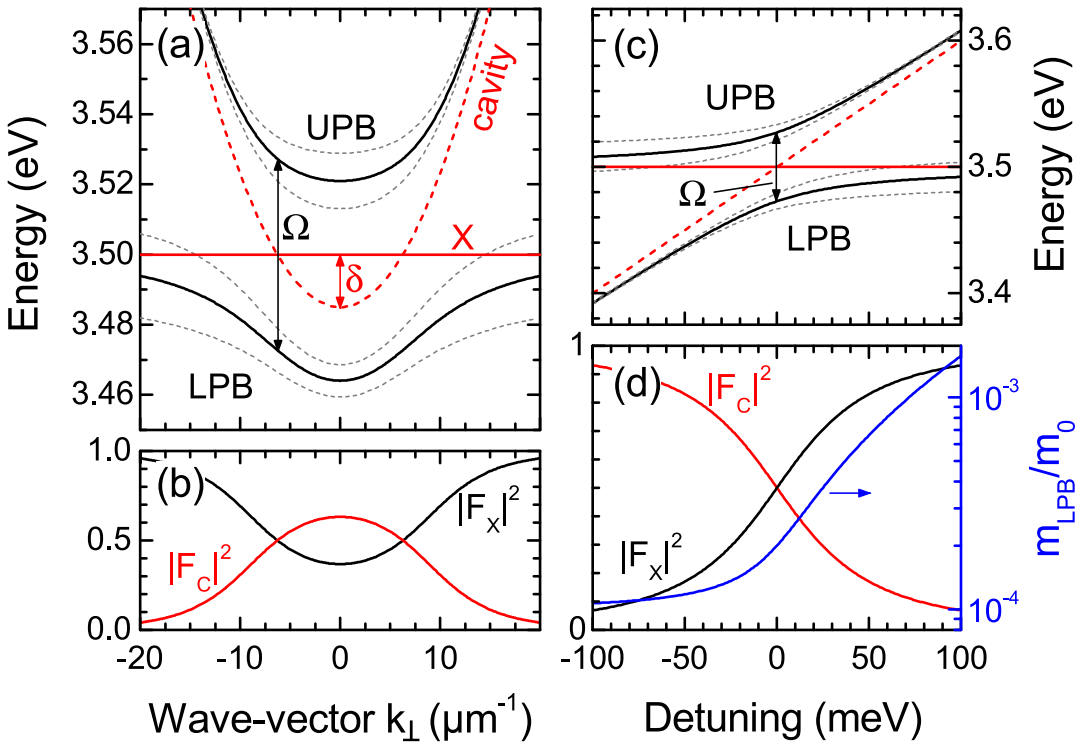

Figure 2.6: **The wave vector and the detuning dependence of the lower and the upper polariton branches. a** In-plane dispersion of lower polariton branch (LPB), upper polariton branch (UPB) (black), cavity mode and exciton (X) (red). By tuning the exciton-cavity detuning (δ) lower and upper polariton dispersion shift in energy (dash line). **b** Corresponding evolution of Hopfield coefficients for lower polariton branch. **c** The effect of the detuning on the energy positions at k=0 and anti-crossing effect. Cavity mode (red dash line) and exciton energy (red line) are shown. **d** Respective evolution of $|F_X|^2$, $|F_C|^2$ and the effective mass of lower polariton ground state (blue). From [45].

dispersion is flat at exciton energy. The lower and the upper polariton states exhibit a well-defined energy minimum at k=0. At high k, the LP (UP) dispersion converges toward the exciton (photon) dispersion. In Figure 2. 6 **b** the respective evolution of the Hopfield coefficients along the LP dispersion is shown. As we can see, for the low and the high in-plane momentums the lower polariton is more exciton-like and around k=0 it is more photon-like. All intrinsic properties of polaritons, like homogeneous linewidth, lifetime and effective mass, are mainly affected by their photonic and excitonic fraction.

The simplest signature of the strong-coupling regime is the anticrossing behaviour for different exciton-cavity detunings. Figure 2. 6 **c** displays the energy of the coupled (LP, UP) and uncoupled (exciton, photon) modes for k=0 versus δ. For a large positive exciton-cavity detuning, the lower polariton branch is more exciton like while the upper polariton branch is more photonic. This is completely reversed for the opposite case with negative δ. The

polariton effective mass depends directly on the ratio between the exciton and the photon fractions. Figure 2. 6 **d** shows LP effective mass (m_{LP}), evidencing that m_{LP} increases with (F_x).

In this simple coupled oscillator model polariton linewidth (γ_p) is given by

$$\gamma_p = F_C^2(0)\gamma_c + F_X^2(0)\gamma_x \tag{2.25}$$

where γ_x denotes the exciton linewidth. This gives correct value for low excitation regime and for a limited exciton-cavity detuning around zero.

3 Optical bistability and multistability in zero-dimensional polaritons

3.1 Introduction

Bistability is a general phenomenon which can be investigated in wide range of fields like physics and chemistry. Generally speaking, in a bistable system, for a given input parameter, two different output values are possible depending on the history of the system. Optical bistability (OB) means that both input and output signals are optical. This can be achieved under conditions in which light and matter are closely coupled together. Two important ingredients for OB are the nonlinear media and the positive feedback mechanism. These conditions can be achieved in a Fabry-Perot interferometer filled with non-linear materials. In 1976 Gibbs and his coworkers demonstrated the first optical bistability [19]. They used a continuous wave dye laser to excite sodium atoms in a cell between the plates of a Fabry-Perot. Since this pioneering work, optical bistability has been shown with several nonlinear mechanisms such as soliton formation in liquid crystals [46], Kerr effects [47] and absorption saturation [48, 49]. However, all experiments just mentioned are performed in the regime of weak coupling, where the light and matter interaction can be considered just as a perturbation. In 2004, Bass et al., reported the observation of polariton bistability in the strong coupling regime. They showed that polariton-polariton interactions give rise to a Kerr-like nonlinearity [13]. Bistability is commonly used for device applications [50, 51, 52, 53], particularly in polariton systems as spin switch and optical memory [11, 10], optical transistor [54], laser [55], and logic functions [56]. Among all device oriented proposals, spin dependent devices have the possibility to improve greatly the possibilities in optical communications.

Polariton multistability, as a promising effect in the development of spintronics, has been studied theoretically and experimentally during the last decade [14, 57, 58, 59, 60]. Spin multistability denotes the opportunity for a system to switch between several stable spinor states for a given excitation condition. Strong spin coherence and the control of spin interactions are two main conditions which for spin multistability observation should be fulfilled.

In this chapter, first we present the sample with zero-dimensional polaritons. In section 3. 3, we discuss about the theory of the optical bistability in the polariton system. Then, we

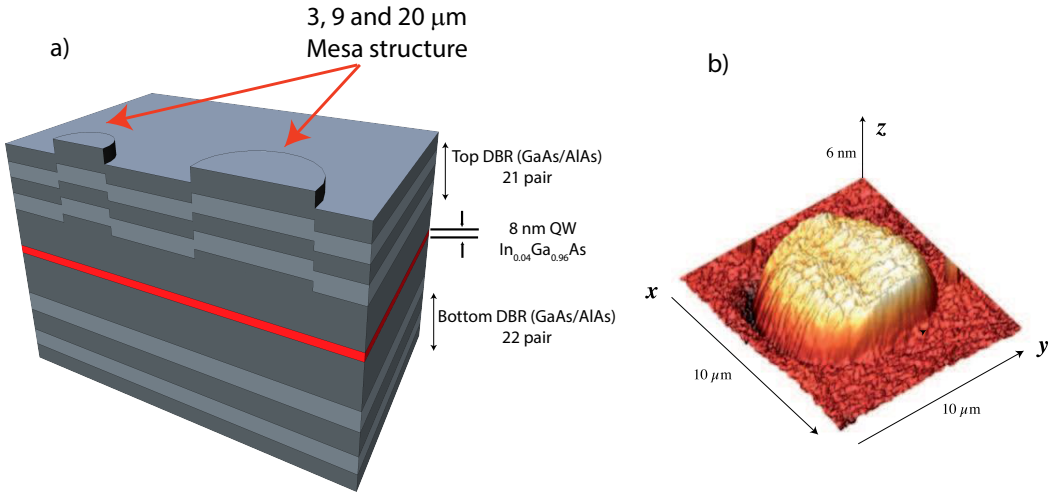

Figure 3.1: **The microcavity and mesa structure.** From [61]. **a** The schematic of the GaAs λ cavity with two GaAs/AlAs DBRs. $In_{0.04}Ga_{0.96}As$ quantum well and the mesa structure create two dimensional and zero dimensional structures for excitons and photons respectively. The Rabi splitting is 3.5 meV and the quantum well exciton energy lies at 1484.2 meV **b** AFM image of a 9 μm mesa. Due to the anisotropic mobility of the atoms during the MBE growth, the step is sharper along the x-axis than along the y-axis.

introduce the concept of spin dependent nonlinear interactions and biexciton creation. In the last section we will present our experimental results. We will discuss about the effect of the biexciton resonance respect to the polariton ground state and laser energy in details. It will be shown how the competition between several nonlinear mechanism, such as biexciton formation, parallel and antiparallel spinor polariton interactions can effectively modify the polariton spinor bistability and consequently polariton multistability.

3.2 Zero-dimensional polariton

3.2.1 Sample

All experimental results presented in this thesis have been performed using a sample grown by O. El Daif and F. Morier-Genoud [61]. The sample has been grown by molecular beam epitaxy (MBE) on a GaAs substrate. It is a GaAs λ microcavity with a 8 nm $In_{0.04}Ga_{0.96}As$ quantum well introduced in the middle of the cavity at an anti-node position of the confined optical mode. The microcavity is sandwiched between quarter-wave stack distributed Bragg reflectors made of AlAs/GaAs (22pairs for the lower DBR and 21 pairs for the upper DBR) (Fig. 3. 1 **a**). The sample is grown with 4 percent wedge so that, over the whole sample, the cavity resonance shifts of more than 50 meV.

In order to obtain zero-dimensional microcavity polaritons, a photonic lateral confinement is

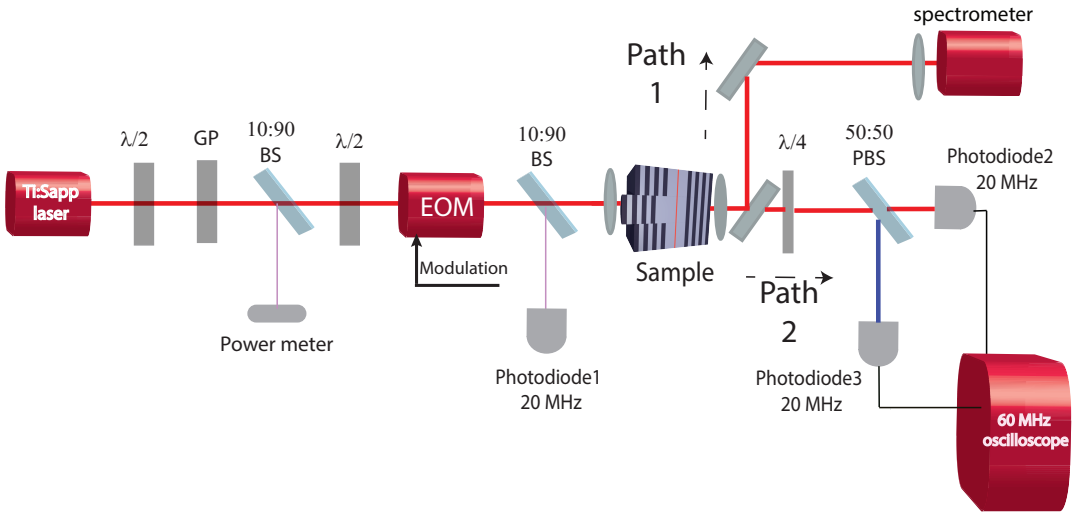

Figure 3.2: **Experimental setup.** The cw single mode laser excites a microcavity polariton gas. Using a half-wave plate ($\lambda/2$), mounted on motorized rotation stage, and a Glan polarizer (GP) the power of the excitation laser is tuned precisely. Using an electro-optic modulator (EOM), the laser polarization is tuned from left circular to right circular. In path number 1, the polariton photoluminescence is focused on the entrance slit of a 1 m spectrometer with a 600 grooves per millimeter grating. These specifications lead to a spectral resolution of 25 μeV. In path number 2, using a quarter-wave plate ($\lambda/4$) the transmitted light is converted to linear polarization. Horizontal and vertical components of the polarized emission are separated by a polarizing beam splitter (PBS). Spin-up and Spin-down polaritons are detected simultaneously using two fast photodiodes and a 60 MHz bandwidth oscilloscope. Excitation power and photon time streams are detected through power meter and photodiode 1, respectively.

achieved through a mesa structure. Local elevation of the planar microcavity spacer layer is so called as mesa. In fact, inside the mesa, the cavity length is increased and hence the resonant energy of the cavity is reduced. This leads to the quantization of the electromagnetic wave in the (**x**, **y**) plane. The mesas of 20, 9 and 3 μm with a height of 6 nm are placed along the wedge, resulting in optical traps with different exciton-cavity detunings. An atomic force microscopy image of a 9 μm mesa is shown in Figure 3. 1 **b** [61].

3.2.2 Polariton photoluminescence

As explained in chapter 2, in a planar microcavity, exciton-polaritons are only confined along the growth axis of the structure, and they can move freely in the (**x**, **y**) plane. However, in mesa

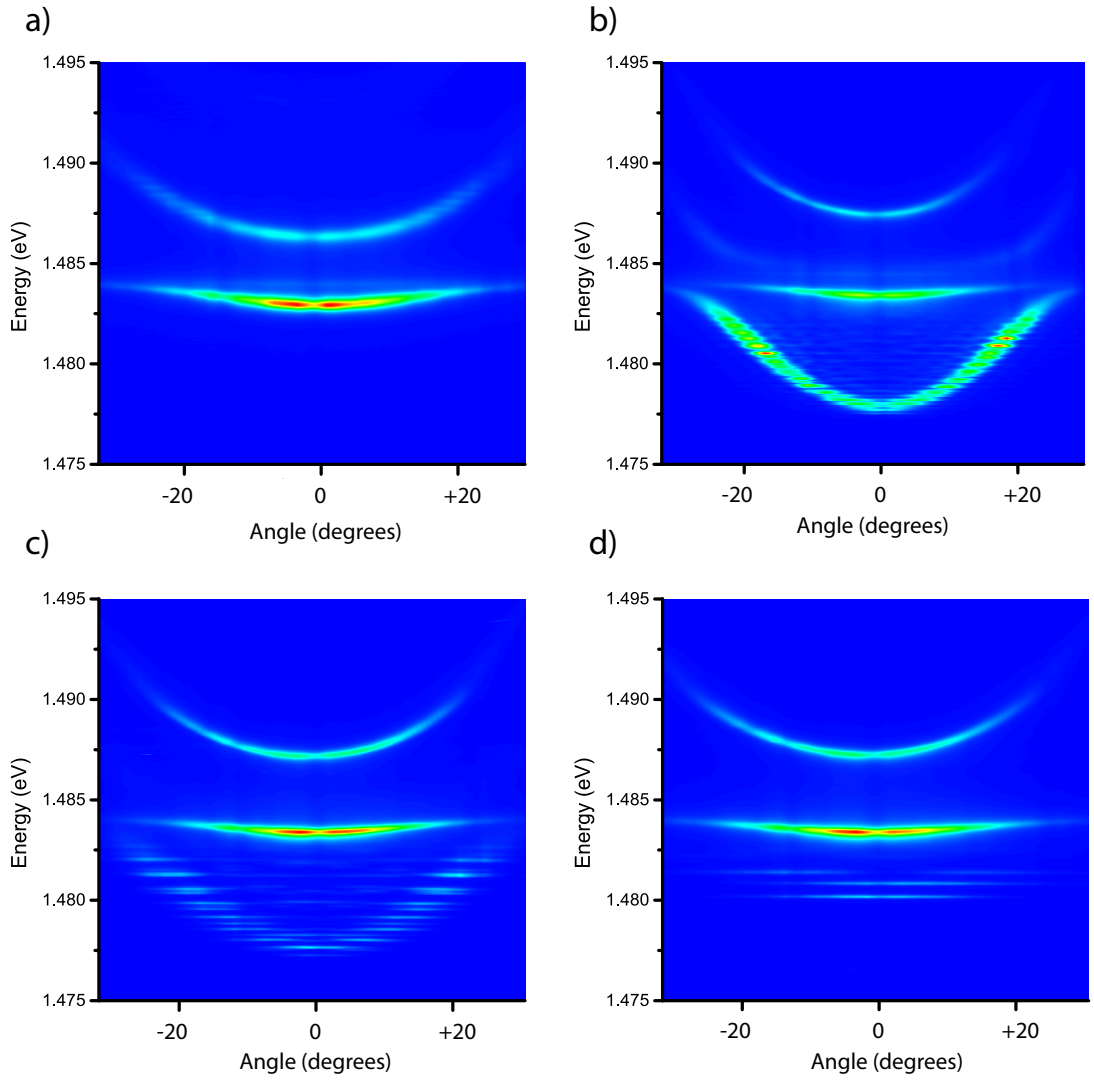

Figure 3.3: **Far-field imaging spectroscopy.** Polariton spectra along one direction of the momentum space. **a** The polariton dispersion of planar microcavity. Two new eigenstates of the system in strong coupling regime, lower and upper polariton states. The exciton-cavity detuning is around $\delta = +1.3meV$ **b** The co-existence of delocalized two-dimensional polaritons and confined polaritons in 20 μm mesa. The dispersion of confined states are almost continuous ($\delta = -6.4meV$). **c** Clear confinement of the lower confined polariton states in a 9 μm mesa ($\delta = -6.42meV$). **d** Polariton dispersion in 3 μm mesa. Due to the strong confinement, discrete energy states are extended in momentum space ($\delta = -3.2meV$).

structures a photonic confinement potential for polaritons is achieved, while the potential depth depends on the mesa height. By decreasing the lateral size of the mesa, it is possible to obtain zero-dimensional polariton with discrete energy levels [62, 63].

The optical characterization of the sample is performed using a photoluminescence setup

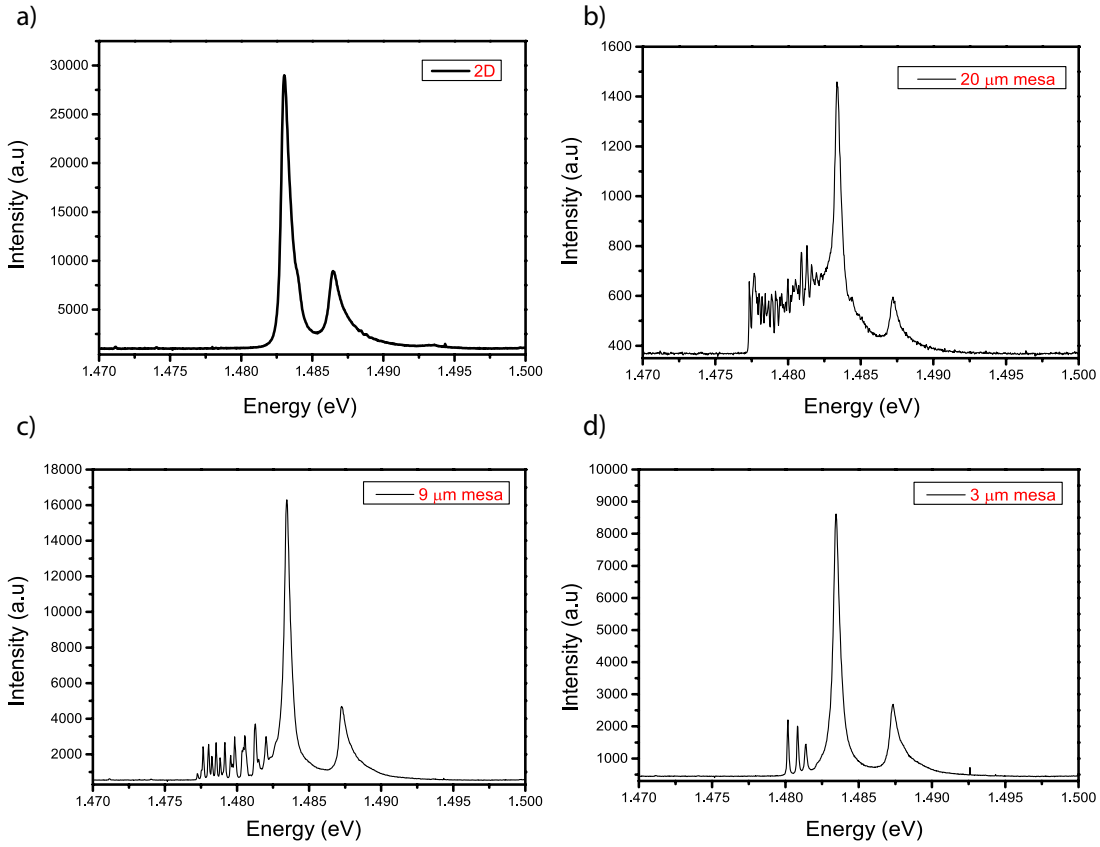

Figure 3.4: **Transmission spectra in planar microcavity and mesa structure corresponding to Figure 3. 3. a** lower and upper polariton with 670 μeV and 878 μeV full width half maximum (FWHM), respectively. The exciton-cavity detuning is around $\delta = +1.3meV$ **b** 20 μm dispersion with exciton-cavity detuning of $\delta = -6.4meV$. FWHM of quantized polariton states is comparable with their energy spacing. **c** 9 μm dispersion with exciton-cavity detuning of $\delta = -6.42meV$. Quantization effect is more significant. **d** 3 μm mesa with $\delta = -3.2meV$. The linewidth of the confined polariton state is 110 μeV.

(Fig. 3. 2). The sample is cooled down to liquid helium temperature (4 K) in a cryostat. Using a continuous wave (cw) Ti:Sapph laser, we excite the sample at the first reflectivity minimum above the DBRs stopband. This nonresonant excitation creates free electrons and holes which relax to the lower and upper polariton energies. Due to the finite reflectivity of the cavity mirrors, the photonic part of the polariton population escapes the microcavity. Emitted photons are collected with a microscope objective and, through path number 1, imaged on the entrance slit of a spectrometer. Figure 3. 3 **a** to **d** presents the polariton dispersion of planar microcavity (**a**) and 20, 9 and 3 μm mesas (**b**-**d**). As expected theoretically, the energy quantization in the mesa structure is observed, and by reducing the lateral size of the mesa, the energy difference between these quantized states increases. Their corresponding transmission spectra are shown in Figure 3. 4. The energy spacing between the ground state and the first excited state is 670 μeV in the 3 μm mesa and 390 μeV in the 9 μm mesa. The ground state

polariton linewidth in a 3 μm mesa is around 110 μeV and the two dimensional lower polariton linewidth is 670 μeV . However, as mentioned before, the polariton linewidth depends on the exciton-cavity detuning and does not show a fixed value. In the 3 and 9 μm mesas, the energy spacing between the states is larger than the linewidth of these confined states, while in the 20 μm mesa the energy separation is comparable to the linewidth of the states. For all exciton-cavity detunings, the lower two dimensional polariton dispersion at large momentum is close to the exciton resonance [61]. Based on several measurements in a wide range of mesa structures and what we observe in Figure 3. 3, the quantum well exciton energy is located around 1484.2 meV. The quantum well photoluminescence shows also a sharp exciton resonance of 500 μeV FWHM [61].

In the strong coupling regime, the inhomogeneous broadening of the exciton line does not directly lead to the inhomogeneous broadening of the lower and upper polariton states [64]. Furthermore, here, the mesa size is smaller than the typical size of the photonic disorders in the distributed Bragg reflectors. Therefore, the polariton lifetime can be directly estimated from polariton linewidth. This means that 110 μeV polariton linewidth correspond to about 10 ps polariton lifetime.

3.3 Optical bistability

In our experiment, we consider the resonant excitation of the lower polariton state by a continuous wave (cw) laser. Therefore, we will focus on the evolution of the lower branch. In chapter 2 we introduced the linear Hamiltonian in the polariton basis (equation 2.21). For our experimental conditions, the Hamiltonian changes to $\hat{H}$=$\hat{H}_{LP}$+$\hat{H}_{eff}$. The first term corresponds to the free lower polariton Hamiltonian defined as $\hat{H}_{LP}$=$\sum_k E_{LP}\hat{p}_k^\dagger\hat{p}_k$. The second term represents the polariton-polariton interaction and is defined as:

$$\hat{H}_{eff} = \frac{1}{2}\sum_{k,k',q} V_{k,k',q}\hat{p}_{k+q}^\dagger\hat{p}_{k'-q}^\dagger\hat{p}_k\hat{p}_{k'} \tag{3.1}$$

where V is positive and represents a repulsive interaction due to the interactions governed by the exciton fraction of the polaritons [65, 66, 13].

$$V_{k,k',q} = V_0 F_X(|k'-q|)F_X(k)F_X(|k+q|)F_X(k') \tag{3.2}$$

$$V_0 = 6e^2\frac{a_B}{\epsilon_0 A} \tag{3.3}$$

where a_B, ϵ_0 and A denote the two-dimensional Bohr radius of exciton, the dielectric constant of the quantum well and the quantization area. In the following, we consider a resonant excitation at k=0 with $p_k = p_{k'} = p$. This Hamiltonian describes polariton interactions in a lossless environment. In reality, the system witnesses some loss through the DBRs, which

should be considered as a damping rate. We add phenomenologically this loss term into the Hamiltonian. We include also the H_{pump} which describes the coupling between the external pump field of frequency (ω_L) and amplitude A_{in} and the cavity mode:

$$H_{pump} = i\hbar\sqrt{2\gamma_1}[A_{in}exp(-i\omega_L t)\hat{a}^\dagger] \tag{3.4}$$

where γ_1 represents the loss through the front DBR. The Langevin equation for polariton mode reads as:

$$\frac{dp}{dt} = -(\gamma_p - i\Delta)p - i\alpha_1 p^\dagger pp - F_C(0)\sqrt{2\gamma_1}A_{in} \tag{3.5}$$

where $\Delta = \hbar\omega_L - E_{LP}$ is the energy detuning between the laser energy and the lower polariton energy at k=0. α_1 is the polariton effective nonlinear coefficient defined as $\alpha_1 = F_X(0)^4 V_0/\hbar$. The steady-state response of the system can be solved within a mean field approximation:

$$i\frac{d\Psi}{dt} = (-\Delta - i\gamma_p)\Psi + \alpha_1 n_p \Psi - F_C(0)\sqrt{2\gamma_1} < A_{in} > \tag{3.6}$$

where (Ψ=$< p >$) is the polariton field and $n_p = |\Psi|^2$ is the mean number of polaritons. This equation is called the Gross-Pitaevskii equation. Multiplying equation (3. 6) with its conjugate we obtain:

$$n_p[\gamma_p^2 + (-\Delta + \alpha_1 n_p)^2] = 2\gamma_1 F_C(0)^2 I_{in} \tag{3.7}$$

The solutions exist if $\Delta^2 - 3\gamma_p^2 \geq 0$. In this condition polariton population shows a bistable behaviour versus the laser intensity. Consider a continuous wave laser which is blue detuned respect to the lower polariton energy ($\Delta > 0$). By increasing the laser intensity, the polariton population increases linearly. The growth of the polariton population activates the nonlinear polariton interactions, and, as a consequence, the polariton energy blue shifts ($\Delta E = \alpha_1 n_p$). However, this supply mechanism competes with the polariton lifetime loss mechanism (γ_p). At a given threshold power, the feedback mechanism becomes dominant and polaritons reach a population for which polariton interactions become large enough to blueshift the polariton energy in resonance with the laser. This, results in a better polariton state coupling to the laser, and corresponds to the upper power threshold (I_{upper}) of the hysteresis cycle. In this condition, the emission intensity jumps to the upper branch. In the backward direction, when decreasing the laser power, the emission remains in the upper branch until it reaches the lower threshold power (I_{lower}), which is lower than the upper one. This originates from the fact that the polariton state and therefore the polariton population are clamped to the laser. At this lower threshold, the losses due to the polariton lifetime, dominate the feedback mechanism, which reduces the polariton population. As a consequence, the nonlinear polariton interaction and accordingly the polariton energy decrease. Therefore, the emission falls to a low intensity branch. Figure 3. 5 **a** shows the polariton mean number as a function of the laser intensity for two different case of $\Delta = \sqrt{3}\gamma_p$ and $\Delta > \sqrt{3}\gamma_p$. For the first case the two nonlinear thresholds overlap and the width of the optical bistability (I_{upper}-I_{lower}) is zero. This regime is called

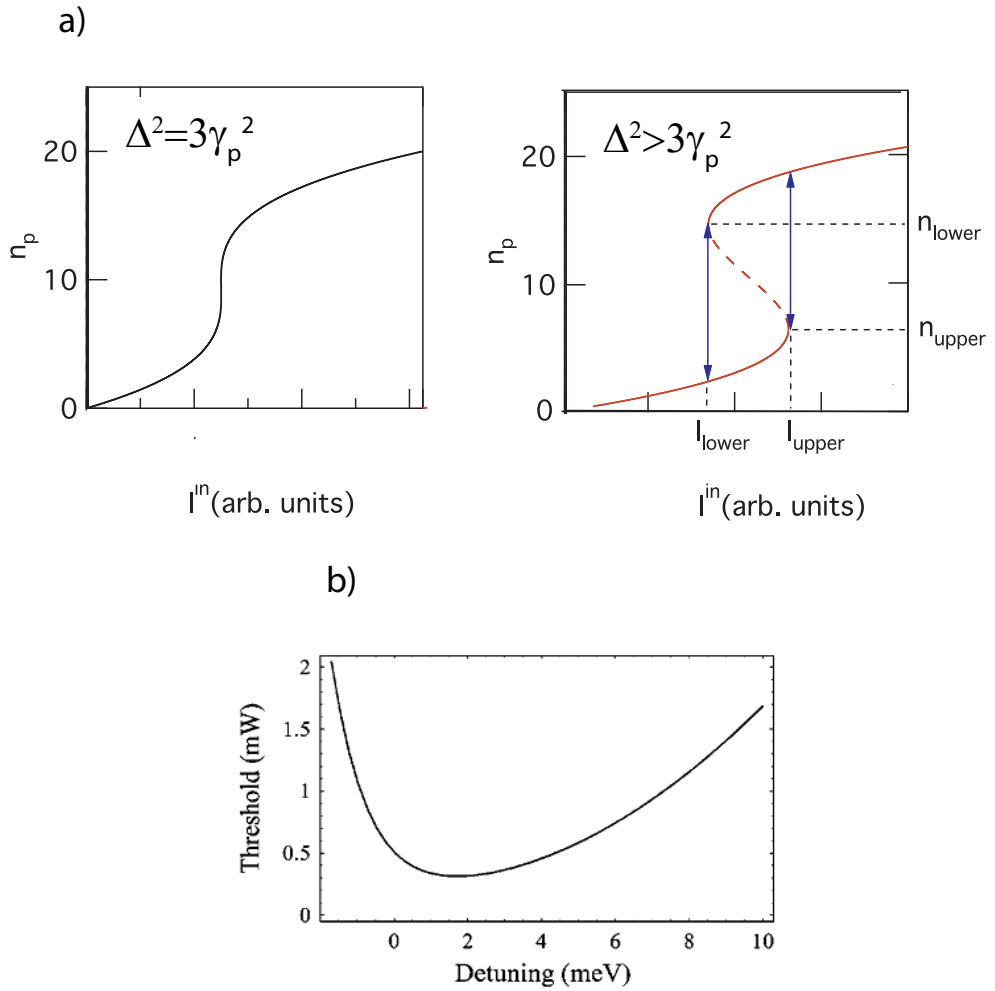

Figure 3.5: **Optical bistability a** From [67]. Two instability regimes: optical discriminator for $\Delta = \sqrt{3}\gamma$, and optical bistability for $\Delta > \sqrt{3}\gamma$. **b** From [13]. Effect of exciton-cavity detuning (δ) on the nonlinear threshold in optical discriminator regime. Due to the trade-off between nonlinearity and coupling to the external field, there is an optimum condition for reducing the discriminator threshold.

"*optical discriminator*". According to Equation 3. 7, the bistability intensity thresholds and the bistability width (ΔB) are obtained as [13]:

$$I_{lower} = \frac{2\Delta + \sqrt{\Delta^2 - 3\gamma_p^2}}{27\alpha_1 F_C(0)^2 \gamma_1}(3\gamma_p^2 + \Delta^2 - \Delta\sqrt{\Delta^2 - 3\gamma_p^2}) \tag{3.8}$$

$$I_{upper} = \frac{2\Delta - \sqrt{\Delta^2 - 3\gamma_p^2}}{27\alpha_1 F_C(0)^2 \gamma_1}(3\gamma_p^2 + \Delta^2 + \Delta\sqrt{\Delta^2 - 3\gamma_p^2}) \tag{3.9}$$

$$\Delta B = \frac{2(\Delta^2 - 3\gamma_p^2)^{\frac{3}{2}}}{27\alpha_1 F_C(0)^2 \gamma_1} \tag{3.10}$$

As mentioned before, for different exciton- cavity detunings, the polariton linewidth and also the Hopfield coefficients are modified. Figure 3. 5 **b** shows the variation of the nonlinear threshold in an optical discriminator regime ($I_{lower} = I_{upper}$) as a function of the exciton-cavity detuning. We observe that, for large positive and negative δ, the laser intensity needed for nonlinear jump between the upper and the lower state is large, while for an optimum exciton-cavity detuning, the threshold intensity is minimum. This behaviour is due to a trade-off between the nonlinear interaction (which is stronger for positive detuning with large exciton properties) and coupling with the external laser (which increases when polaritons become more photon-like at large negative detuning) [13].

In the forward direction of optical bistability (increasing the excitation power), polariton population increases linearly with laser power and for high enough excitation power (I_{upper}) it shifts to laser energy resonance through a nonlinear jump. For a fixed exciton-cavity detuning, by increasing the polariton-laser detuning (Δ), the slope of the linear part decreases while the effective difference between lower and upper states increases. For 3μm mesa structures, with various exciton-cavity detunings (δ) also the shape of bistability can be modified. These modifications are due to different nonlinear strength and coupling to external light sources.

3.4 Multistability and spinor Gross-Pitaevskii

All the theoretical descriptions discussed up to now are valid as far as only one spinor polariton population exists in the microcavity. As discussed in the second chapter, the polariton spinor state is in one-to-one correspondence with the polarization state of the laser light. Spin-up ($\uparrow$) and spin-down ($\downarrow$) polaritons are created via right and left circularly polarized light ($\sigma+$, $\sigma-$), respectively. In case of linearly polarized light, polaritons are created in a coherent superposition of spin-up and spin-down states. Under linear or elliptical polarization first of all, polariton-polariton interactions will be significantly modified. In fact, the strength of the interactions between polaritons with the same (α_1) and opposite (α_2) spinor states are not equal. Consequently, each spin populations, having different populations, experience different blueshift: $\Delta E\uparrow,\downarrow=\alpha_1 n\uparrow,\downarrow+\alpha_2 n\downarrow,\uparrow$, where α_1 and α_2 are respectively nonlinear interaction constants between polaritons of the parallel and antiparallel spins .

The second important mechanism is the biexciton creation and its impact on the polariton dynamics, which has been studied in several experimental and theoretical works [68, 69, 70, 71]. The exciton-exciton interaction can lead to the formation of a molecular state called as biexciton. The energy of a biexciton is given by:

$$E_{BX} = 2E_X - E_b^{BX} \tag{3.11}$$

that E_b^{BX} is the biexciton binding energy and expected to scale with the electron-hole mass ratio and the structure dimensionality. In microcavities with InGaAs quantum well this parameter is about 2.5 meV [68]. We consider the biexciton energy is approximately located around 1483 meV. Due to the biexciton formation, spin dependent nonlinear losses within the polariton population exist. The more the density of one spin population is, the larger would be the damping of the opposite spin population. This nonlinear mechanism has been shown to play an important role in the observation of polariton multistability [14, 57].

Finally, the energy states of the mesa structures indicate a linear polarization splitting along the crystallographic axis of the sample [14]. This is the third significant mechanism in case of a linearly polarized laser excitation. If the linear polarization of the pump laser is not along the eigenaxes of the polarization, depending on its orientation, spin up (↑) or spin down (↓) polaritons are favored. This will result in a small rotation of the polariton spin in the Poincaré sphere, and affects remarkably the multistability regime [57].

Considering all the effects mentioned up to now, polariton dynamics can be modeled qualitatively with the following five equations [57]:

$$i\frac{d\chi_{\uparrow,\downarrow}}{dt} = [-\epsilon_x - i(\gamma_x + \beta|\chi_{\downarrow,\uparrow}|^2) + \alpha_1|\chi_{\uparrow,\downarrow}|^2 + \alpha_2|\chi_{\downarrow,\uparrow}|^2 + g_R n_R]\chi_{\uparrow,\downarrow} + \frac{\Omega_R}{2}\phi_{\uparrow,\downarrow} \tag{3.12}$$

$$i\frac{d\phi_{\uparrow,\downarrow}}{dt} = [-\epsilon_c - i\gamma_c]\phi_{\uparrow,\downarrow} + \frac{\Omega_R}{2}\chi_{\uparrow,\downarrow} + \frac{\epsilon_{lin}}{2}\phi_{\downarrow,\uparrow} + F_{\uparrow,\downarrow}e^{-i\omega_L t} \tag{3.13}$$

$$\frac{dn_R}{dt} = 2\beta|\chi_\uparrow|^2|\chi_\downarrow|^2 - \gamma_R n_R \tag{3.14}$$

where $\chi(\phi)$ represent the exciton (photon) field with energy $\epsilon_{x(c)}$ and linewidth $\gamma_{x(c)}$. β, ϵ_{lin} and Ω_R represent respectively the nonlinear loss through biexciton creation, the strength of the linear polarization splitting and the Rabi splitting. n_R, γ_R and g_R denote the reservoir density, linewidth and the exciton-reservoir interaction constant. Notice that, due to the biexciton formation, the nonlinear loss and energy renormalization of the exciton field are both possible. F and ω_L represent the amplitude and frequency of the excitation field. In the next section, we will discuss about the effect of each of the parameters of Eqs. 3. 12 to 3. 14 on polariton bistability and multistability.

3.5 Experimental results

In order to investigate the polariton bistability and multistability we used the experimental setup shown in Figure 3. 2. We tune the laser power, with high resolution, through a motorized rotating half-wave plate ($\lambda/2$) and a Glan polarizer (GP). The laser polarization is adjusted trough an electro-optic modulator (EOM). The EOM can be seen as a voltage-controlled wave plate, and can modulate the polarization state of the incoming light with a DC or low-frequency electric field. In order to optimize the range of its modulation, the input beam should be vertically polarized. To satisfy this requirement, we used a Glan polarizer followed by a half wave plate. By applying a sinusoidal electric field, with frequency within the EOM bandwidth (500 KHz), we are able to tune laser polarization from left circular to right circular state passing through linear polarization. The detection has two different passes which are separated via a mirror mounted on a flip mount adapter. We measure polariton photoluminescence (as described in section 3. 2) and polariton bistability, through paths number 1 and 2, respectively. In path number 2, the transmitted signal is projected onto the circular polarization basis using a quarter-wave plate ($\lambda/4$), which converts spin-up and spin-down populations into cross-linear polarization. The two linear polarizations are separated using a 50:50 polarized beam splitter. We record simultaneously the two spin populations with two 20 MHz bandwidth photodiodes connected to a 60 MHz bandwidth oscilloscope. Experiments are performed as follows:

(a) We measure the polariton dispersion, and define the position of the lower polariton ground state in addition to the exciton-cavity detuning.

(b) We detune the laser energy above the polariton ground state.

(c) For a fixed laser polarization, we study the behaviour of both polariton spin populations as a function of the laser power (P). The laser polarization is set using the EOM.

(d) For a fixed laser power, we study both polariton spin populations versus laser polarization. This measurement is performed using the usual X-Y method [72]. Using an external function generator, a sinusoidal signal (with frequency around 1KHz) is applied to the electro-optic modulator controller. Accordingly, the laser polarization state should be modulated with the same frequency. By adjusting the amplitude of the sinusoidal signal, we are able to tune the laser polarization from $\sigma-$ to $\sigma+$. After calibrating the laser polarization and applied sinusoidal signal, using three fast photodiodes we measure laser polarization (in excitation) and polariton intensities (in detection) (Fig. 3. 2). Plotting the first quantity as **x** axis and polariton intensities as **y** axis we measure two polariton spin populations as a function of the laser polarization. This experimental technique helps us to find out the experimental error for nonlinear thresholds while they are less affected by low frequency mechanical vibrations.

(e) We present the results based on excitation (ρ_{in}) and emission (ρ_{out}) circular polarization

degree defined as:

$$\rho_{in,out} = \frac{I_{\sigma+} - I_{\sigma-}}{I_{\sigma+} + I_{\sigma-}} \tag{3.15}$$

(f) In order to study the effect of the biexciton formation on polariton dynamics, we repeat the experiments for different exciton-cavity detunings.

3.5.1 The polariton bistability dependence on laser polarization

In order to study the effect of the polarization of the excitation laser, we performed the experiment in a 3 μm mesa with large negative exciton-cavity detuning of δ=-3.9 meV. At this detuning condition, the lower polariton ground state is far from the biexciton reservoir, and consequently we investigate only the effect of polariton-polariton interactions in the spinor polariton bistability (Fig. 3. 6 **e**). The laser energy is blue detuned Δ=0.12 meV with respect to the polariton ground state. Figure 3. 6 shows transmitted polariton intensity in $\sigma+$ (black) and $\sigma-$ (red) polarization winding, which correspond respectively to spin-up and spin-down polariton population inside the microcavity. We tune the laser power between 0.5 mW and 7 mW in forward (solid lines) and backward (dash lines) directions. By increasing the power, the polariton emission increases linearly until reaching the upper threshold. For a circular laser polarization (ρ_{in}=1), we observe the polariton bistability for spin-up polaritons, which is due to the polariton-polariton interactions between copolarized populations (α_1) (Fig. 3. 6 **a**). By tuning slightly the laser polarization to ρ_{in}=0.8, we observe two optical bistability curves (one for $\sigma+$ and one for $\sigma-$) with the same lower and upper thresholds for both spin-up and spin-down polariton populations. As we can observe, for all excitation powers the total polarization of the transmitted light is elliptical when $0 < |\rho_{in}| < 1$. Due to the linear splitting between two linear modes in mesa structure the true eigenstates of the system can be presented in linear basis. By increasing the excitation power the polariton state blue shifts to resonance with the excitation laser, and therefore the polariton population jumps to the upper state. We observe that the polariton intensities on the upper state for two spin populations are different. Although both spin ensembles in the microcavity experience the blue shift, but the majority spin population is larger than the minority one (Fig. 3. 6 **b**). However, for linear polarization (ρ_{in}=0), the two bistability loops overlap and the intensity of both spinor polariton populations on the upper state are the same (Fig. 3. 6 **c**). For ρ_{in}=-0.58, we observe the same behaviour however reversed as in part **b** (Fig. 3. 6 **d**). Notice that in all excitation polarizations the upper and lower power thresholds are the same for the majority and minority spin populations. The results show that the total polariton population undergoes the bistable behaviour.

3.5.2 The effect of polariton-laser detuning and biexciton resonance

In this section, we focus on the effect of the biexciton resonance and laser-polariton ground state (Δ) detuning on the polariton spinor bistability and multistability. In the first part all

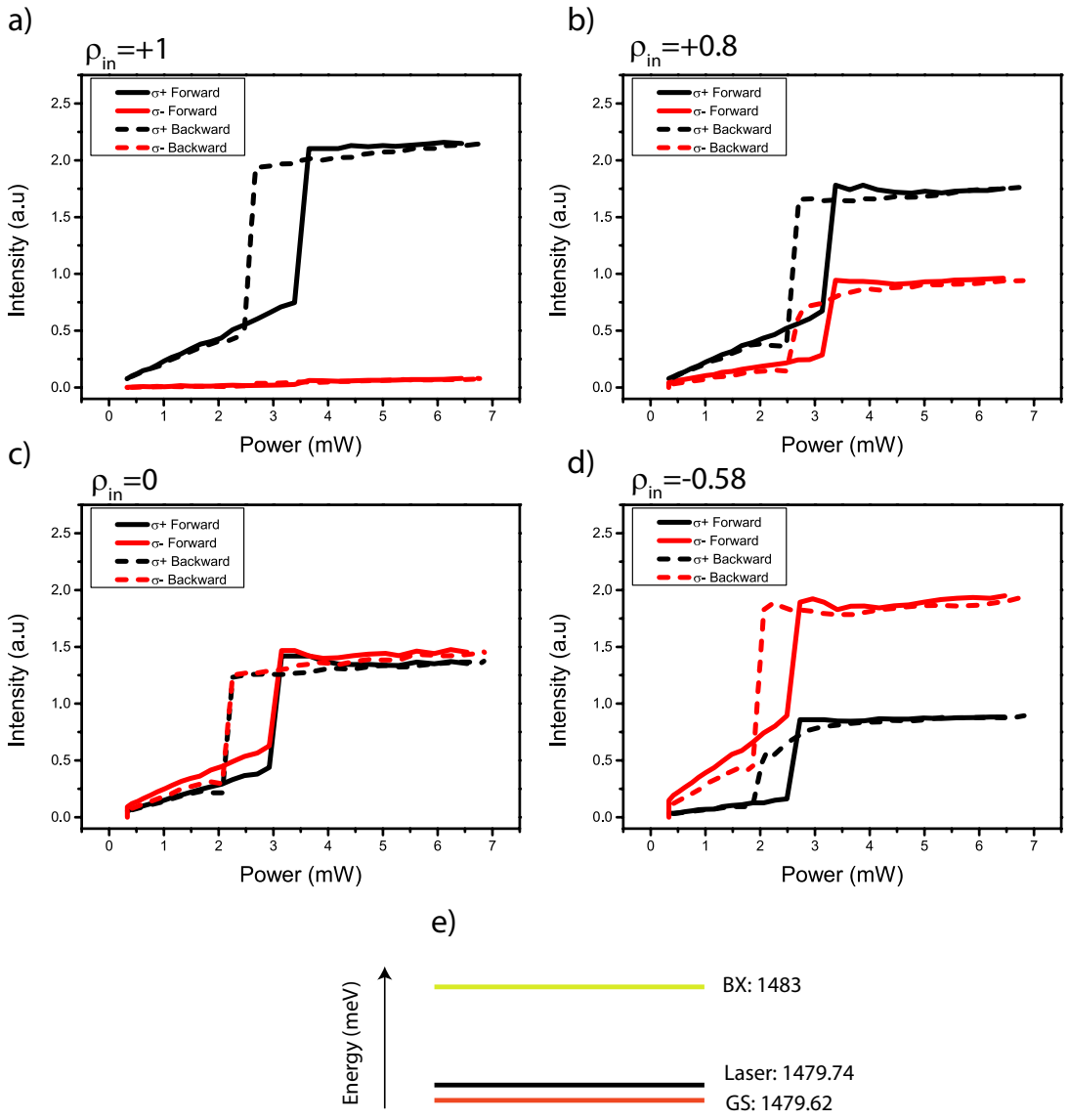

Figure 3.6: **The effect of the laser polarization on optical bistability.** The two polariton spin populations ($\sigma+$, $\sigma-$) versus excitation power in forward direction by increasing laser power (solid line), and backward direction by decreasing laser power (dash line). **a** Under circular polarization (ρ_{in}=1), the conventional bistability for one spin population is observed. **b** At ρ_{in}= 0.8 spin-up polariton population is greater than spin-down polariton population. Both spin populations show a conventional bistability with the same lower and upper thresholds. **c** At linear polarization ρ_{in}= 0, the bistability of the two spin populations overlap. **d** Corresponds to laser polarization ρ_{in}= -0.58. All curves are obtained for exciton-cavity detuning of (δ=-3.9 meV) and a polariton-laser detuning of (Δ=0.12 meV). **e** Energy diagram for mesa ground state (E_{GS}=1479.62 meV), cw laser (E_{cw}=1479.74 meV), and biexciton resonance (E_{BX}=1483 meV).

experiments are performed in a 3 μm mesa with polariton ground state slightly above the biexciton resonance. For this case, we prepared the experiment in three different laser-polariton detunings. Then, for the next part all studies are done in a 3 μm mesa with ground state energy below the biexciton resonance. In this case also the effect of Δ has been investigated.

Polariton bistability above the biexciton resonance

We performed this series of experiments in a 3 μm mesa structure with an exciton-cavity detuning of δ=2.18 meV. To study the effect of laser-polariton detuning, we performed the experiment for three different laser-polariton detunings (Δ). We will discuss one by one the effect of laser power and polarization on an ensemble of exciton-polaritons in microcavity.

Laser-polariton detuning of Δ=0.88 meV For a negative laser polarization of ρ_{in}=-0.32, we observe the normal bistability behaviour for spin-down and spin-up polaritons, noticing that they present the same upper and lower power thresholds however the intensity of the upper state for majority population is much larger than the minority one (Fig. 3. 7 **a**). Figure 3. 7 **b** shows the optical bistability in case of ρ_{in}=-0.20. We observe that in the forward direction, both spin populations jump to a same upper value at the same excitation power. Then, in the backward path, at P=8 mW the minority population falls down to the lower state, and simultaneously the majority population jumps to higher intensity in the upper state. This behaviour has been understood as due to biexciton formation which affects as a source of nonlinear loss[57]. In fact, in the backward direction, for a certain amount of excitation power (here P<8 mW) the minority spin population falls down to the lower branch. As a consequence, the majority spin polaritons undergo less losses and its population is enhanced. As we can see in spinor Gross-Pitaevskii for one spin population the nonlinear loss through biexciton state is proportional to the intensity of the reverse spin population. Figures 3. 7 **c** and **d** show spinor bistabilities for ρ_{in}=-0.15 and -0.06 respectively. We observe that spin-up polaritons are majority populations while the excitation polarization is still more $\sigma-$. This is mainly due to the effect of the linear splitting. The orientation of the excitation linear polarization can effectively modify the ratio between spin-up and spin-down polaritons, and consequently shift the multistability behaviour along the polarization axis [67]. The second important behaviour that one, by comparing these two parts, finds is the width of the optical bistability for minority population. By increasing the laser polarization towards $\sigma+$, the width of the bistable loop for $\sigma-$ reduces. It is worth mentioning that, tuning the laser polarization from circular to linear has no significant influence on the upper thresholds of both spin populations. It is due to the fact that, for linear excitation, the reservoir blueshift can compensate for the attractive interactions between counter circularly polarized polaritons.

In the next step, we fixed the excitation power and using X-Y method we studied two spin populations as a function of the laser polarization ρ_{in} (Fig. 3. 8). There is a direct link between this Figure and Figure 3. 7. For large excitation power (P=10.78 mW) we observe four polariton bistability loops at positive and negative ρ_{in} for the two spin populations (Fig. 3. 8 **a**). We start

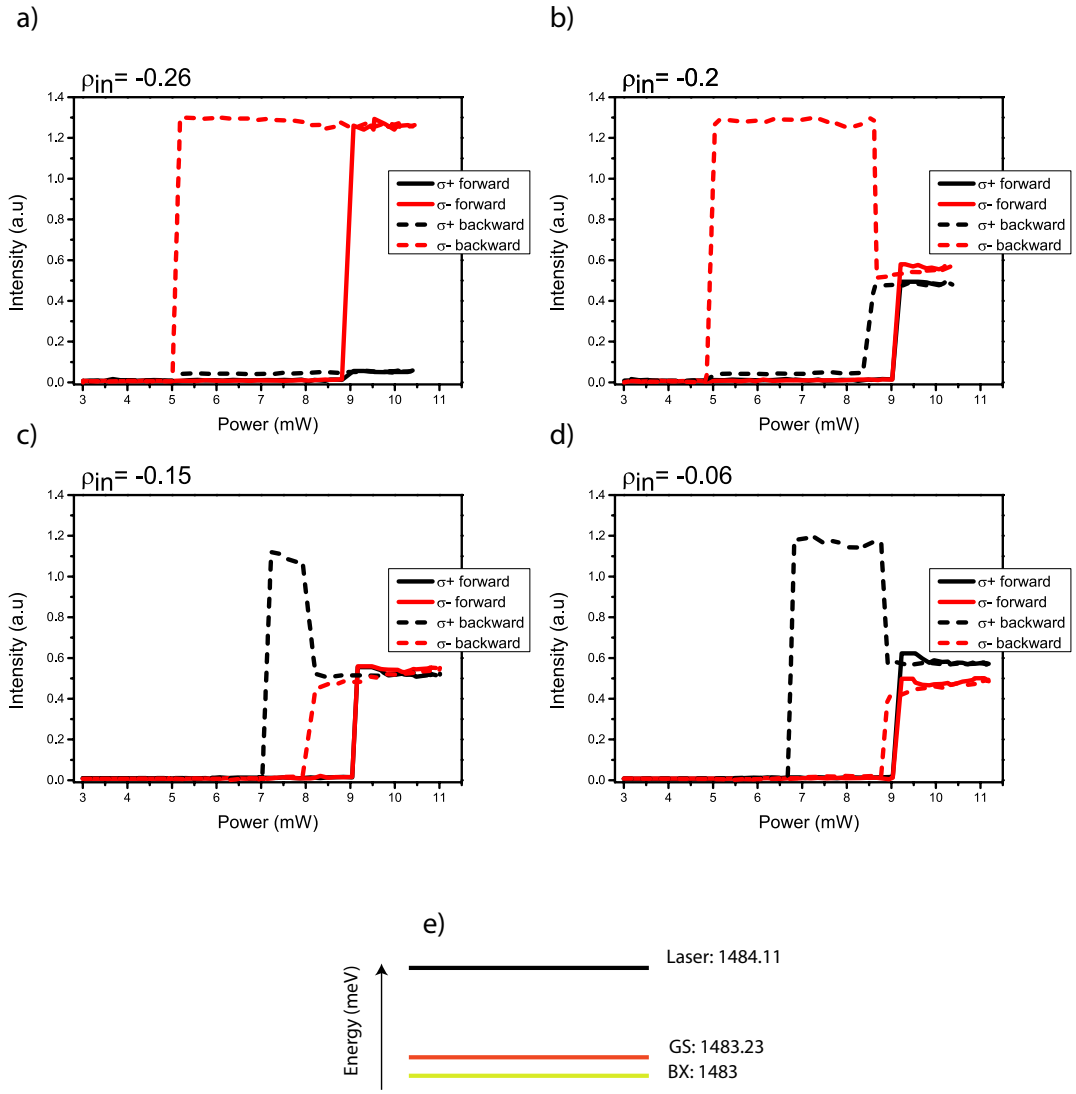

Figure 3.7: **The effect of polarization laser and biexciton resonance on polariton bistability.** Two polariton spin populations ($\sigma+$, $\sigma-$) versus excitation power in forward direction by increasing laser power (solid line), and backward direction by decreasing laser power (dash line). **a** At laser polarization ρ_{in}=-0.32, only spin-down polariton bistability exist and all spin-up polariton populations are fed to exciton reservoir. **b** By increasing ρ_{in} to -0.24, two related polariton hysteresis is observed. In forward path two spin populations jump simultaneously to the middle state. In backward path, the minority polariton ($\sigma+$) falls to the lower state while the majority polariton ($\sigma-$) jumps to the higher intensity in the upper state. **c** For ρ_{in}= -0.15, we observe the same behaviour as part **b** for reverse populations. Due to the linear splitting at negative laser polarization, spin up polaritons are dominant [57]. **d** Correspond to laser polarization ρ_{in}=-0.06. In backward path the width of minority population decreases in addition to the reduction of the lower threshold for the majority bistability. Polariton bistabilities are obtained for exciton-cavity detuning of (δ=2.18 meV) and a polariton-laser detuning of (Δ=0.88 meV). The biexciton formation leads to the middle stable state around linear polarization. **e** Energy diagram for mesa ground state (E_{GS}=1483.23 meV), cw laser (E_{cw}=1484.11 meV), and biexciton resonance (E_{BX}=1483 meV).

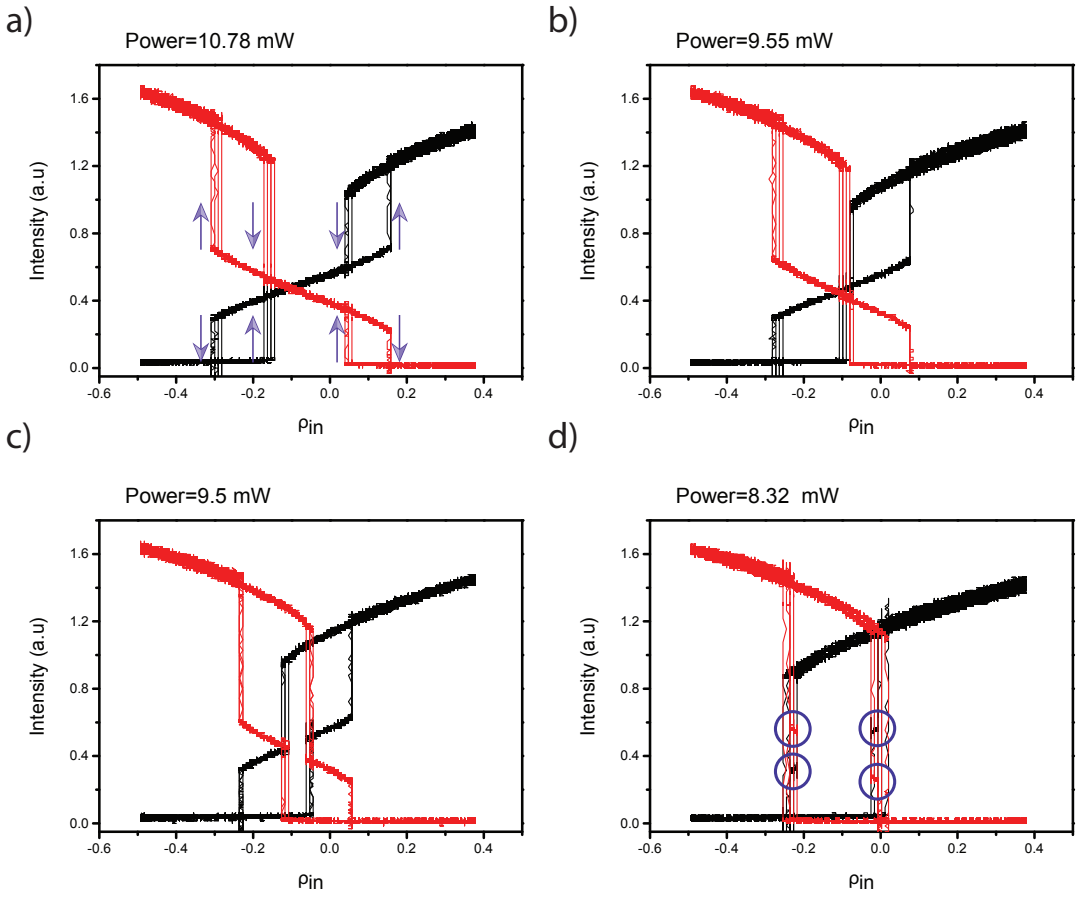

Figure 3.8: **The effect of excitation power on two polariton spin populations.** Two polariton spin populations ($\sigma+$, $\sigma-$), for the same experimental condition as Figure 3. 7, as a function of the laser polarization (ρ_{in}). **a** At high excitation power (P=10.78 mW) polarization hysteresis for spin-up and spin-down polariton populations is observed. On the forward direction, a first jump of spin-up polaritons to the middle branch is concomitant with decreasing the spin-down populations and their corresponding jump to the middle branch. The second nonlinear threshold occurs when spin-up polariton jumps to the upper branch while spin-down polariton falls back to the lower branch. On the backward direction, process is reversed with a hysteresis behavior. **b** Further decrease of laser power 9.55 mW, brings two polarization hysteresis close to each other. **c** to **d** At lower excitation power (9.5 mW and 8.32 mW) two polarization hysteresis merge. The results are measured using the usual X-Y method.

from ρ_{in}=-0.4, where spin-down polaritons are dominant and on the upper state while spin-up polaritons are on the lower state. Around ρ_{in}=-0.3 both spin populations jump to the middle state. By increasing the ρ_{in}, $\sigma+$ ($\sigma-$) intensity increases (decreases) linearly. The crossing point of these linear parts for two spin populations corresponds to the laser polarization for which we expect the majority population change in Figure 3. 7. The second nonlinear jump in the forward path happens around ρ_{in}=+0.2. Under this condition, spin-up polaritons jump in resonance with the excitation laser. In the backward direction, we observe two other nonlinear

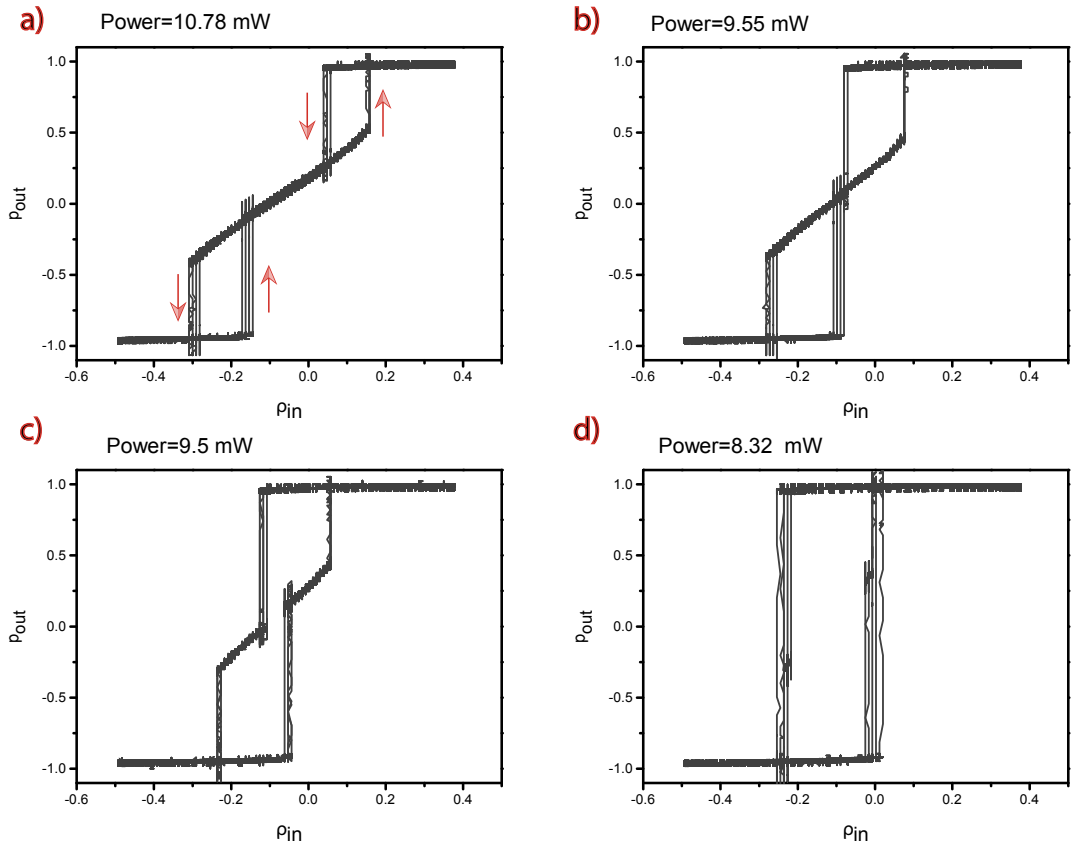

Figure 3.9: **Evidence for spinor interaction and multistability versus excitation power.** Emission polarization degree in circular basis (ρ_{out}) versus laser polarization (ρ_{in}) for the same experimental condition as Figures 3. 7 and 3. 8. **a** to **d** Correspond to laser power P= 10.78, 9.55, 9.5 and 8.32 mW. Three output polarization (ρ_{out}) are allowed in the bistability region .

jumps which lead to the optical bistability in polarization. Decreasing the excitation power brings two optical bistabilities for each polariton population close to each other (Fig. 3. 8 **b**). Upon a further decrease to P= 9.5 mW and 8.32mW, the polarization bistabilities merge together (Fig. 3. 8 **c**, **d**). In part **d** we observe small horizontal lines as middle states which means we are still dealing with three stable states; lower state, middle state and upper state. We observe an uncertainty around each nonlinear jump. This error bar originates from the internal noise in the system. Thanks to the X-Y method we are able to measure each graph in a fraction of a second.

Using equation 3. 15 we compute the polarization of the transmitted light in circular basis for the same experimental results presented in Figure 3. 8. For P=10.78 mW, we observe two polarization bistability separated by a linear part (Fig. 3. 9 **a**). For positive excitation polarization ($\rho_{in} > 0$) the polariton spinor state jumps between spin-up ($\rho_{out} = 1$) and linear ($\rho_{out} = 0$) states. While for negative excitation polarization ($\rho_{in} < 0$) the polariton spinor

state jumps between spin-down ($\rho_{out} = -1$) and linear ($\rho_{out} = 0$) states. By reducing the laser power, the two hysteresis loops move toward each other (Fig. 3. 9 **b**). Finally, for even smaller excitation powers, two polarization bistabilities overlap. In fact, for a fixed excitation polarization around ρ_{in}=-0.1 polariton population can switch between three stable states. This is so called polariton multistability.

Laser-polariton detuning of Δ=0.8 meV In order to investigate the effect of polariton-laser detuning on polariton bistability and multistability, we repeat the same set of experiments carried out for Δ=0.8 meV. It is worth mentioning that considering the exciton energy at 1484.2 meV and considering 1 to 1.2 meV biexciton binding energy, by decreasing Δ, the laser energy would come closer to the biexciton resonance.

In Figure 3. 10, we present the intensity of two polariton spin populations versus excitation power for four different laser polarizations in circular basis. Figure 3. 10 **a** shows the normal bistability for majority and minority spin populations. In case of ρ_{in}=-0.13 we observe a new type of behavior. The upper thresholds of the two spin populations are no more superimposed. Around 8 mW excitation power, the spin-down polariton population jumps into resonance with the laser energy. Due to the significant nonlinear loss, spin-up polaritons fed biexciton state. At the certain power (9 mW) spin-up polariton population reaches the upper threshold. A sudden jump for the spin-up population modifies the nonlinear losses for the spin-down intensity (see spinor GPE). Consequently we observe that the $\sigma-$ intensity decreases to the middle state. In the backward direction we observe the same process, which finally leads to the discriminator regime for $\sigma+$ emission (Fig. 3. 10 **b**). For ρ_{in}=-0.06 and +0.28 we observe the same mechanism as what we discussed in case of Δ=0.88 meV (Fig. 3. 10 **c**, **d**). Notice that we observe no slope for the lower state and a negative slope for the upper state, which are both due to the nonlinear losses through the biexciton formation.

As before, in the next step we study two polariton spin populations as a function of the laser polarization for fixed excitation laser power (Fig. 3. 11). The general behaviour is same as what we present in Figure 3. 8. Although two main differences are observed. First, by reducing the laser-polariton detuning, the width of optical bistability for each spin population decreases. This means that the hysteresis behavior in one spin domain is directly linked to what we observe in intensity domain for an optical bistability. Second, for P=7.79 mW, we observe a new mechanism. The polariton spin populations directly jump between lower to upper state (Fig. 3. 11 **d**).

In Figure 3. 12 we present the polariton polarization versus laser spinor state in a circular basis. We clearly observe that the width of both spin bistabilities decrease (Fig. 3. 12 **a**-**c**). For an excitation power of P=7.79 mW, the polariton spinor state directly switch between two well-defined spinor states: spin-up (+1) to spin-down (-1), and reverse. This is the so called "*spin-trigger*" regime, which is implemented for device applications and fast polariton switches [10].

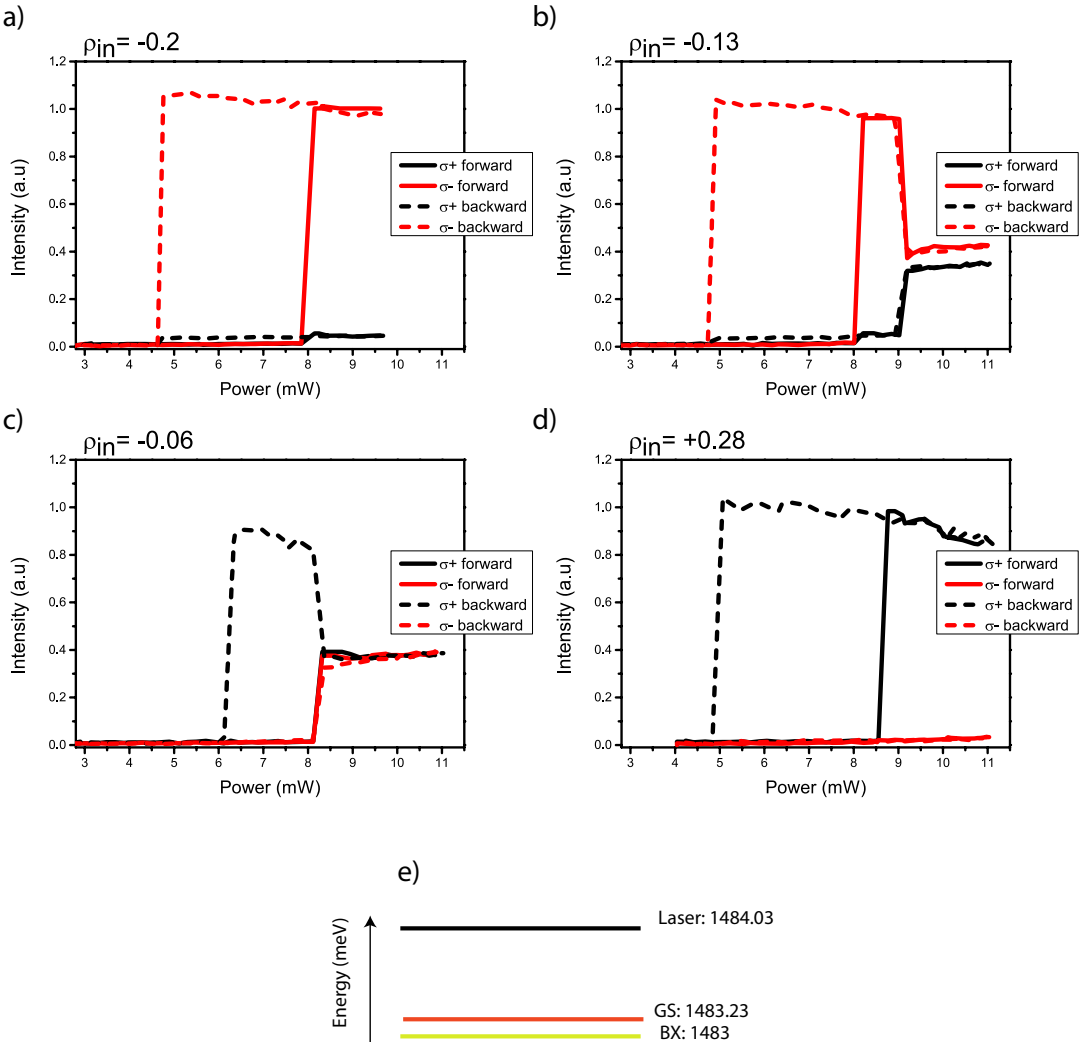

Figure 3.10: **Competition between nonlinear polariton-polariton interaction and nonlinear reservoir.** Two polariton spin intensities ($\sigma+$, $\sigma-$) versus excitation power in forward direction by increasing laser power (solid line), and backward direction by decreasing laser power (dash line). **a** At laser polarization ρ_{in}=-0.2, only spin-down polariton bistability exist and all spin-up polariton populations fed exciton reservoir. **b** For ρ_{in}=-0.13, majority spin population jumps to the upper state for P=8mW, while the minority population is flat on the lower state. By increasing the laser power minority population jumps to the middle state and correspondingly $\sigma-$ falls to the middle state. **c** For almost linear polarization (ρ_{in}=-0.06) two spin populations jump at the same power. The minority bistability width is close to zero. **d** At positive emission polarization degree (ρ_{in}=+0.28), we observe optical bistability for $\sigma+$ polariton with a negative slope on the upper state. Polariton bistabilities are obtained with the same mesa as Figure 3. 7 for exciton-cavity detuning of (δ=2.18 meV) and a polariton-laser detuning of (Δ=0.8 meV). **e** Energy diagram for mesa ground state (E_{GS}=1483.23 meV), cw laser (E_{cw}=1484.03 meV), and biexciton resonance (E_{BX}=1483 meV).

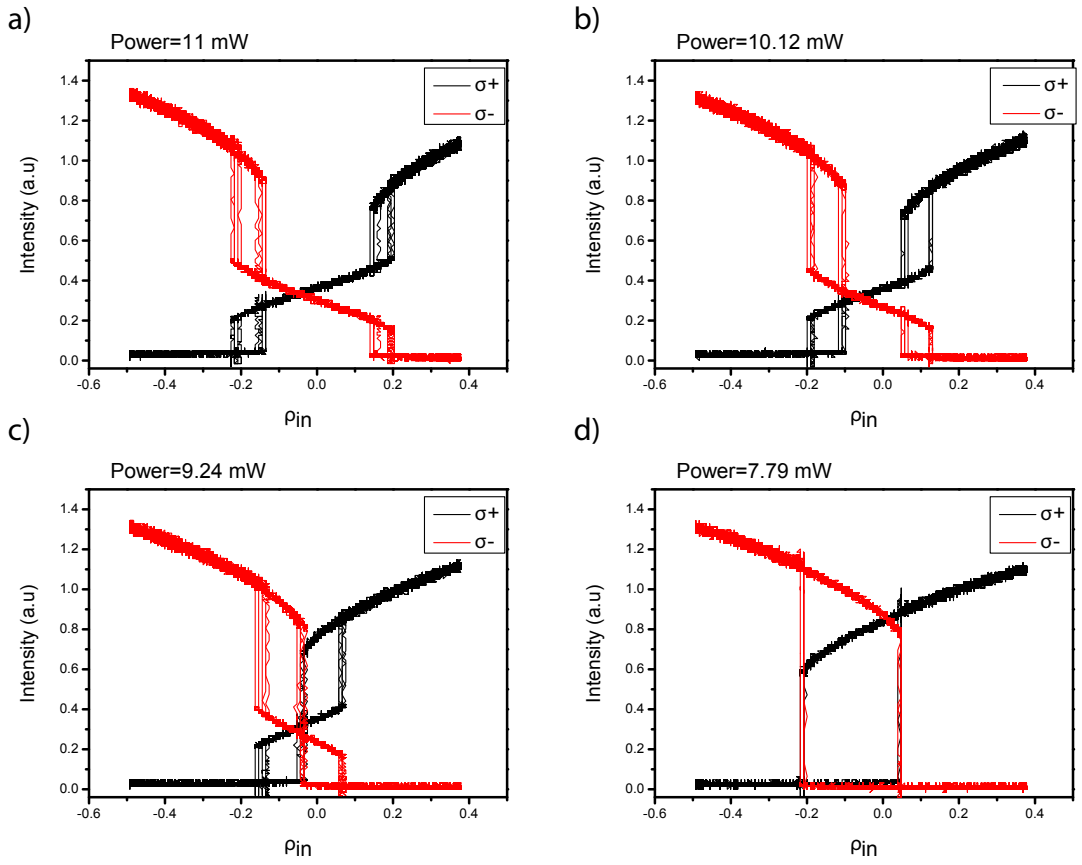

Figure 3.11: **Two polariton spin populations through excitation power dependence.** **a** At high excitation power two spin populations show clear hysteresis in positive and negative laser polarization. **b**, **c** By decreasing P to 10.12 mW (part b) and 9.24 mW (part c), two polarization bistabilities get closer and start to merge. **d** At laser power between the both lower thresholds of two spin populations P=7.79 mW (see Figure 3. 10) the polariton population directly jump from lower to upper states without passing through the middle state. Experimental condition is same as Figure 3. 10.

Laser-polariton detuning of Δ=0.64 meV In a next step, we reduce the laser-polariton detuning to Δ=0.64 meV. In Figure 3. 13 **a**, **b** we observe the same behaviour as what we discussed already in the last part. As mentioned before, polariton ground state is located just above the biexciton resonance. Therefore, by reducing Δ, polariton population in the upper state will be more and more affected by biexciton formation and consequently nonlinear loss. This is the reason that we notice a remarkable negative slope for the polariton majority population on the upper stable state. For ρ_{in}=+0.28, although the absorption mechanism is evident respectively via increasing and decreasing intensities of $\sigma-$ and $\sigma+$ photons, within the experimental excitation power minority spin population is not large enough to cause any nonlinear behaviour (Fig. 3. 13 **c**). For a large circular polarization (ρ_{in}=+0. 8) the slope of the upper state decreases, because the minority polariton population is very small, and we observe a normal bistability

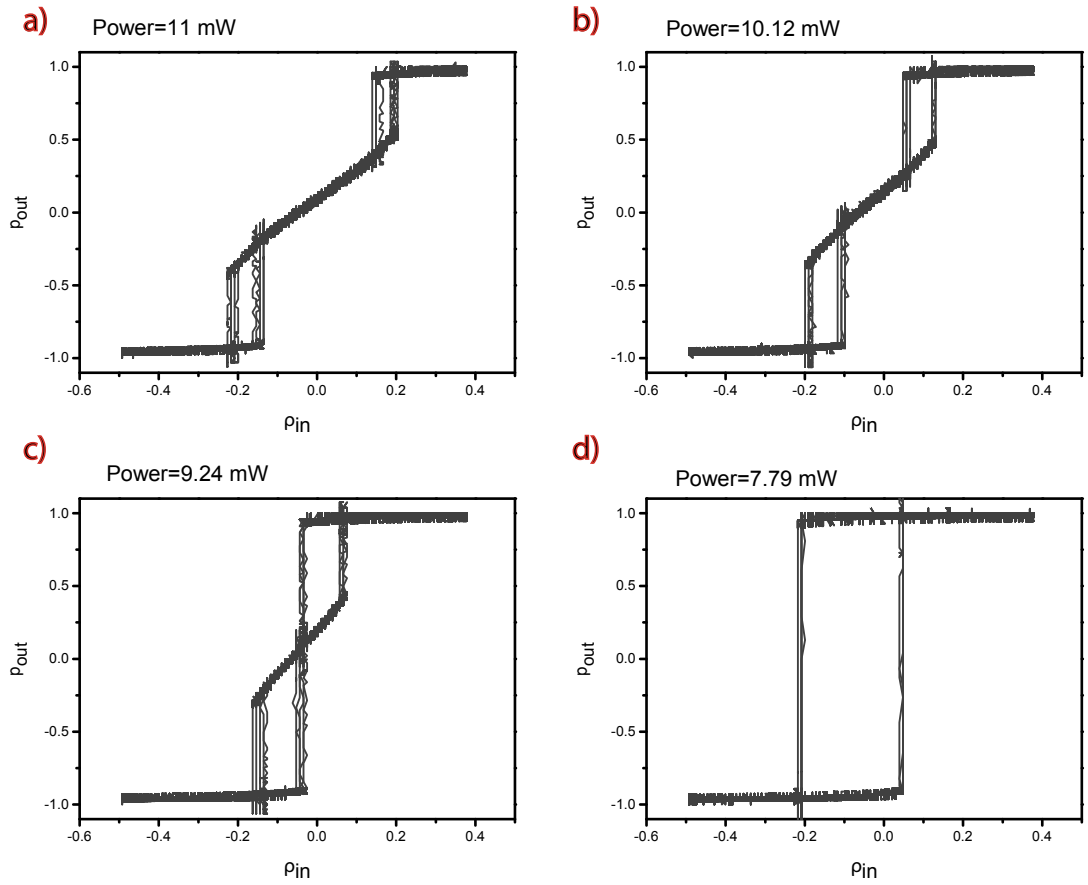

Figure 3.12: **Polariton spin-trigger.** Emission polarization degree in circular basis (ρ_{out}) versus laser polarization (ρ_{in}) for the same experimental condition as Figures 3. 10 and 3. 11. **a** to **c** Correspond to laser power P= 11 mW, 10.12 mW and 9.24 mW, respectively. **d** For small enough laser power (P=7.79 mW), output polarization shows a bistable behavior versus excitation polarization. This is so called spin-trigger regime. Because of linear splitting in the studied mesa, the polarization bistability is not centered on linear state.

behaviour for spin-up polaritons.

Similarly to the last experiments, in the next step we studied polariton bistability as a function of the ρ_{in} (Fig. 3. 14). For high excitation power the bistability regime altered to discriminator regime (3. 14. **a**, **b**). This observation is in the continuity with our explanation for Figure 3.11. Decreasing the excitation power leads to the spin-trigger regime (3. 14. **c**). Further reduction of the laser power causes a spin-trigger regime with larger polarization width. This difference originates from the fact that, due to the nonlinear loss the upper threshold powers for majority population decreases and for minority population increases (Fig. 3. 13 **a** to **d**). In Figure 3. 15 we preset the corresponding graphs in polarization basis.

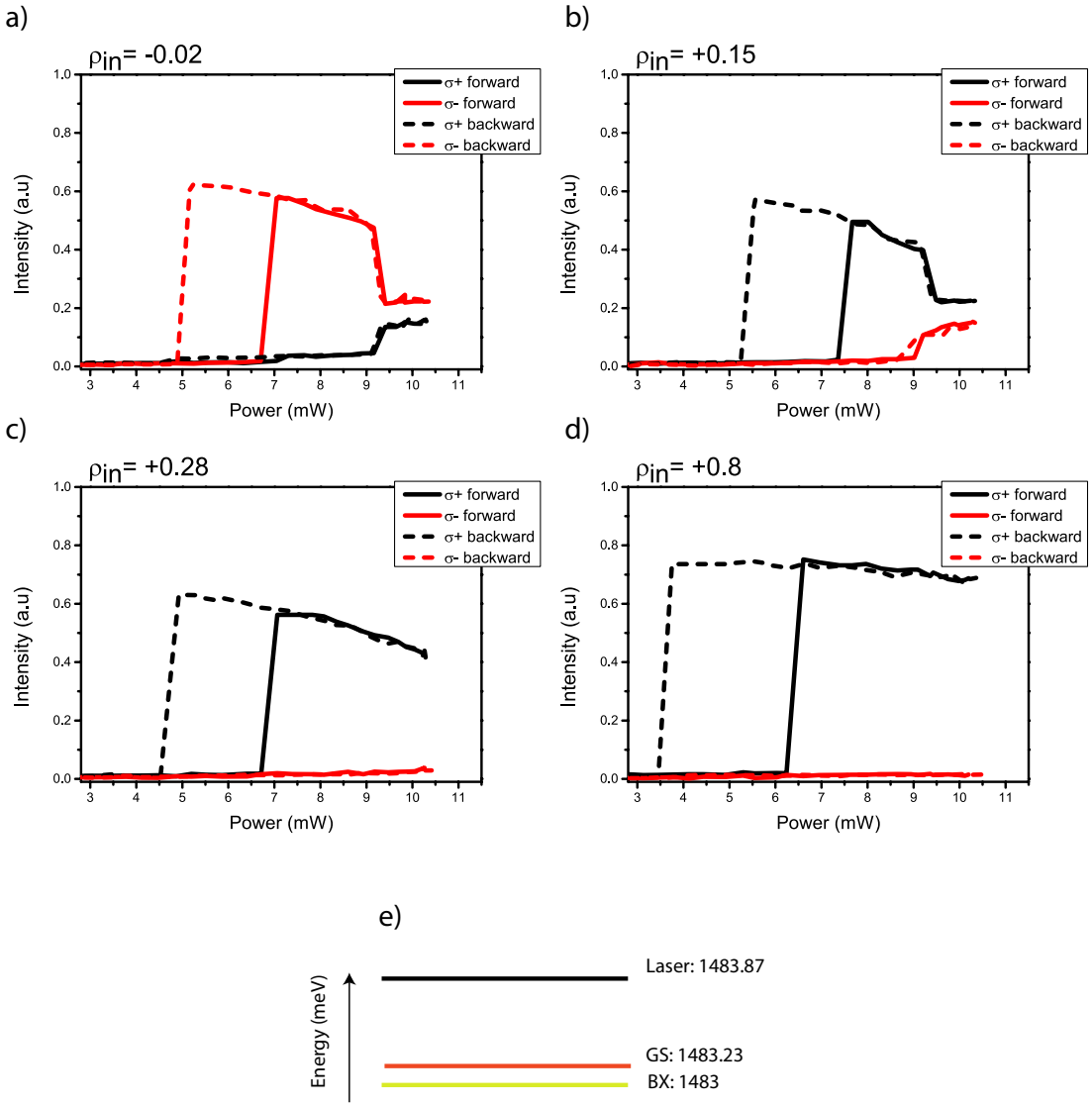

Figure 3.13: **Two spin populations behaviour close to biexciton resonance.** Two polariton spin populations ($\sigma+$, $\sigma-$) versus excitation power in forward direction by increasing laser power (solid line), and backward direction by decreasing laser power (dash line). **a** At slightly negative laser circular polarization degree (ρ_{in}=-0.02), spin down population jumps to the upper state. By increasing further the excitation power, minority population increases while the majorities decrease. Around P=9 mW both populations jump to the middle state. **b** The same behaviour as part a for $\sigma+$ emission as majority polaritons for ρ_{in}=0.15. **c** Polariton bistability for $\sigma+$ emission for ρ_{in}=0.28. The upper state shows the absorption through biexciton state. **d** At a large positive circular polarization (ρ_{in}=+0.8) the absorption effect on the upper state strongly decreases. Polariton bistabilities are obtained with the same mesa as Figures 3. 7 and 3. 10 with exciton-cavity detuning of (δ=2.18 meV) and a polariton-laser detuning of (Δ=0.64 meV). **e** Energy diagram for mesa ground state (E_{GS}=1483.23 meV), cw laser (E_{cw}=1483.87 meV), and biexciton resonance (E_{BX}=1483 meV).

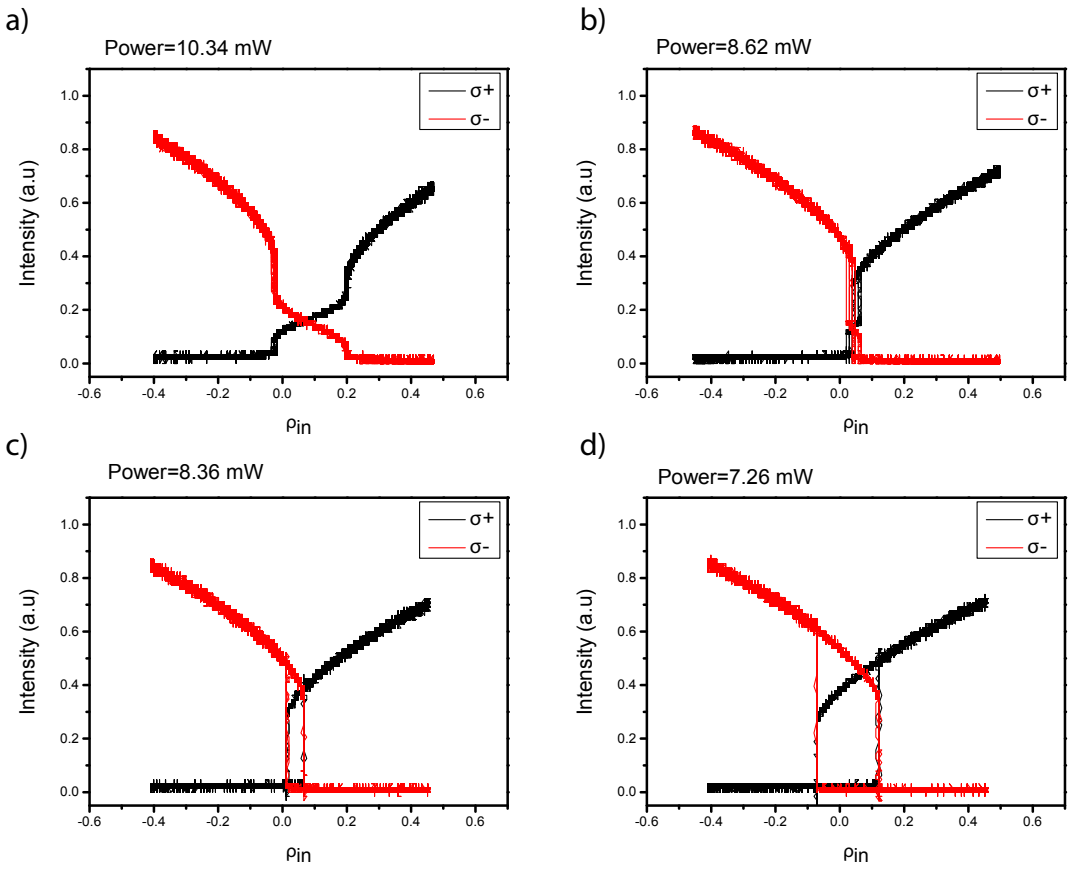

Figure 3.14: **Polariton discriminator regime through laser polarization dependence. a** At high excitation power (P=10.34 mW), two spin populations show discriminator behaviour in positive and negative polarization degree. **b** By reducing the laser power to 8.62 mW two discriminator regimes move toward each other's and merge together. **c** For further decrease of the excitation power (P=8.36 mW) two spin bistabilities between lower and upper states are observed. **d** The width of spinor bistability increases by reducing the excitation power to 7.26 mW. Experimental condition is same as Figure 3. 13.

Polariton bistability below the biexciton resonance

The last complete set of experimental results was performed in a mesa structure with lower polariton ground state energy at 1481.05 meV, i. e. above the biexciton resonance (Fig. 3. 13 **e**). Here we will study the polariton bistability for different laser polarizations inside a 3 μm mesa, with exciton-cavity detuning of δ=-2.24 meV. For this new condition, the laser and the polariton state are located below biexciton energy (1483 meV). We performed the experiment at two different polariton-laser detuning of Δ=0.23 meV and 0.13 meV.

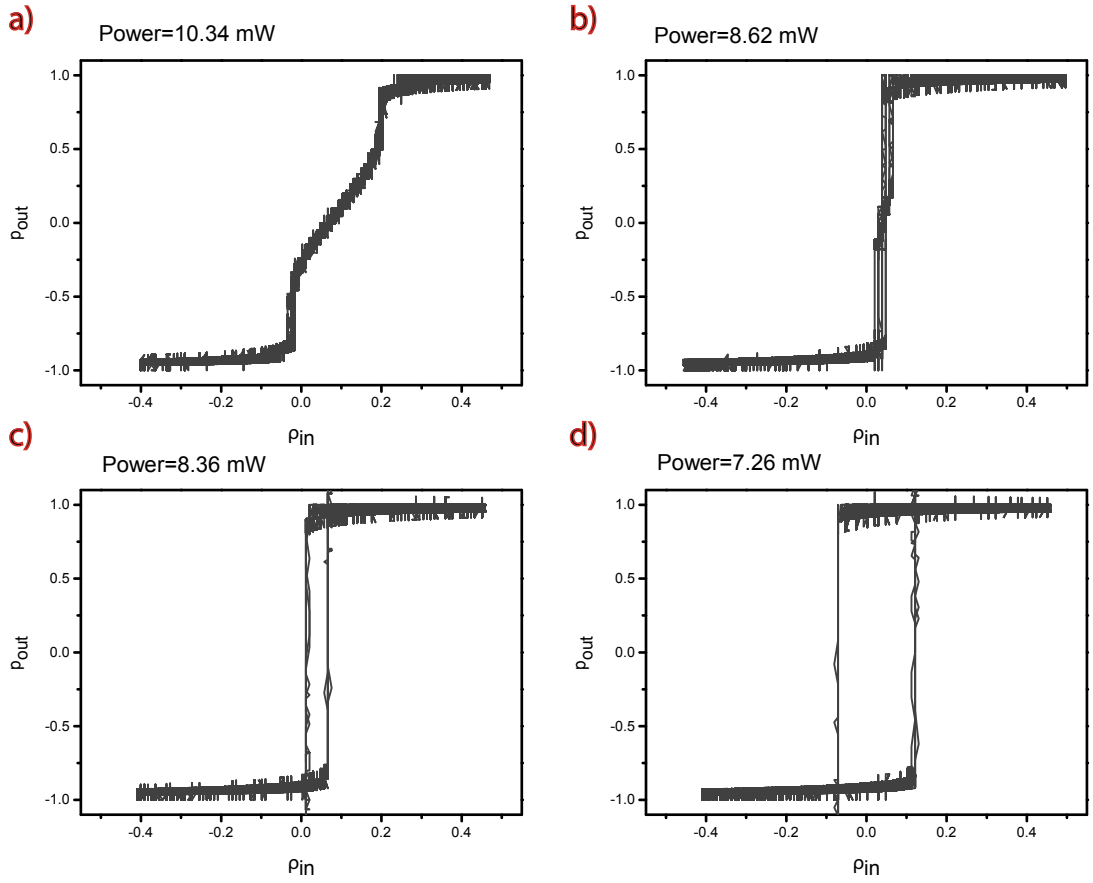

Figure 3.15: **Discriminator and spin-trigger regimes for small enough polariton-laser detuning.** Emission polarization degree in circular basis (ρ_{out}) versus laser polarization (ρ_{in}) for the same experimental condition as Figures 3. 13 and 3. 14. **a**, **b** For larger excitation powers exciton-polariton polarization jump between three polarization state (ρ_{out}=-1, 0, +1) through hysteresis behavior with zero width. **c**, **d** Polariton spin-trigger for smaller excitation power is observed.

Laser-polariton detuning of Δ=0.23 meV

In Figure 3. 16, we presents the polariton intensity in $\sigma+$ (black) and $\sigma-$ polarization basis in forward (solid line) and backward (dash line) directions. For nearly circular polarization degree (ρ_{in}=+0.95), we observe the usual polariton bistability for the majority spin population (Fig. 3. 16 **a**). In case of the elliptic laser polarization, we observe the routine behaviour which has been explained in the previous section. The upper thresholds of two spin populations coincide, while the lower thresholds can be separated (Fig. 3. 16 **b**, **d**). We are then dealing with three stable states due to the biexciton formation within the microcavity. Figure 3. 16 **c** shows a linear increase of both polariton populations without any nonlinear jump. In fact the excitation power needed for nonlinear threshold is larger than 14 mW. This is completely different from what we observed in last regimes. The other important dissimilarity is the

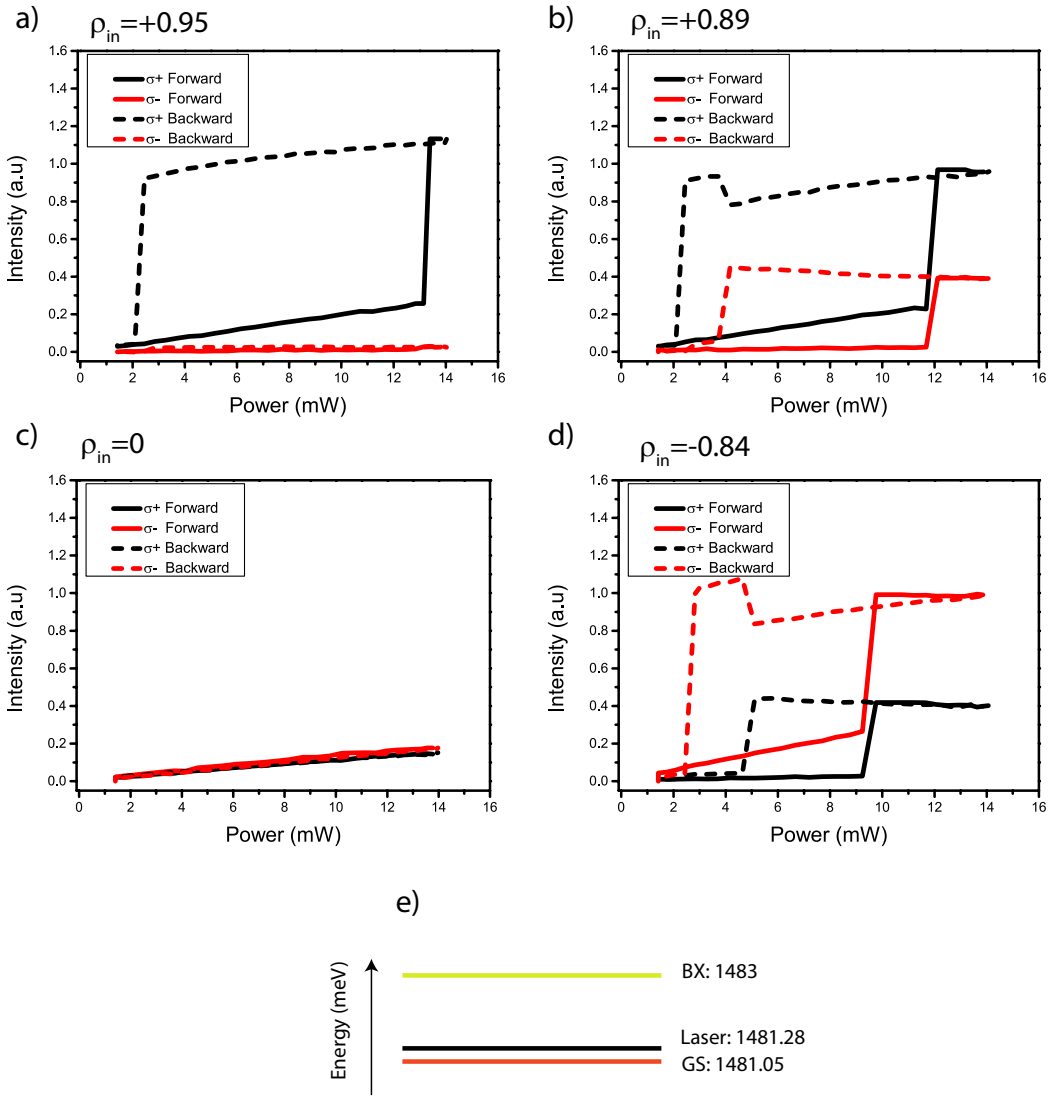

Figure 3.16: **Spinor bistability below biexciton resonance.** Two polariton spin populations ($\sigma+$, $\sigma-$) versus excitation power. **a** Spin-up polariton bistability for ρ_{in}=0.95. **b** For ρ_{in}=0.89, two spin populations jump simultaneously to the middle state in forward direction. In backward path, the minority population jump to the lower state which leads to second nonlinear jump of spin-up polaritons to the upper state. The middle state shows two different gradients for both spin populations. **c** $\sigma+$ and $\sigma-$ polaritons increase linearly without any nonlinear threshold (ρ_{in}=0). **d** For ρ_{in}=-0.84 we observe the same behaviour as part b with reverse majority spin population. Polariton exciton-cavity detuning is δ=-2.24 meV, and cw laser is blue detuned of Δ=0.23 meV respect to the polariton ground state. **e** Energy diagram for mesa ground state (E_{GS}=1481.05 meV), cw laser (E_{cw}=1481.28 meV), and biexciton resonance (E_{BX}=1483 meV).

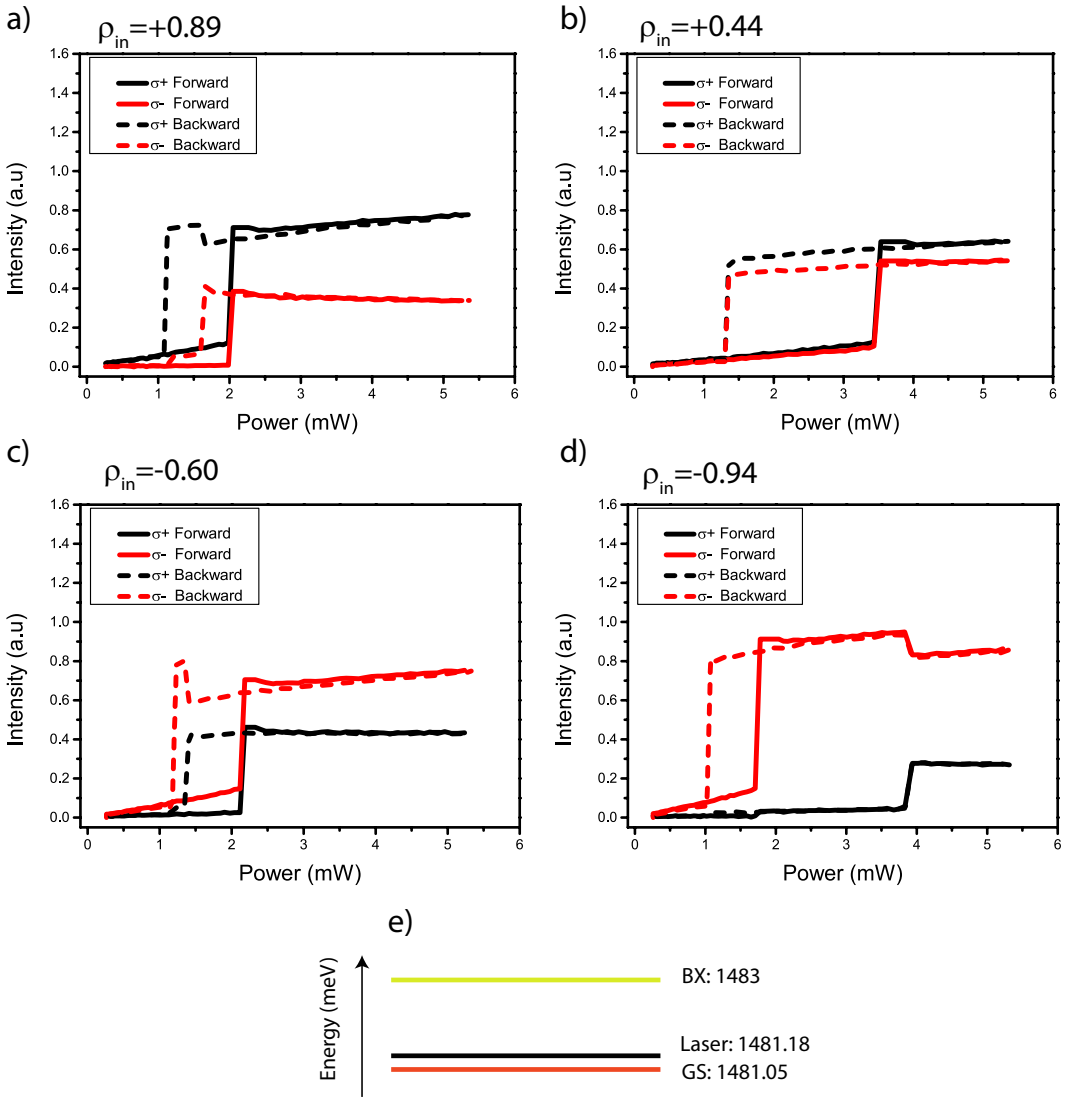

Figure 3.17: **The effect of Δ on spinor bistability below biexciton resonance.** Two polariton spin populations ($\sigma+$, $\sigma-$) versus excitation power for the polariton-laser detuning of Δ=0.13 meV. **a**-**d** polariton spinor bistability for four fixed laser polarization in circular basis ρ_{in}=+0.89, +0.44, -0.6 and -0.94. **e** Energy diagram for mesa ground state (E_{GS}=1481.05 meV), cw laser (E_{cw}=1481.18 meV), and biexciton resonance (E_{BX}=1483 meV).

slope of two spin populations on the upper bistable states. We notice that the gradients of the upper bistable state for majority polariton population are positive while for minority it is zero or even negative (Fig. 3. 16 **b**, **d**). We interpret this observation to a negative value for antiparallel spinor nonlinearity constant α_2. For the case that ground state of the studied mesa was located above the biexciton resonance, we observe the same upper thresholds for both linear and elliptical excitations, which means that nonlinear loss through the biexciton

formation was the dominant mechanism. Here, polariton ground state is located below the biexciton resonance. For linear excitation, upper threshold for both populations are higher than circular excitation. Moreover, the nonlinear jump of majority population between the middle and upper states, in backward direction, is not as large as what has been observed in Figures 3. 7, 3. 10 and 3.13. It seems in this condition nonlinear loss through biexciton formation is no more dominant. These effects can be explained by the positive α_1 and large negative α_2 in studied condition [73, 74].

Laser-polariton detuning of Δ=0.13 meV

Figure 3. 17 shows the polariton bistability for a laser-polariton detuning of Δ=0.13 meV. We observe almost the same behaviour as Figure 3. 10. Although like Figure 3. 16, the majority spin population decreases gradually in the backward direction, which is similar to normal bistability without the effect of nonlinear loss through the biexciton reservoir. Because of the observation of the middle state, we believe that in this experimental condition polariton dynamics are still affected by biexciton creation. The discrepancy between two sets of results originates from different position of laser and lower polariton ground state energy respect to the biexciton resonance.

3.5.3 Conclusion

In conclusion, in the present chapter we studied the effect of the polarization of the driving laser on the nonlinear mechanisms in an ensemble of exciton-polariton confined in a microcavity and consequently on polariton bistability and multistability. We demonstrate the multistability and the spin-trigger regime. We showed that, in the sample that we have studied, biexciton creation can be considered as the main mechanism for polariton tristability. The effect of the laser polariton detuning on the spinor bistability has been studied in detail. We validate the fact that, depending on the excitation power and polarization different types of spinor bistabilities are recognizable. We show that the energy of polariton ground state with respect to the biexciton energy can effectively modify the characteristic of the spinor bistability. In fact, the intensity of each polariton population, and also the nonlinear threshold for both populations are strongly affected by β, α_1 and α_2. Depending on the experimental condition, one of these parameters can dominate the others and reveal a new type of spinor bistability regime.

4 The effect of noise on polariton bistability

4.1 Introduction

The presence of noise-random disturbances of signal-typically interferes with systems reliability for information processing. Moreover, since it is not possible to isolate a system from its environment, noise is fundamentally unavoidable. For all systems the thermal reservoir plays an important role in their dynamics. Even at zero temperature, when classical noise disappears, zero-temperature reservoirs which are sources of quantum noise are present[23].

Optical bistability is a model system for investigating nonequilibrium fluctuation phenomena with coexisting stable states. A large variety of bistabilities can be described effectively by a single dynamical equation: a harmonic oscillator with a quartic double-well potential force. Brownian movement in a double-well potential is a classic model of the statistical physics. In 1940, Kramers developed a theory on the thermally activated escape rates from one potential well to the other [21]. Afterwards, the experimental visualization of particle escape time has presented in several bistable systems. Among them we can mention Brownian particle in a dual optical trap [75], passive all-optical bistable system affected by additive and multiplicative noise [76], and bistability in three dimensional optical traps [77].

In this chapter, using time resolved photon statistics we study fluctuation-induced transitions of exciton-polaritons in an optical bistability. In a general view, the origin of these fluctuations can be internal noise, as exciton reservoir, or external noise like intensity or phase fluctuations of external driving laser [78]. Practically we study the effect of an external Gaussian noise, imprinted on the excitation laser intensity, on the polariton dynamics. We evidence that due to the laser noise the polariton emission intensity fluctuates between lower and upper states of the polariton bistability. We determine the lower and upper state residence times as a function of the noise strength and the excitation power. Furthermore, we study the Kramers time as a function of the noise in the excitation power. The investigation is pursued by studying the effect of noise on the quality of the bistable polariton emission system. In fact, in the presence of fluctuations the bistability width can decrease drastically [78]. In order to have insight in the actual bistable behaviour of the system, we need to investigate the output intensity signal

in time. This reveals the genuine instability of the system, which should be considered in the realization of devices. We show that the presence of noise causes decreasing of the hysteresis cycle in a residence time scale. Moreover, the results reveal the noise strength threshold in which the bistability is seen as a discriminator. Numerical simulations using Gross-Pitaevskii equation driven by a stochastic excitation reproduce the experimental results.

4.2 Noise-induced transitions in bistability

4.2.1 Standard example

In order to investigate the polariton dynamics affected by external Gaussian noise, we start with the theoretical approach used by Dykman et al., in which a nonlinear oscillator is subjected to the combined effect of a driving force ($Fcos(\omega_F t)$), with amplitude F and frequency ω_F, and a random force ($\xi(t)$) [79]. Statistical differential equation of motion of the nonlinear oscillator is described as:

$$\ddot{q} + 2\gamma\dot{q} + \omega_0^2 q + \alpha q^3 = F\cos(\omega_F t) + \xi(t) \tag{4.1}$$

where γ, α and ω_0 are oscillator damping, nonlinear constant and oscillator frequency, respectively. The random force, ξ(t), is a Gaussian variable with characteristic noise intensity D:

$$< \xi(t)\xi(t') >= D\delta(t - t') \tag{4.2}$$

The oscillator is assumed underdamped:

$$\gamma, |\Delta| \ll \omega_F \tag{4.3}$$

where $\Delta = \omega_F - \omega_0$ is the detuning between the driving field and the oscillator frequency. Changing from the fast oscillating function (q, $\dot{q}$) to slow complex functions "a" and "$a^\dagger$", the second-order equation will reduce to a complex equation of first order [79]:

$$\frac{da}{d\tau} = L + \nu\widetilde{\xi}(\tau) \tag{4.4}$$

$$L = -\nu a + i a(|a|^2 - 1) - i\beta^{0.5} \tag{4.5}$$

$$\tau = |\Delta| t \tag{4.6}$$

$$\nu = \frac{\gamma}{\Delta} \tag{4.7}$$

$$\beta = \frac{3\alpha F^2}{32\omega_F^3 \Delta^3} \tag{4.8}$$

where ν and β are respectively the reduced damping coefficient and the dimensionless field intensity. The dynamics of this system depends on the values of the relative field intensity β, damping parameter ν and noise intensity D [80].

In Figure 4. 1 **a** the bistable region of a nonlinear oscillator with two stable states "1" and "2" is shown. The upper and lower states are separated by the middle unstable state called as separatrice [78]. This system can be considered as a double-well potential as typically used for Brownian motion of particles (Figure 4. 1 **b**, **c**). The potential is bistable with minima located at '1' and '2'. For different excitation amplitudes (F_1<F_2<F_3), the potential shape and consequently the stable state are modified. We recall that for a thermal equilibrium system, the transition probability can be given by the Arrhenius law $W \propto exp(-E_a/T)$, where E_a is the activation energy of the transition and T denotes the temperature of the system. For a potential with the Brownian motion, the activation energy E_a is represented by the depth of the potential barrier (ΔV) from which the particle scape. The characteristic activation energy for the transition '1' to '2' and '2' to '1' are different. As a matter of fact, the transition probabilities W_{12} and W_{21} differ for diverse external amplitudes. The probability of noise-induced transitions over the potential barrier can be written in the form [81, 80]:

$$W_{12,21} = const. \exp(-\frac{Q_{1,2}}{D}) \tag{4.9}$$

where Q_1 and Q_2 are the activation energy of the transition W_{12} and W_{21}, respectively. For $\nu^2 \ll \beta \ll 1$ it has been derived that these two parameters can be estimated as following expressions [80]:

$$Q_1 = \frac{2\sqrt{\beta}}{\nu} \tag{4.10}$$

$$Q_2 = \frac{0.5 - 0.98\beta^{\frac{1}{4}}}{\nu} \tag{4.11}$$

As we can see, when increasing the noise intensity (D), the transition rate in both directions increases exponentially. Furthermore, for larger excitation amplitudes (F), the probability of transition towards state '2' (W_{12}) increases while the reverse transition probability (W_{21}) decreases. All other parameters like oscillator damping and frequency, nonlinearity, energy detuning and laser frequency effectively modify the transition probability between two stable

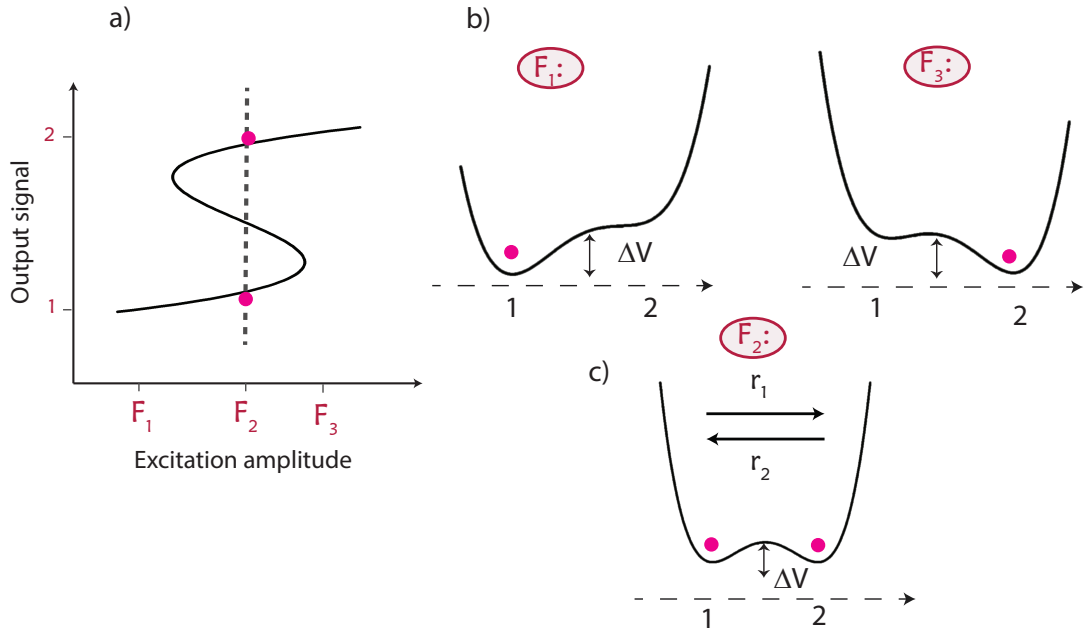

Figure 4.1: **Double-well potential and bistability. a** Bistability of a nonlinear oscillator with two stable states '1', '2'. For a fixed value of excitation amplitude there are two possibilities for the output signal. **b, c** Classical particle in a double well potential with potential barrier of ΔV. **b** For different external amplitudes (F_1, F_2), the potential shape and the activation energy for transition is modified. **c** In case of the symmetric potential (F_2), noise induced transition rate between the two wells is equal to Kramers rate r_k=r_1=r_2.

states.

It is worth mentioning that if ξ (t)=0 we have a deterministic equation and the system jumps from one state to the other state with the driving force F. For F_2 value the system is stable in one state where V′(x)=0 either '1' or '2' . If we switch on the random force and if the noise intensity (D) is smaller than potential barrier (ΔV), the system can switch from one stable state to the other stable state with the same probability given by the Kramers rate.

4.2.2 Polariton bistability and external Gaussian noise

Let us consider exciton-polaritons in a bistable system. If the polariton system is free of noise, at a given excitation power, polariton population would rest either in the lower or upper stable branches of the bistability. Otherwise, in the presence of some noise and when the input power is within the bistable cycle, because of the coupling with fluctuations, polaritons can escape from one of the stable states to the other. The time scale in which these noise-assisted transitions occur is defined as the "*residence time*", which is the average time over which the system stays in one state before escaping to the other. For a small range of excitation powers

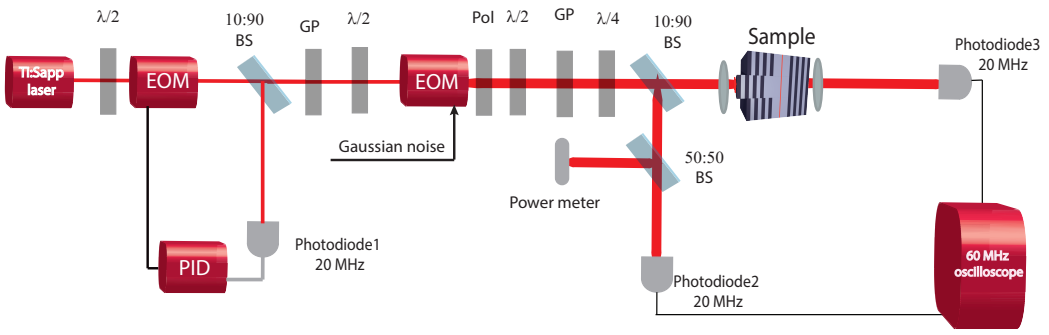

Figure 4.2: **Experimental setup** Microcavity sample is excited using the cw Ti: Sapphire laser. The laser noise intensity is reduced to 0.02 percent through the first electro-optic modulator and the feedback loop (photodiode 1 and PID). Second EOM imprints 500 kHz Gaussian noise on the laser intensity. Excitation and transmission light are detected with two fast photodiodes. BS, Pol, GP, $\lambda/2$, $\lambda/4$ represent beam splitter, polarizer, Glan polarizer, half-wave plate and quarter-wave plate, respectively.

close to the middle of the optical bistability, the effective double-well potential should be symmetric (Fig. 4. 1 **c**), and consequently the residence time in the lower and upper states should be comparable. This residence time is called as Kramers time. To understand the polariton dynamics with intensity noise, it is very important to reconsider how the bistable polariton system behaves. Non-linearity and optical feedback constitute the basis of optical bistability. Note that, in the bistable polariton system, the intensity of the polariton emission is governed by the polariton lifetime and the polariton-polariton interaction, which strongly depend on the polariton population. In addition the emission intensity depends on the spectral overlap between the laser field and the polariton state. However, by introducing fluctuations on the laser power, we directly induce fluctuations on the polariton population, which in turn, due to the nonlinearity of the system, bring fluctuations on the polariton energy. Therefore, the presence of noise in the system disturbs the competition between feedback and loss mechanisms. Depending on the excitation power and noise intensity we can measure a large variety of photon statistics and consequently residence times.

4.3 Experimental setup

The experiment is performed at 4K with a mesa structure of 3 μm diameter and exciton-cavity detuning of δ=-1.15 meV. The linewidth of the zero-dimensional polariton ground state is of 100 μeV. This allows for working with the single ground state level well isolated from intrinsic noise fluctuations. The experimental set-up is shown in Figure 4. 2. We use a linearly polarized single mode cw Ti:Sapphire laser with 10 MHz linewidth and 2 percent noise intensity standard deviation. In order to stabilize its intensity fluctuations, we separate 10 percent of the laser light. Then, using the first photodiode in addition to a proportional-integral-derivative (PID) controller and an electro-optic modulator (EOM) in a feedback loop, we stabilize the noise

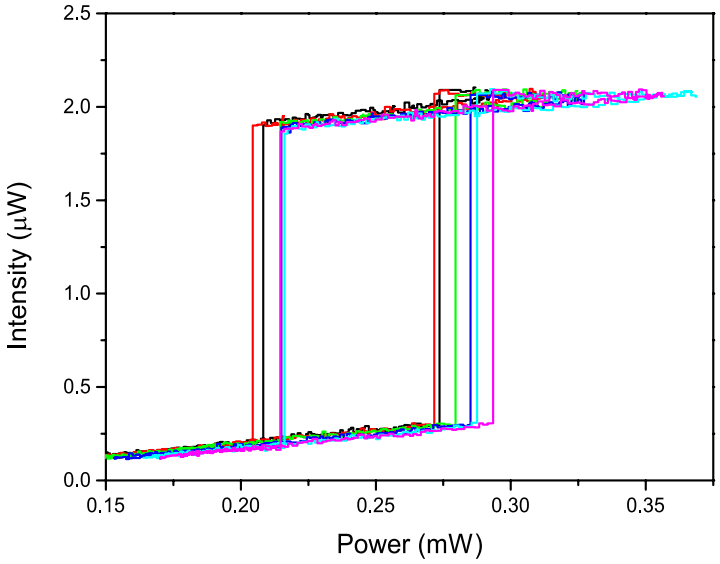

Figure 4.3: **Zero-dimensional polariton bistability.** 0D polariton bistability for the minimum laser noise intensity. Due to the mechanical noise or even internal noise (such as temperature fluctuations) we measure an uncertainty for the bistability width ΔB=68 ± 8 μW. The experiment is performed in a 3 μm diameter mesa with the exciton-cavity detuning of δ=-1.15 meV and the laser-polariton ground state detuning of Δ=0.24 meV.

intensity standard deviation to 0.02 percent. As mentioned in the third chapter, by means of a half-wave plate, the input polarization of EOM is prepared along the vertical axis. The laser beam passes through a second EOM, which imprints 500 KHz bandwidth Gaussian noise with a controllable intensity standard deviation on the DC laser power. We quantify the noise strength as normalized noise standard deviation compared to the bistability width ΔB measured without imprinting any noise on the laser. The laser power is tuned, with a resolution of 1 μW, through a motorized rotating half-wave plate and a Glan polarizer. The sample is excited at normal incidence, the laser being circularly polarized through a quarter wave plate, to ensure polariton repulsive interactions and therefore polariton energy blueshift [74]. In order to control and measure the excitation power using a non-polarizing beam splitter 10 percent of the light is separated. Half of it goes to the power meter and the other half is collected by the second photodiode. The laser has a spot diameter of 20 μm and is detuned by Δ=0.24 meV above the polariton ground state energy, consequently within the excitation bistability condition $\Delta > \sqrt{3}\gamma_p$ [13]. The input power variation in the forward and backward directions builds the bistability curve in the output power. The experiments are performed by varying the input power and measuring the transmission intensity with the third photodiode. These conditions give a polariton bistability width ΔB=68 ± 8 μW (Fig. 4. 3). The error bar comes from any kind of intrinsic noise in the polariton system or even low frequency mechanical or thermal vibration during the experiment .The excitation and transmitted light are detected with 20 MHz bandwidth photodiodes. The time-resolved measurements are

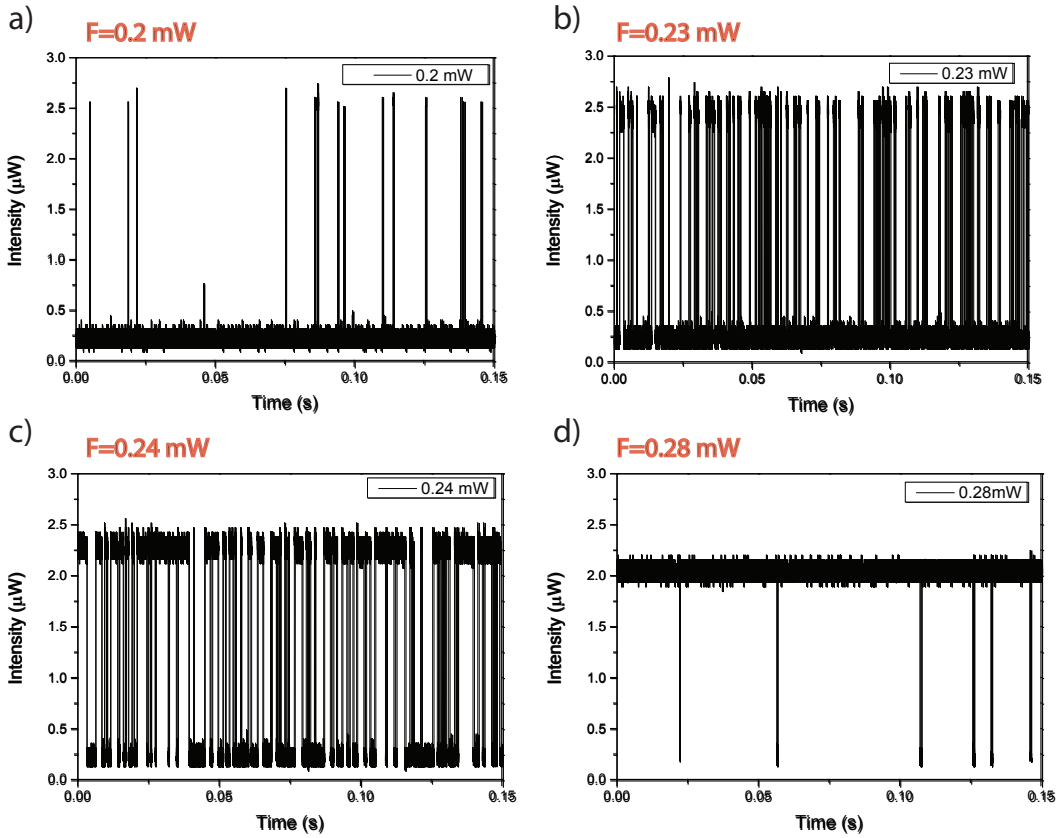

Figure 4.4: **A single realization of polariton transitions between two stable states. a, b** For laser power below the middle of bistability (F=0.2, 0.23 mW) the lower state is the more stable state. **c** For the laser power around the middle of bistability (F=0.24 mW) polariton transitions between the two stable states occurs with the same probability. **d** For the laser power around the upper threshold (F=0.28 mW), the upper branch is the more stable state and we observe some random jumps to the lower state. The applied noise strength is of D=0.30 ΔB.

performed with a 60 MHz bandwidth oscilloscope.

4.4 Experimental results

4.4.1 Residence time and Kramers time

In order to investigate noise-induced polariton transitions we perform time-resolved analysis of the polariton emission. We measure, at different input powers (F), the time behaviour of the polariton emission intensity for a wide range of noise power. In Figure 4. 4 **a**-**d** we display the polariton emission intensity time streams recorded for different input laser powers and with applied noise strength of D=0.30 ΔB. At F=0.2 mW, which is located near the lower threshold, we notice that the lower state is the stable state (Fig. 4. 4 **a**). Then, when increasing the laser power, the probability of transition from the lower to the upper state increases (Fig. 4. 4 **b**). At

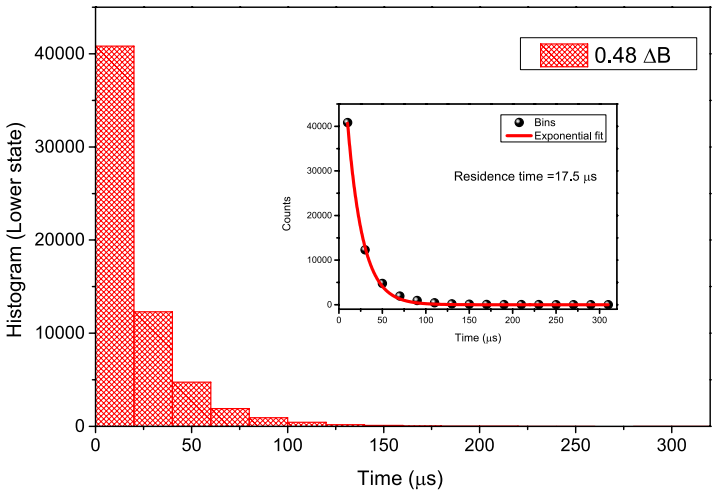

Figure 4.5: **Residence time probability distribution.** Histogram of the lower state residence time distribution for the noise intensity D=0.48 ΔB at F=0.25 mW. Inset: Histogram of the distribution showing the exponential decay of 17.5 μs.

F=0.24 mW we observe almost the same probability for transitions from one bistability branch to the other one (Fig. 4. 4 **c**). Finally at F=0.28 mW which is close to the upper threshold, polaritons tend to become stable on the upper state (Fig. 4. 4 **d**). All the time streams are acquired for a 2s time window with experimental temporal resolution of 2 μs.

To quantify the effect of the external power (F) and noise intensity (D) in a precise way, we study the probability distribution of the residence times, i. e. , of the time intervals spent in the lower (upper) branch before transition to the upper (lower) branch. We report in Figure 4. 5 the histogram of the lower state residence time distribution for the input power of F=0.25 mW and D=0.48 ΔB applied noise. As expected for a two-state bistable system, the histogram clearly evidences an exponential form with the value of the residence time as a characteristic time [75]. We fit the data with the exponential function:

$$f(x) = A\exp(\frac{-x}{k}) \tag{4.12}$$

which k is the characteristic time, here found to be 17.5 μs (inset of Fig. 4. 5).

In Figure 4. 6 **a**, **b**, we plot respectively, for different input laser powers, the residence time in the lower and upper branch as a function of the noise strength. We observe that the residence time decreases with increasing noise strength. For low noise amplitude, the residence time is large because it is difficult to get the system over the bistability threshold. For larger noise intensity, it is easier for the noise intensity to exceed the bistability thresholds. Thus, the transition between the two states takes place fast and shows a weak dependence on the fluctuations. It is worth mentioning that the minimum value measured for both residence times are determined by the noise correlation time (2μs). In the lower branch the residence

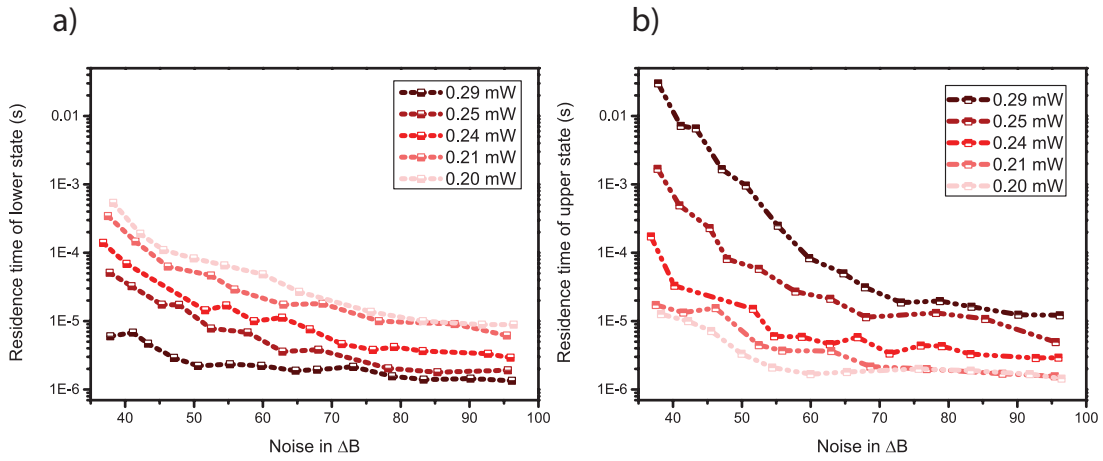

Figure 4.6: **Polariton residence time for lower and upper states.** **a** Residence time of the lower state for five different laser powers : F=0.20, 0.21, 0.24, 0.25 and 0.29 mW. The noise intensity is increased from D=0.37 ΔB to 0.96 ΔB. **b** Residence time of the upper state for the same amounts of laser powers and noise. At F=0.24 mW residence times of the lower and the upper states are nearly the same.

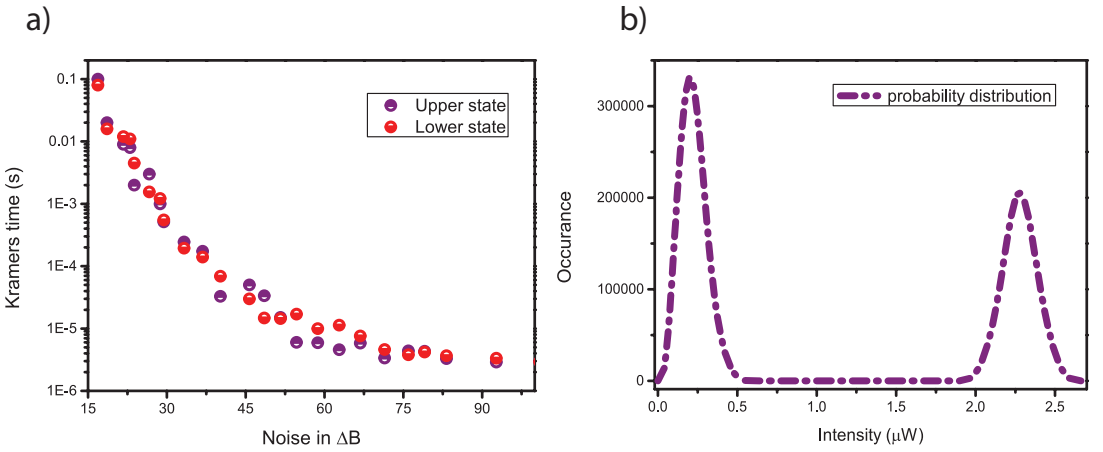

Figure 4.7: **Polariton Kramers time and double-peaked probability distribution.** **a** Polariton residence time for the lower (pink) and the upper (purple) states versus laser noise at the middle of polariton bistability (F=0.245 mW). At this position, the two residence times are nearly equal, which are then labelled as the Kramers time. The noise intensity is tuned from D=0.16 ΔB to 0.93 ΔB. When increasing the noise intensity, the Kramers time is observed to decrease. The minimum measured Kramers time is limited to the experimental bandwidth. **b** Double-peaked probability distribution of polariton time stream for the laser power and the noise intensity of F=0.245 mW and D=0.30 ΔB, respectively. The area of the left-hand and the right-hand peaks is 0.56 and 0.44 of the total area, respectively. Polaritons have equivalent probability to be in both stable states for excitation power around the middle of the polariton bistability.

time decreases as the power is increased toward the upper threshold, and the reverse occurs in the upper branch. Note that at lower noise power, for excitation powers close to nonlinear thresholds, the residence time of the upper state is larger than the lower state residence time. We attribute this discrepancy to large uncertainty around bistability thresholds due to the fluctuations. Notice that for F=0.24 mW the residence time for the lower and the upper branches coincide. This is the so called Kramers time. It has to be pointed out that this power nearly corresponds to the middle of the hysteresis loop, when measured without external noise. To be more precise, following Figure 4. 3, the middle of the polariton bistability is at 0.25 ± 0.008 mW. This result shows that, at this value of the excitation power, the polaritons have the same probability to be in the lower state than in the upper bistable state.

We display in Figure 4. 7 **a** the Kramers time in the upper and the lower branch for a large variation of noise strength measured at power 0.245 mW. We observe that both residence times coincide showing that the probability to remain in the upper and lower branch is the same whatever is the strength of the applied noise. In Figure 4. 7 **b** the lower and upper state probability distribution is shown for D=0.30 ΔB. We observe a double-peak probability distribution. The area of the left-hand side and the right-hand side peaks are 0.56 and 0.44 of the total area respectively, which shows equivalent probability for polaritons to be in both states.

4.4.2 The effect the noise on polariton bistability

In order to peruse the effect of the external noise on the stability of the hysteresis behaviour, we repeat the polariton bistability measurements for a wide range of applied noise strengths. In Figure 4. 8 **a**, we display a set of bistability curves obtained for different amounts of the applied noise. We observe that the increase in the noise strength results in a decrease in the hysteresis width. A small amount of noise perturbs the emission behaviour close to input power bistability thresholds inducing a unique transition to the other branch in which the system stays stable. This reduces the hysteresis width. For given amount of intensity noise (D=0.142 ΔB) the hysteresis is screened and the system appears as an optical discriminator at input power F=0.25 mW. For larger noise amplitudes instability in the hysteresis cycle appears and polariton populations randomly jump between lower and upper branches (Figure 4. 8 **b**).

To understand the dependence of the hysteresis cycle with the noise, let us first focus on the polariton bistability mechanism without additional noise. In the hysteresis cycle, in the forward direction we observe that the emission intensity in the lower branch increases linearly with laser power. Due to the small overlap between the laser and the polariton ground state, the laser power enhancement leads to the increase of the polariton population which activates the nonlinear polariton interactions (see chapter 3). Consequently, the polariton energy blue shifts with the laser power. Nevertheless, this supply mechanism competes with the polariton lifetime loss mechanism. At a given threshold power, the feedback mechanism becomes dominant and the polariton population reaches a condition where the polariton interactions

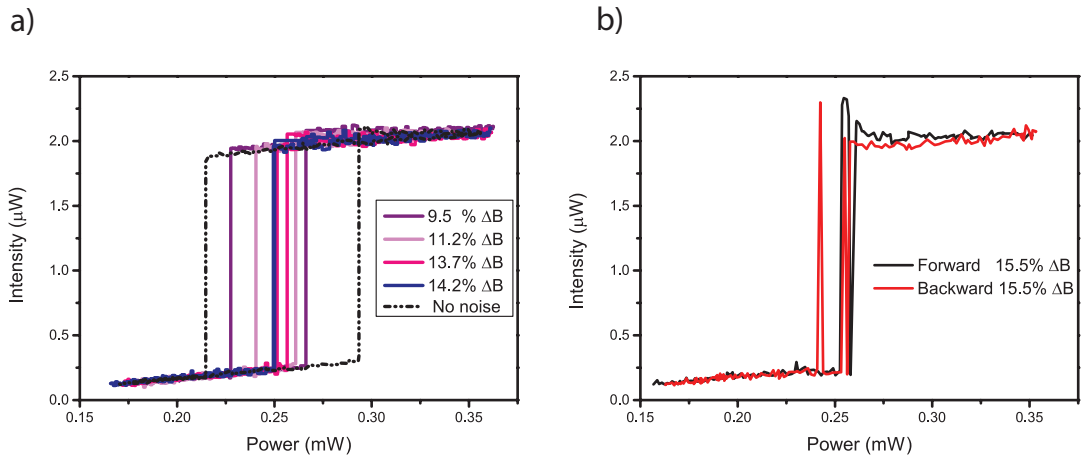

Figure 4.8: **Zero-dimensional polariton bistability affected by the external Gaussian noise.** **a** The initial polariton bistability (dash line) and polariton bistabilities for different amounts of the laser noise: D=0.095 ΔB, 0.112 ΔB, 0.137 ΔB and 0.142 ΔB. Fluctuations on the applied laser intensity make the polariton bistability unstable. We measure the collapse of the optical hysteresis. **b** For larger amounts of the laser noise (D=0.155 ΔB) we start to observe transition between two states.

bring the resonance energy in coincidence with the laser. This appears as the upper power threshold in the hysteresis cycle, and the emission intensity jumps. In the backward direction, by decreasing the excitation laser intensity, the emission remains in the upper branch until reaches the lower power threshold, which is lower than the upper one. At this lower threshold, the losses due to the short polariton lifetime dominate over the feedback mechanism, which reduces the polariton population. As a consequence the blue shift linked to the polariton interaction decreases and accordingly the polariton population decreases to a low value corresponding to the lower stable state. By imprinting the intensity noise on the laser power, we directly induce fluctuations on the polariton population. Because of the polariton-polariton interactions, the population noise is transferred to the fluctuations of the polariton energy. As a result, it affects drastically the competition between polariton loss and feedback mechanism. This appears to be more sensitive close to the upper and lower threshold powers when the equilibrium between both mechanisms is more critical. Consequently, fluctuations induce transitions from one to the other stable state before attaining the threshold powers. This happens for input powers close to the thresholds for small fluctuations. However for larger fluctuations, the power needed for transitions between two stable states gets away from two thresholds. Therefore, noise in polariton population causes the narrowing of the bistability width which can bring instability for device applications. In Figure 4. 9 **a**, **b**, we plot the measured hysteresis width and the middle position of the respective hysteresis loop as a function of the applied noise strength respectively. This result reveals a linear dependence of the bistability width with noise intensity. By extrapolating the straight line we may obtain the genuine width for the system free of any noise which would be of ΔB=76 μW without

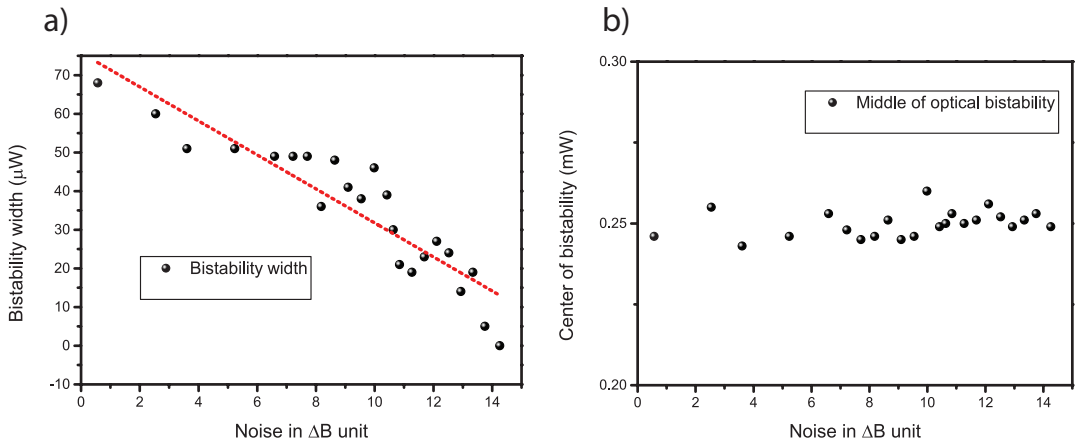

Figure 4.9: **Characteristics of polariton bistability for different amounts of external noise.** **a** Bistability width versus intensity of laser fluctuations. By increasing noise power bistability width decreases and for D=0.142 ΔB it is equal to zero. **b** For different amplitude of laser fluctuations the middle point of each hysteresis fluctuates around 0.245 mW.

considering the low frequency mechanical noise. The reduction of the hysteresis loop evolves symmetrically to collapse in the center position.

4.5 Theoretical model

In order to model the polariton dynamics in a noisy bistability regime, we consider two different approaches. First, we performed numerical simulation using the Gross-Pitaevskii equation (GPE) with a stochastic perturbation and second, we considered the statistical behaviour of the system starting with the polariton bistability without external noise.

For the numerical simulation we use the nonlinear GPE:

$$i\frac{d\Psi}{dt} = -\Delta\Psi - i\gamma_p\Psi + \alpha_1|\Psi|^2\Psi + F \tag{4.13}$$

where Ψ, γ_p and α_1 are the polariton field, the polariton linewidth and the interaction constant respectively. Δ is the energy detuning between the laser energy and the polariton ground state. The driving field F is defined as :

$$F(t) = \sqrt{I + D(t)} \tag{4.14}$$

where I is the laser intensity and D is the random perturbation term which acts on the intensity. The perturbation is considered as a white noise following a Gaussian distribution with a standard deviation of σ.

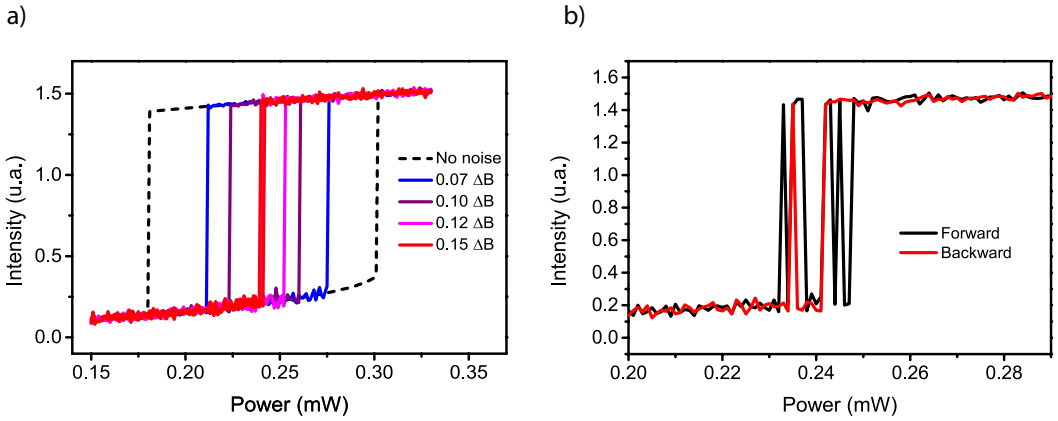

Figure 4.10: **Theoretical study of the effect of the external Gaussian noise on the zero dimensional polariton bistability. a** The initial polariton bistability (dash line) and polariton bistabilities for different amounts of the laser noise: D=0.07ΔB, 0.10 ΔB, 0.125 ΔB and 0.15 ΔB.**b** For a larger amount of the laser noise (D=0.16 ΔB) we start to observe transitions between two states. The parameters used for the GPE are γ_p=0.1 meV, α_1=0.35 meV and Δ=0.24 meV. ΔB is the width of the hysteresis without applying any noise.

In Figure 4. 10 we display the simulated polariton bistability, without noise (black dashed line) in order to extract the theoretical bistability width ΔB. We also display the bistabilities for noise with different standard deviation values normalized with respect to ΔB. The parameters used for the GPE, to reproduce the experimental bistable behaviour, are γ_p=0.1 meV, α_1=0.35 meV and Δ=0.24 meV. We observe a qualitative agreement between the experimental (Fig. 4. 8) and theoretical (Fig. 4. 10) results. It is worth mentioning that the transition power between the lower and the upper state depends on the characteristic time of the experiment compared to the residence time for a given noise strength, which is taken into account by the number of iterations in the simulation.

In Figure 4. 11 **a**, **b** we display the simulated hysteresis width and the input power corresponding to the middle position of the respective hysteresis loops as a function of the applied noise strength, respectively. As clearly seen, the numerical simulations reproduce well the three characteristic behaviour of the polariton dynamics in a noisy bistability regime: 1) the reduction of the bistability width for increasing noise power, 2) the linear dependence of this reduction and 3) the conservation of the hysteresis middle point.

Figure 4. 12 **e** to **h** shows the simulated output time streams for different input powers and a fixed noise standard deviation D=0.2 ΔB. The parameters of the GPE, the noise strength and input powers, are chosen to reproduce the experimental conditions. By using the same analysis procedure as for experimental data, we extract the residence time (Fig. 4. 13 **a, b**) and Kramers time (Figure 4. 13 **c**).

To model the dynamics of the system between the lower and the upper states we use also a statistical approach based on the hysteresis curve without noise. Considering that the

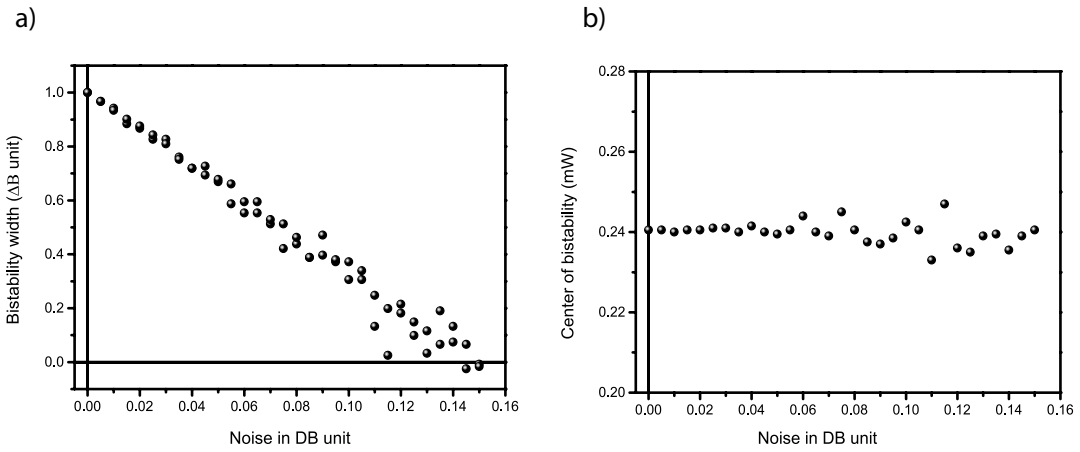

Figure 4.11: **Theoretical characteristics of polariton bistability for different amounts of Gaussian noise. a** Bistability width (normalized to the experimental ΔB) versus noise power in ΔB unit. By increasing the noise power bistability width decreases and for D=0.15 ΔB it is equal to zero. **b** For different amplitudes of the laser fluctuations, the middle point of each hysteresis loop fluctuates around 0.24 mW.

noise affects only the intensity and not the phase of the driving field, both thresholds on the hysteresis loop are fixed and perfectly defined. We name these intensity thresholds I_{up} when the polaritons pass from the lower state to the upper state and I_{down} for the opposite transition.

In this context, the noise perturbation D is modeled by a standard normal distribution with a characteristic correlation time (τ_{cor}) given by the bandwidth of the experimental components. For a given mean power I_0 the noise intensity distribution becomes:

$$I(x) = \frac{1}{P_\sigma \Delta B\sqrt{2\pi}} \exp -\frac{1}{2}(\frac{x-I_0}{P_\sigma \Delta B})^2 \tag{4.15}$$

where I_0 and σ are defined as a function of the ΔB=$I_{up} - I_{down}$:

$$I_0 = I_{down} + P_I \Delta B \tag{4.16}$$

$$\sigma = P_\sigma \Delta B \tag{4.17}$$

where P_I=0, 0.5 and 1 represent lower threshold, middle of optical bistability, and upper threshold, respectively. Finally, we can determine the conditional probability for the system to transit from the initial state by the cumulative distribution function (CDF). For example, when the polariton population is in the lower state, the probability to pass to the upper state is given

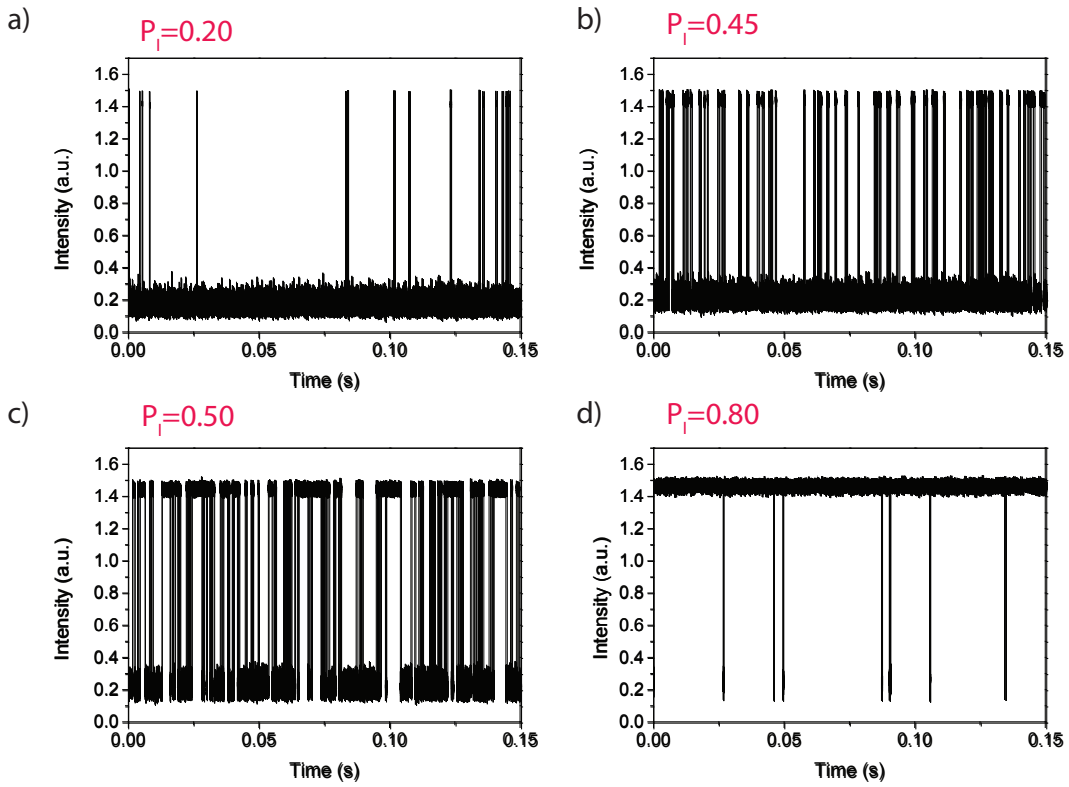

Figure 4.12: **Theoretical description of polariton transitions between two stable states. a, b** For laser power below the middle of bistability (P_I=0.2, 0.45) the lower state is the more stable state. **c** For a laser power close to the middle of the bistability loop (P_I=0.5), transitions between the two stable polariton states occur with the same probability. **d** For a laser power around the upper threshold (P_I=0.8), the upper branch is the most stable state and we observe some random jumps to the lower state.

by:

$$P(I > I_{up}|down) = \int_{I_{UP}}^{\infty} I(x)dx = \frac{1}{2}(1 - erf(\frac{1-P_I}{P_\sigma\sqrt{2}})) \tag{4.18}$$

where erf(x) is the error function.

From a statistical point of view, the histogram built in figure 4. 5 represents the non-normalized probability to jump at time **t** knowing that the system was located on the lower state for **t** second. This probability function can be written as an analytical form:

$$W(t) = P_s^{(n-1)}P_j \tag{4.19}$$

where P_j is the probability to jump from initial state to the other stable state, and $P_s = 1 - P_j$ is the probability to stay in the initial state. n represents the number of iteration. Equation 4.

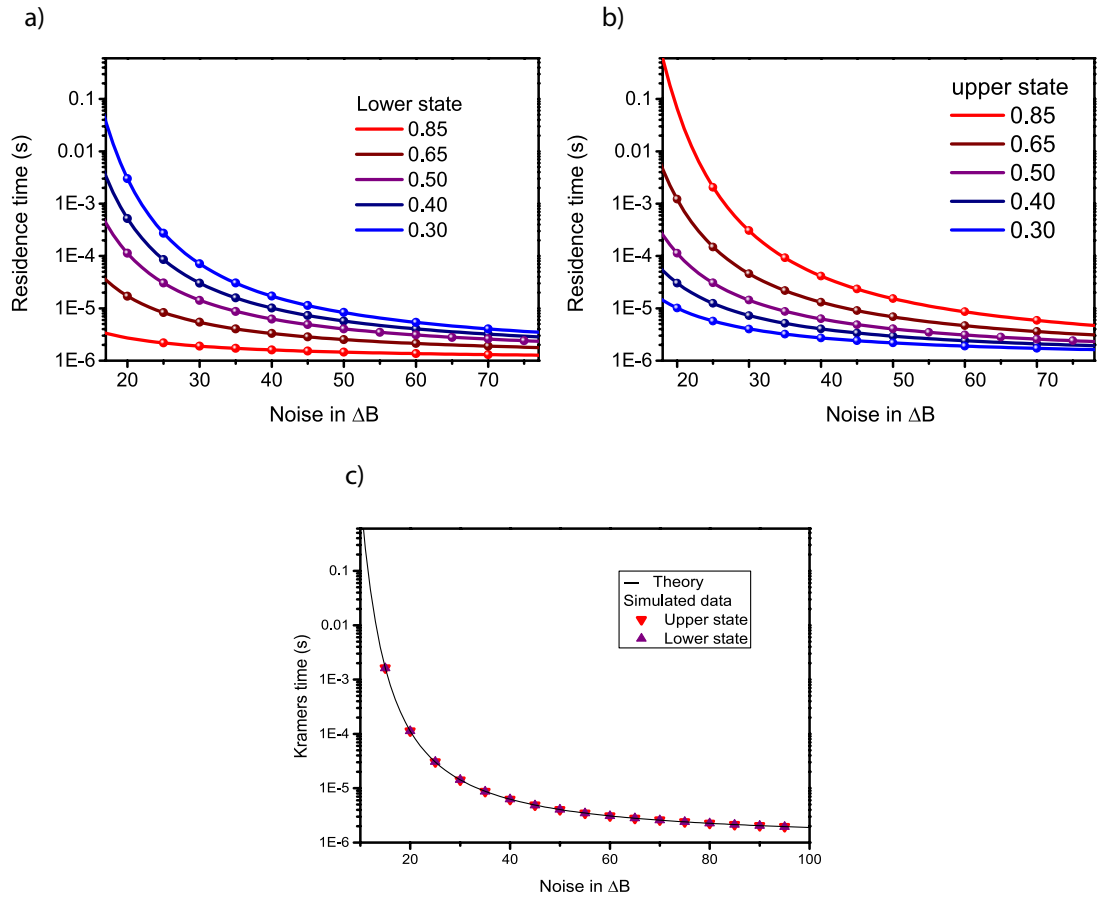

Figure 4.13: **Theoretical residence time for lower and upper states. a** Residence time of the lower state for five different laser powers :P_I=0.30, 0.40, 0.50, 0.65 and 0.85. The noise intensity is increased from D=0.2 ΔB to 1 ΔB. **b** Residence time of the upper state for the same amounts of laser power and noise. **c** The residence times of the lower and the upper states for the laser power around the middle of bistability (P_I= 0.5), which is called as Kramers time. Calculation from GPE (points), and theoretical model (line) are both presented.

19 can be written as:

$$W(t) = \frac{P_j}{P_s} \exp(nln(P_s)) \tag{4.20}$$

Considering the noise correlation time (τ_{cor}) as the minimum time step, this equation can be rewriten as:

$$W(t) = \frac{P_j}{P_s} \exp(\frac{t}{\tau_{cor}} ln(P_s)) \tag{4.21}$$

Same as experimental procedure, we can extract the general residence time (τ_{res}):

$$\tau_{res} = -\frac{\tau_{cor}}{ln(P_s)} \tag{4.22}$$

and the particular Kramers time when

$$P(I > I_{up}|down) = P(I < I_{down}|up) = \frac{1}{2}(1 + erf(\frac{0.5}{P_\sigma\sqrt{2}})) \tag{4.23}$$

Considering the statistical theory, we add in Figure 4. 13 **a-c** the residence time and the Kramers time for different input laser powers as a function of the noise strength. The statistical description is in agreement both with the experiment and the GPE simulation and allows us to extract certain experimental parameter such as the noise correlation time τ_{cor}=1 μs.

4.6 Conclusion

In conclusion, in this chapter we presented the influence of the intensity fluctuations of the coherent driving laser on the bistable polariton emission system. We evidence that the applied noise acts as an effective source of internal noise on the system. In the low noise regime, the hysteresis is well-defined and presents high-quality emission stability in each branch. The residence time defines the time period of this stability, which is necessary to assure the fidelity for devices. We show that the upper (lower) threshold power decreases (increases) with the noise strength, which originates from polariton escapes to the other branch. This results in the reduction of the bistability width. We demonstrated that, for a given amounts of noise, the bistability loop collapses and the system behaves as a discriminator. For larger amount of noise we determine the residence times for different input powers through time resolved emission measurements. We demonstrate that at collapsing power the probability of polaritons being in the upper and lower branch is the same whatever is the strength of the applied noise. At this particular situation we define the Kramers time, which is measured as a function of a large range applied noise. Through numerical simulations using Gross-Pitaevskii equation driven by stochastic excitation and also the theoretical model we reproduced the experimental results.

5 Stochastic resonance

5.1 Introduction

In everyday life, noise is generally considered as an unavoidable, random and detrimental contribution when detecting and transferring information. Stochastic resonance is an astonishing effect allowing to enhance coherently the response of a nonlinear process by the addition of a noisy perturbation[82]. The notion of this counter-intuitive phenomenon was initially proposed by Benzi and collaborators in the 80's to explain the cycling recurrence of ice ages[83]. Because of its generic nature, stochastic resonance has subsequently been demonstrated in a wide variety of fields such as chemistry, biology, physics, and medicine[22, 84]. The first experimental demonstration was obtained in a discrete two-state electronic Schmitt-trigger circuit[24]. This pioneering work stimulated several experimental and theoretical works on stochastic resonance. The first demonstration of stochastic resonance in an optical bistable regime has been reported in a bidirectional ring laser, a ring resonator with a dye as lasing medium [20]. Afterwards, this phenomenon has appeared in a large variety of systems like passive optical cavity[76], polarized emission of a vertical cavity surface emitting laser [85] and atomic system in an electromagnetically induced transparency configuration[86].

Over the past decade, the concept of stochastic resonance has been widened to describe a number of different mechanisms. Classical stochastic resonance encompasses a very large class of stochastic resonances in the macroscopic world around us. It has been studied in double well potential[87], excitable systems[88] and also in coupled processes such as network of neurons [23]. It is worth to mention a proposal to observe stochastic resonance even without any threshold-like system[89]. Quantum stochastic resonance has been also the subject of theoretical studies[90], but an experimental demonstration is still lacking.

Nowadays, stochastic resonance appears to be not only an interesting phenomenon for fundamental reasons, but also a potential means for several practical purposes like neuron transmission enhancement in neurobiology [91], or signal and image processing [92]. In that way, this effect can be realized as a locking technique to extract and magnify weak signal hidden in noise[93]. In this chapter, we present our studies on stochastic resonance in microcavity

exciton-polaritons. We focus on two different types of two-state systems: one is the polariton population bistability and the other is the polariton spin-trigger regime. First, in part 5. 2 we explain in simple terms the principle of stochastic resonance through the motion of a particle in a double well potential. Then, in part 5. 3 we present our experimental and theoretical results for "*intensity stochastic resonance*": stochastic resonance in polariton bistable system [94]. The effect is evidenced through two well defined criteria namely the spectral magnification factor and the signal-to-noise ratio (SNR). The robustness of the process is witnessed as a function of the weak modulated amplitude of the coherent driving field. In part 5. 4, we take advantage of the exclusive spin properties of exciton-polaritons in the spin-trigger regime. This allows us to unveil an original possibility for stochastic resonance based on the ordering of the spin of a collective ensemble of particles through spin noise. We name this phenomenon: "*spinor stochastic resonance*". The effect is the spin polarization amplification, which is evidenced by the enhancement of the degree of polarization of a noisy polarized modulated input signal into a fully circular polarized signal. Experimental observations for both intensity and spin stochastic resonance are reproduced by numerical solution of the Gross-Pitaevskii equation driven by a stochastic excitation.

5.2 Principle of stochastic resonance

In simple terms, the mechanism of stochastic resonance is the following. Let us consider a Brownian particle moving in a double well potential. The particle, which is subjected to noisy forces (such as a thermal noise) undergoes transitions between the two minima of the potential according to the Kramers rate (see chapter 4), i. e. ,

$$r_k \propto exp(\frac{-\Delta V}{D}) \tag{5.1}$$

ΔV and D being the height of the potential barrier and the noise intensity, respectively. If we apply small periodic force on the potential, the potential barrier will be periodically raised and lowered. We consider here a small enough modulation amplitude, such that it does not cause any deterministic hopping of the particles between the two wells. Synchronization between the periodic signal and the noise induced hopping can take place for some optimal noise intensity (D_{SR}) (Fig. 5. 1 **a**). This statistical synchronization happens when the average residence time between two interwell transitions ($1/r_k$) is comparable with half of the period of the external force (T).

$$T \cong \frac{2}{r_k} \tag{5.2}$$

In this condition, we reach stochastic resonance. It is important to mention for large modulation amplitudes deterministic jumping occur and the synchronization is not so obvious [95].

As we mentioned before, bistability can be modeled as a double well potential where each

potential well simply represent one of the two stable states. Let us consider a nonlinear system with well-defined bistable behaviour in which the system has two stable states for a given input force (Fig. 5. 1 **b**). By applying a sinusoidal signal in the middle of the bistability with small modulation amplitude, we cannot switch the system from the lower to the upper state

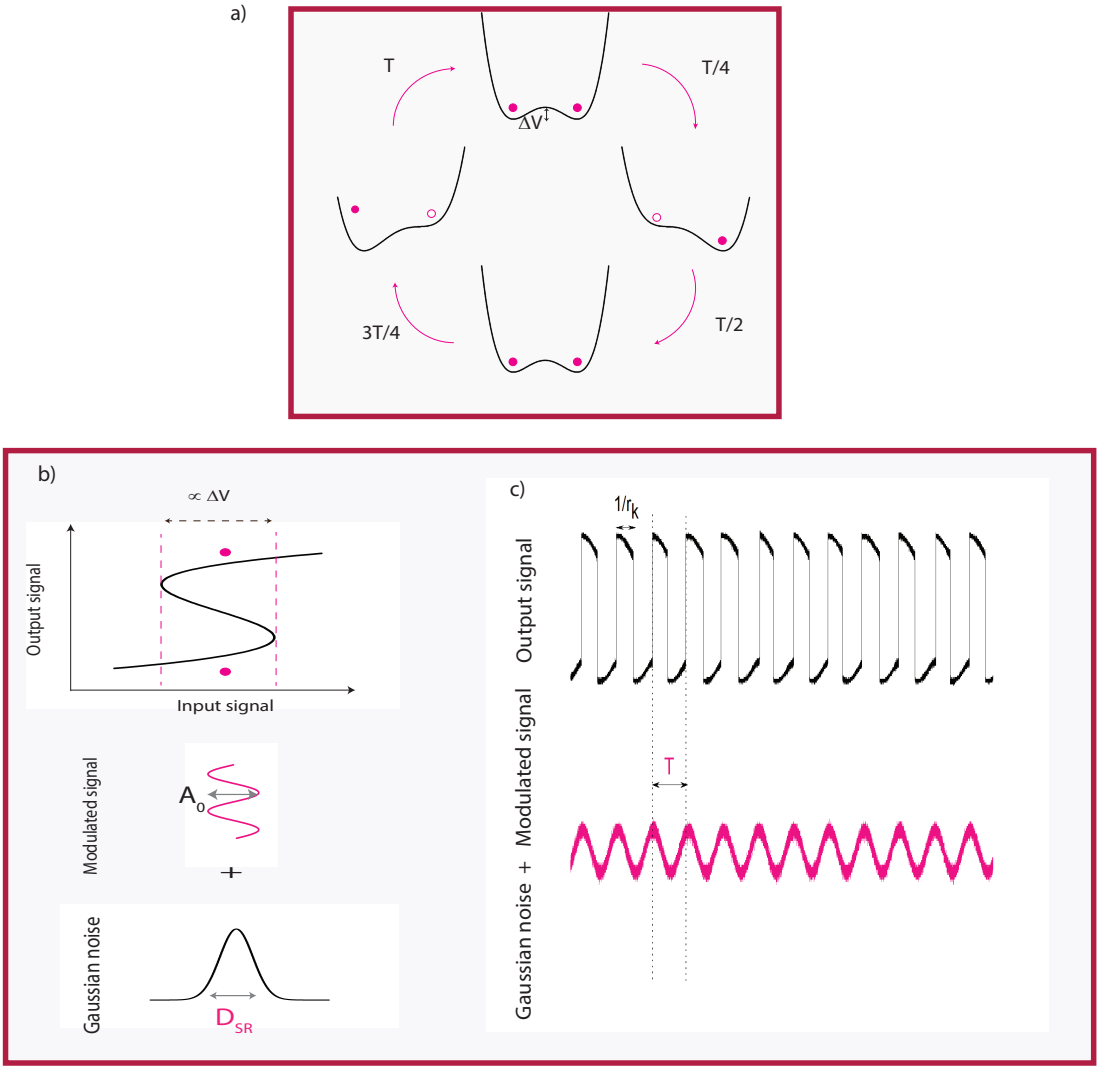

Figure 5.1: **Principle of stochastic resonance. a** Double-well potential. By applying a small modulated signal within one periodic cycle (T), potential barrier (ΔV) will be periodically raised and lowered. For the optimal noise value, filled circle jumps to the stable potential well with the same frequency as the external periodic force. For the symmetric double-well potential, two stable states have occupied with equal probabilities (filled circles in two potential wells). **b** The optimal amount of Gaussian noise and external modulated signal in the middle of bistability, forcing the filled circle between lower and upper states periodically. **c** The output signal as a stochastic parameter jumps between two states with the same period as applied periodic force, which is about twice the residence time in each state.

and vice-versa. However, by adding an optimal amount of external noise, synergic interplays between these two forces can activate hopping events between two states with the same frequency as the periodic force (1/T), which is about twice the Kramers time (Fig. 5. 1 **c**).

5.3 Intensity stochastic resonance

5.3.1 Experimental setup

In order to investigate stochastic resonance in polariton bistability, we have designed the experimental setup as follows (Fig. 5. 2). We use a continuous-wave mode Ti:Sapph laser with 2% of noise intensity standard deviation. We work in transmission configuration as described in third and fourth chapters. The sample is excited at normal incidence (k=0) and cooled down to 4K. In order to use an electro-optic modulator (EOM) the laser beam is vertically polarized using a Glan polarizer and a half wave plate. By means of EOM, we imprint a 500 kHz bandwidth Gaussian noise in addition to a weak periodic signal on the DC component of the laser power. EOM, which works based on polarization modulation, is followed by Glan polarizer in order to modulate the laser intensity (see section 3. 4). The excitation is fully controllable and allows varying the modulation amplitude and the frequency of the signal as well as the noise intensity. It is then possible to study in detail the stochastic resonance response for a wide range of input parameters. Using a quarter wave plate, the polarization of the laser is prepared in a circular state to avoid any spinor related effects[14]. Using a 10:90 non-polarizing beam splitter (BS), 10 percent of the excitation beam is separated. Then, by means of a 50:50 non-polarizing beam splitter, half of the separated beam is sent to the power meter to control the excitation power, and the other half is sent to photodiode 1. The other 90 percent of the laser beam is used for exciting the sample. In order to realize polariton bistability, the laser energy is tuned slightly above the polariton ground state (Fig. 5. 3 **a**). We record simultaneously the time evolution of both the input excitation signal and the transmitted light under conditions of polariton bistability by using 20 MHz bandwidth low noise photodiodes. Time streams are acquired through an oscilloscope with 60 MHz bandwidth.

5.3.2 Stochastic resonance in 0D polariton bistability

Input-output syncronization

We choose to use confined mesa structures of 3 μm diameter in our microcavity sample [62]. This structure can be seen as a perfect system to investigate stochastic resonance. The photonic confinement allows separating efficiently the polariton ground state from intrinsic noise perturbations. This noise-free polariton level allows to accurately control the important parameters of the experiment, i.e. the polariton bistability condition and the extrinsic applied fluctuations, which in turn, determine the characteristic time scale of the stochastic resonance.

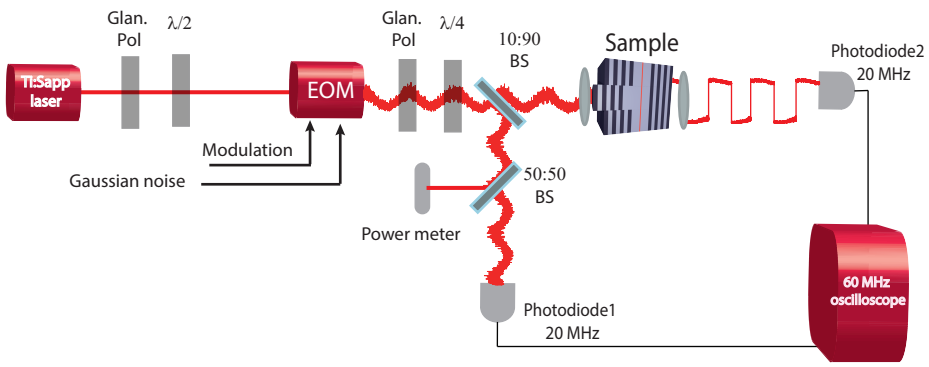

Figure 5.2: **Intensity stochastic resonance setup.** The cw single mode laser excites resonantly a microcavity polariton gas. By means of a Glan polarizer (GP) and half wave plate ($\lambda/2$), entrance light of the electro-optic modulator (EOM) is prepared in vertical direction. A weak modulation in addition to Gaussian noise is applied on the laser intensity using the EOM. Using Glan polarizer and quarter wave plate ($\lambda/4$), the laser excitation is circularly polarized. Using a lens of 5 cm focal length, the laser is focused onto a 20 μm spot on the sample. The transmitted output signal is collected with a microscope objective. Two fast photodiodes record the excitation and transmitted signal simultaneously. The power meter controls the input excitation power.

Experiments are performed at negative exciton-cavity detuning (-3.58 meV) for which the ground state polariton linewidth is in the order of $\gamma = 100$ μeV. First we obtain power dependent polariton bistability curve by scanning the excitation power back and forth. Then, in order to decrease the effect of mechanical noise, we measure polariton bistability using the usual X-Y method [72]. First, we fix the laser power in the middle of the bistability loop. Then, using EOM we imprint a large enough modulated signal on the laser intensity. This periodic force reaches lower and upper thresholds of bistability and can push the polaritons from lower to upper states and vice versa. Considering the modulated input signal as an input (x axis) and polariton intensity as the output parameter (y axis) polariton bistability is determined. For blue detuned ($\Delta = 0.4$meV) continuous wave laser respect to the polariton ground state (Fig. 5. 3 **a**), the system shows polariton bistability with a width $\Delta B = 2.27 \pm 0.43$ mW (Fig. 5. 3 **b**). We fix then the laser power at 4.5 mW in the middle of the bistable hysteresis loop, and we add modulated signal at frequency $\nu_0 = 600$ Hz. Then, by increasing the noise intensity standard deviation D, we record both the excitation power and transmitted signal as a function of time. It is worth highlighting that the driving field modulation frequency ν_0 is orders of magnitude smaller than the intrinsic frequency dynamics of the polariton gas (≈25 GHz).

In Figure 5. 4, we display the results recorded for a modulated signal amplitude $A_0 = 525\mu$W corresponding to $0.23\Delta B$. From top to bottom, we evidence the effect of the increased noise intensity on the time behaviour of the excitation laser and transmitted signal (in black and blue respectively) (Fig. 5. 4 **a-e**). We acquire their corresponding frequency spectrum via Fourier transform of input and output signals for time sequences of 0.63 second (Fig. 5. 4 **f-j**).

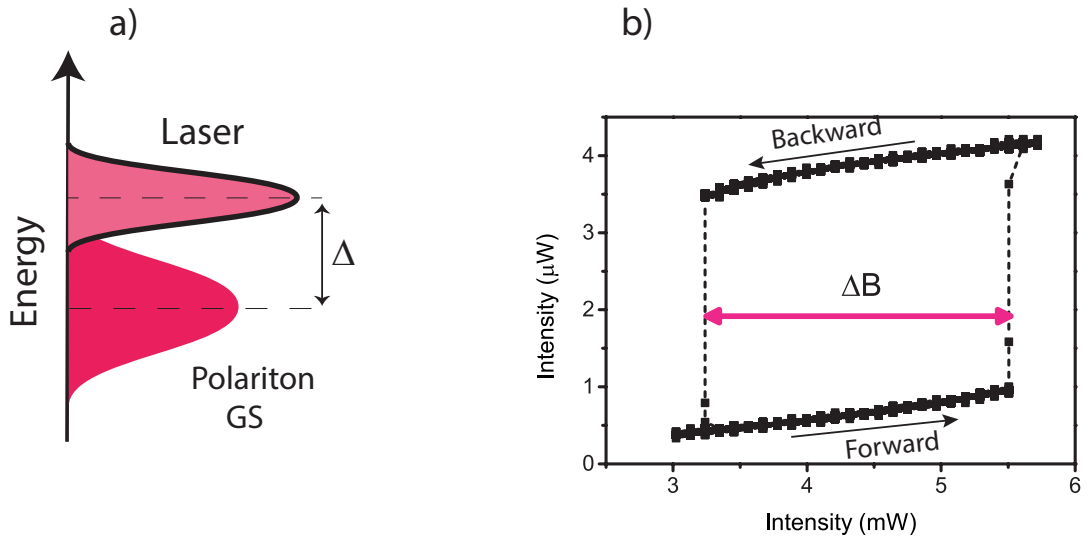

Figure 5.3: **0D polariton bistability. a** Energy diagram of the experimental configuration. The laser energy is tuned (Δ) above the polariton ground state (GS). **b** Polariton bistability obtained using X-Y method. For a negative exciton-cavity detuning (-3.58 meV) and a polariton-laser detuning of Δ = 0.4 meV, bistability width is (ΔB= 2.27 ± 0.43 mW).

Figure 5. 4 **a** shows the input and output signal when only the laser intensity fluctuations D_0= 58 μW (0.02ΔB) are present. Note that the modulation amplitude is not sufficiently large to overcome the bistable intensity threshold by itself. Because of the dissipative character of microcavity exciton polaritons, the system can clearly transfer the modulated input signal. We evidence the modulated polariton intensity with the same frequency as the input beam. As a consequence, the corresponding frequency spectrum (Fig. 5. 4 **f**) shows small but clear peak, located at ν_0 = 600 Hz. By adding an external stochastic perturbation D= 275 μW (0.12ΔB), the outcoming signal displays erratic jumps between the two stable states due to the random nature of the input signal (Fig. 5. 4 **b**). This effect adds large amounts of low frequency noise, and consequently the weak signal is almost buried in the background noise (Fig. 5. 4 **g**). Residual peaks in the input signals at frequencies higher than 600 Hz are due to the nonideal Gaussian noise distribution provided by the electrical noise generator. For larger noise intensity (D=367 μW (0.16ΔB)) synergic interplay between noise and modulated signal displays periodic hopping of polariton gas between lower and upper stable states. In fact, polariton bistability shows a coherent amplification of the weak transmitted signal due to the noise contribution (Fig. 5. 4 **c, h**). Notice that the spectrum displays odd and even harmonics, while the Fourier series of a perfect square signal is only composed of odd harmonics of the fundamental 600 Hz component. We attribute the appearance of those peaks to the stochastic origin of the resonance that represent a breathing of the output signal period. By introducing a larger amount of noise D=408 μW (0.18ΔB), the transmitted signal shows again erratic jumps (Fig. 5. 4 **d, i**). For even larger noise intensity D=976 μW (0.43ΔB), the output signal is completely buried in the noise. The above description carries all the characteristics of the

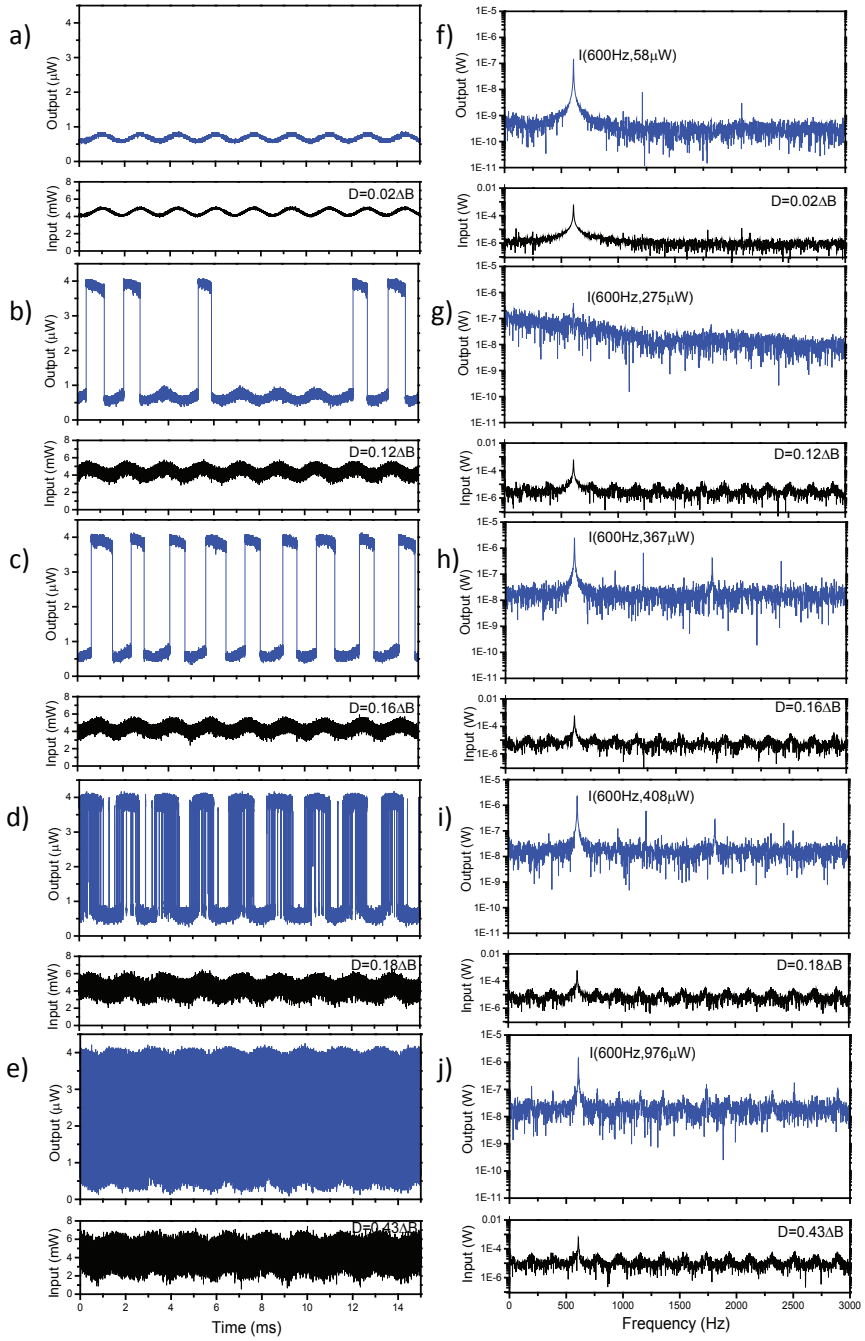

Figure 5.4: **Input-output synchronization for 0D polariton intensity stochastic resonance. a-e** Excitation laser (black) and polariton intensity (blue) while the noise intensity is continuously increased: 58μW (0.02ΔB), 347 μW (0.12ΔB), 367 μW (0.16ΔB), 408 μW (0.18ΔB) and 976 μW (0.43ΔB). **f-j** The corresponding frequency spectra obtained by Fourier transforming time streams acquired for 0.63 second. The resolution of the spectrum is 1.5 Hz. Other parameters are the frequency of modulation $\nu_0 = 600$ Hz and the amplitude of the input signal $A_0 = 525\mu$W (0.23ΔB).

so-called stochastic resonance.

Stochastic resonance quantifiers

Signal-to-noise ratio To quantify the behavior of the polariton stochastic resonance in more detail, we now study a well suited quantifier namely the signal-to-noise ratio (SNR). The spectral power can be defined as the superposition of harmonics (centered at $\nu = (2n+1)\nu_0$ with n=0, ±1, ±2,...) and the background power spectrum. Although as mentioned before, we observe experimentally even as well as odd harmonics. We obtain the signal-to-noise ratio from the ratio between the output spectral power at the driving frequency ($I_{out}(\nu_0, D)$) and the corresponding background power spectrum:

$$SNR = \frac{I_{out}(\nu_0, D)}{N(\nu, D)}, \tag{5.3}$$

Spectral peak intensities ($I_{out}(\nu_0, D)$) are extracted for different noise standard deviations varying from 0 to 0.78 ΔB and the background noise ($N(\nu, D)$) averaged between 760 Hz to 1045 Hz. We plot in Figure 5. 5 **a** the SNR of the input and transmitted signals for a modulation amplitude of $A_0 = 0.23\Delta$B. Both signal-to-noise ratios show large values for low noise contribution ($D < 0.1\Delta$B). This behaviour is due to the dissipative character of polariton gas. Contrary to Schmitt-trigger switches [24], the polariton bistability does not exhibit flat states. Actually the output polariton intensity varies linearly on both stable states as a function of the pump power (Fig. 5. 3 **b**). The behaviour of the input SNR follows the expected decrease when increasing the noise intensity. Conversely, by increasing the noise intensity initially the SNR of the output signal decreases drastically. This behavior corresponds to random hopping of polariton between two stable states and consequently low frequency background noise (Fig. 5. 4 **g**). Then, for optimal noise intensity (D_{SR}), the SNR of both excitation and transmitted signals are comparable. Looking at Figure 5. 4 **c**, it seems that excitation light is more noisy compared to the output polariton intensity around the optimum noise power, while they have same amount of signal-to-noise ratio. Although the amount of imprinted noise on polariton lower and upper states compared to polariton intensity (4. 5 μW) seems small, pulse width breathing also decreases the output signal-to-noise ratio and make it comparable with input SNR. Eventually, for large enough noise intensity, the polariton SNR decreases in a way that is similar to linear systems. This resonance behaviour of the transmitted SNR, which shows a revival of the input SNR for an optimum amount of noise, is directly related to the nonlinear phenomenon in polariton bistability and evidences the stochastic resonance phenomenon.

We study the signal-to-noise ratio for a large range of modulation amplitudes from 0.29 mW (0.13 ΔB) to 1.04mW (0.46 ΔB) (Fig. 5. 5 **b**). As is evidenced by this figure, the SNR peak value increases with the signal amplitude. Therefore, we observe that when increasing the modulation amplitude, the shape of the SNR resonance is less pronounced and also shifts to lower noise intensities. This behaviour comes from the tendency of the system to evolve

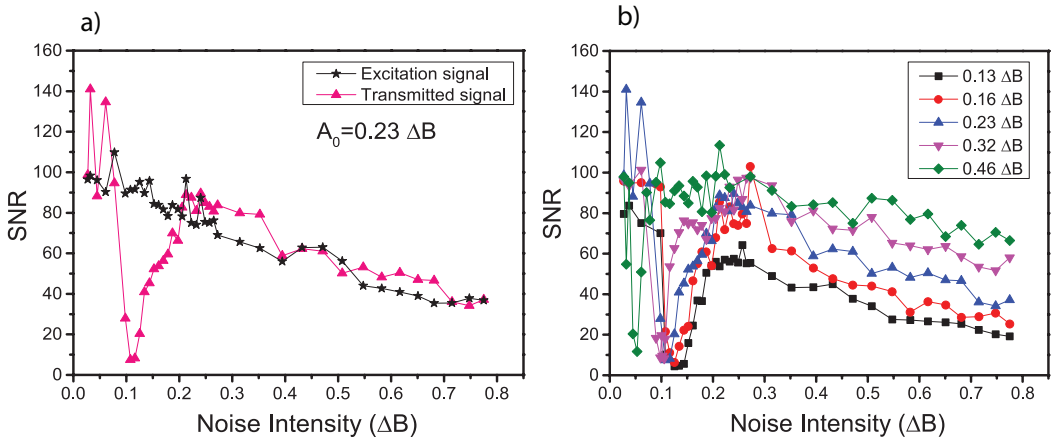

Figure 5.5: **Signal-to-noise ratio for 0D polariton intensity stochastic resonance. a** SNR of the excitation signal (black) and corresponding transmitted signal (pink) for $A_0 = 0.23\Delta B$ as a function of the noise standard deviation. Due to polariton bistability transmitted signal recovers input signal-to-noise ratio using external fluctuations. **b** SNR as a function of noise power for different modulation amplitudes of $A_0 = 0.13\Delta B$, $0.16\Delta B$, $0.23\Delta B$, $0.32\Delta B$ and $0.46\Delta B$. For larger modulation amplitudes, SNR increases while the resonance shape is less pronounced. The activation noise for stochastic resonance formation decreases with sinusoidal signal amplitude.

towards deterministic jumps between the two states without the cooperative interplay between noise and the weak signal.

Magnification factor The magnification factor is another quantifier which measure synchronization between the input signal and the fluctuation-activated polariton dynamics. In order to study the magnification factor, spectral peak intensities of the transmitted signal at the modulation frequency ($I_{out}(\nu_0, D)$) are normalized by the transmitted signal intensity $I_{out}(\nu_0, D_0)$ when only laser fluctuations exist (without additional noise):

$$M = \frac{I_{out}(\nu_0, D)}{I_{out}(\nu_0, D_0)} \tag{5.4}$$

This magnification measurement also shows a clear resonance behaviour: upon introducing noise intensity, the magnification factor increases up to an optimal maximum and then, when increasing further the noise, it falls off (Fig. 5. 6). For a small modulation amplitude (0.13 ΔB), the resonance appears for $D_{SR} \approx 0.2\Delta B$, the weak signal is coherently transmitted and shows a strong amplification. Nevertheless, this large amplification value is not accompanied by the large SNR observed on Figure 5. 5 **b**. Contrary to the increasing behaviour of the SNR, as the modulation amplitude increases, the transmitted signal for the activation noise intensity D_{SR} decreases. This behaviour is accompanied by a decreasing of the activation noise. However, it

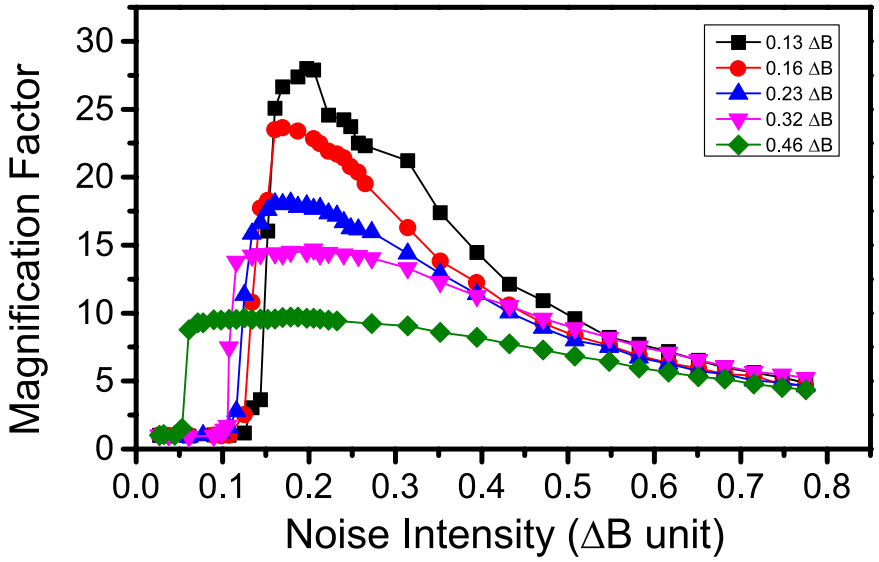

Figure 5.6: **Experimental magnification factors for 0D polariton intensity stochastic resonance.** Experimental spectral magnification factors for modulation amplitudes of $A_0 = 0.13\Delta B$, $0.16\Delta B$, $0.23\Delta B$,$0.32\Delta B$ and $0.46\Delta B$. The noise standard deviation varies from 0 to 0.78 ΔB. For larger modulation amplitude the polariton hopping between two states is less noise induced and more deterministic.

is important to note that both trends , that of the SNR and that of the magnification factor, are related to the same effect evoked in the above paragraph, namely the deterministic behavior of the system for an amplitude of modulation close to the bistability width ΔB. This effect evidences that, contrary to intuition, the weaker the modulated signal, the better can be the benefit of noise in view of magnifying the signal transmission.

Theoretical model

The simplest approach used to model the double-well problem is indeed based on a two-state model, in which the stochastic variable can take only two discrete values [22]. The Schmitt-trigger is an example of such a discrete system with a symmetric bistability [24]. Nevertheless, the dissipative nature of polariton bistability brings an asymmetry in the hysteresis, and using this model reduces the polariton dynamics only to the switching mechanism between the two states, omitting all short time dynamics within each of the two states. Therefore, we performed numerical simulations considering a stochastic perturbation of the Gross-Pitaevskii equation

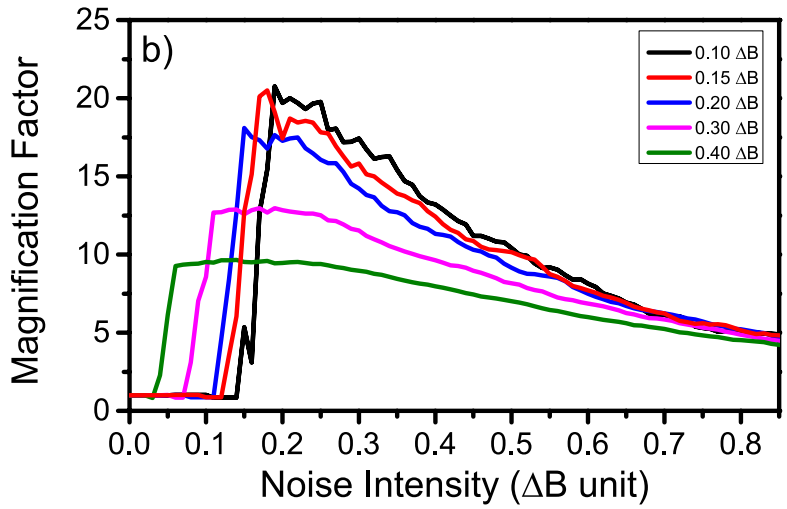

Figure 5.7: **Numerical Magnification factors for 0D intensity stochastic resonance.** Numerical spectral magnification factors for A_0 = 0.1ΔB, 0.15ΔB, 0.2ΔB,0.3ΔB and 0.4ΔB. The noise standard deviation varies from 0 to 0.85 ΔB.

usually employed to model polariton dynamics in bistability regime:

$$i\frac{d\Psi}{dt} = -\Delta\Psi - i\gamma_p\Psi + \alpha_1|\Psi|^2\Psi + F \tag{5.5}$$

where Ψ, α_1 and γ_p are the polariton field, the interaction constant and polariton line width respectively. Since the driving field modulation frequency ν_0 is orders of magnitude smaller than the intrinsic frequency dynamics of the polariton gas (≈25 GHz), the present investigated stochastic resonance fulfills the well-established adiabatic approximation. This means that the temporal changes of the double-well potential affected by applied modulation and noise is slow in comparison to the polariton lifetime in each of wells. Indeed, the cw resonant excitation of the polaritons guarantees our working in the stationary regime. Since the variation of the driving field (μs time scale) is extremely slow with respect to the transient response time of the polariton gas (ps time scale), the driving field amplitude F can be considered as a constant in equation (5. 5).

$$F(t') = E_0 + A_0\cos(2\pi\nu_0 t' + \phi) + D(t'), \tag{5.6}$$

where E_0 is the DC amplitude component, A_0 the modulation amplitude and $D(t')$ the random perturbation term. The modulation frequency ν_0 is set to 30 Hz. ΔB is the bistability width

obtained with the following set of parameters: α_1 = 0.35 meV, $\gamma = \hbar/10$ ps, Δ = 0.45 meV with $\hbar$ the reduced Planck constant. The numerical correlation time of the Gaussian noise distribution is fixed to be 20μs. By Fourier transformation of simulated output time streams, the spectral magnification factor is calculated according to the equation 5. 4. Figure 5. 7 shows the numerical magnification factor for five values of A_0 normalized in terms of the bistability width ΔB. These results qualitatively reproduce our experimental measurements (Fig. 5. 6) . We show a good agreement in terms of the noise activation intensities which shift to lower D when increasing the amplitude of the modulation. Moreover, our simulations also reproduce very well the overall shape of the spectral magnification factor and the maximum gain is well reproduced. The normalization of our results in terms of bistability width allows us to show a good agreement with works related to stochastic resonance in other physical systems where the activation noise intensity is expected to be $D_{\mathrm{SR}} \approx 0.2\Delta$B [22].

5.3.3 Stochastic resonance in 2D polariton bistability

Input-output synchronization

Within the last decade, a large number of polariton based devices such as interferometers[96], logic gates[54, 97] and switches[98] has been proposed, which usually take advantage of polariton propagation. Multiple polariton channels can be also integrated together to form polariton neuron networks [56]. Stochastic resonance could be a tool to enhance SNR in polariton propagating networks. At this point, we did the experiment in two dimensional (2D) microcavity polaritons and we clearly demonstrate stochastic resonance in planar microcavity.

Our experiment has been performed at an exciton-cavity detuning equal to $\delta = 0.89meV$. The sample is excited at normal incidence (k=0) with a continuous wave (cw) mode Ti:Sapph laser. Laser energy is blue detuned by Δ=0.69 meV above the lower polariton state and its polarization is prepared in one circular state. These conditions give rise to a bistable region width of ΔB=0.81$\pm$0.23 mW (Fig. 5. 8). We observe quite different slopes for the two metastable states in the 2D optical bistability. This is in contrast with the case of 0D bistability where the slopes of two stable states were nearly the same. This difference comes from difference in exciton-cavity detunings in the studied mesa structure and 2D part. The slope of each state will determine transmitted modulation amplitude and noise intensity through bistable system.

In order to evidence stochastic resonance in 2D polariton system, we fix the excitation laser power, at 3.45 mW, in the middle of the 2D optical bistability. Then, by imprinting the external 500 kHz Gaussian noise and optical modulation on the DC component of the laser power, we study the transition of polariton gas between the two stable states. The modulated signal frequency is fixed at ν_0 = 780 Hz. We increase the noise standard deviation (D) from 51 μW (0.06ΔB) to 1.81 mW (2.24 ΔB) and we record both the excitation and transmitted signals in

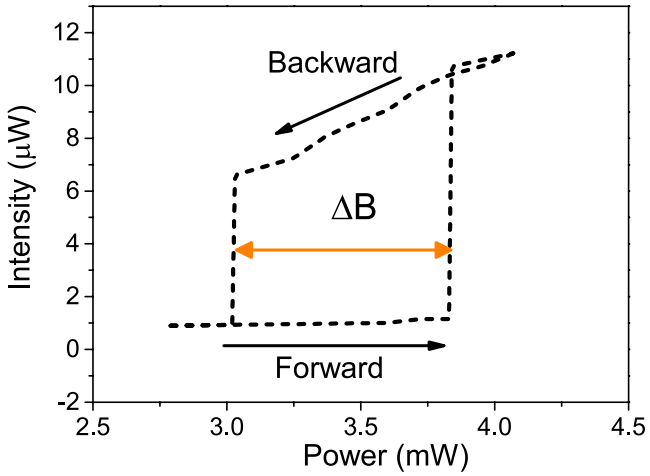

Figure 5.8: **Two dimensional polariton bistability.** 2D polariton bistability obtained for an exciton-cavity detuning of $\delta = 0.89 meV$ meV and the polariton-laser detuning of Δ= 0.69 meV.

function of time.

In Figure 5. 9 we present both excitation and transmitted signals for applied modulation amplitude of 230 μW (0.28ΔB). We study the dynamical response of the 2D polaritons for different noise intensities in time (Fig. 5. 9 **a-e** and frequency domain (Fig. 5. 9 **f-j**). For minimum noise intensity D= 49 μW (0.06ΔB), polariton population is located on the lower state. Because of flatness of this state in 2D polariton bistability, we measure negligible value of main harmonic at ν_0 = 780 Hz (Fig. 5. 9 **a, f**). For larger noise intensity D=57 μW (0.07ΔB) polariton gas jumps to the upper state. However, the superposition of modulated signal and noise is not large enough to reach bistability thresholds more than one occurrence and the weak transmitted signal stays on the upper bistable state (Fig. 5. 9 **b, g**). By increasing noise amplitude D=97 μW (0.12 ΔB), polaritons start to jump between two stable states randomly (Fig. 5. 9 **c, h**). Figure 5. 9 **d, i** shows experimental results obtained for noise intensity D= 130 μW (0.16 ΔB). An effective interplay between the two input forces, the periodic signal and the Gaussian noise, leads to periodic jumps of 2D polariton population between the two bistability states. For larger external perturbation D=243 μW (0.3 ΔB), switching between two states start to be buried with noise. Contrary to 0D stochastic resonance, we observe that the noise amplitude which is imprinted on top of lower and upper branches is different. This observation is directly related to the asymmetry in the slopes of the two stable states in the 2D optical bistability (Fig. 5. 8).

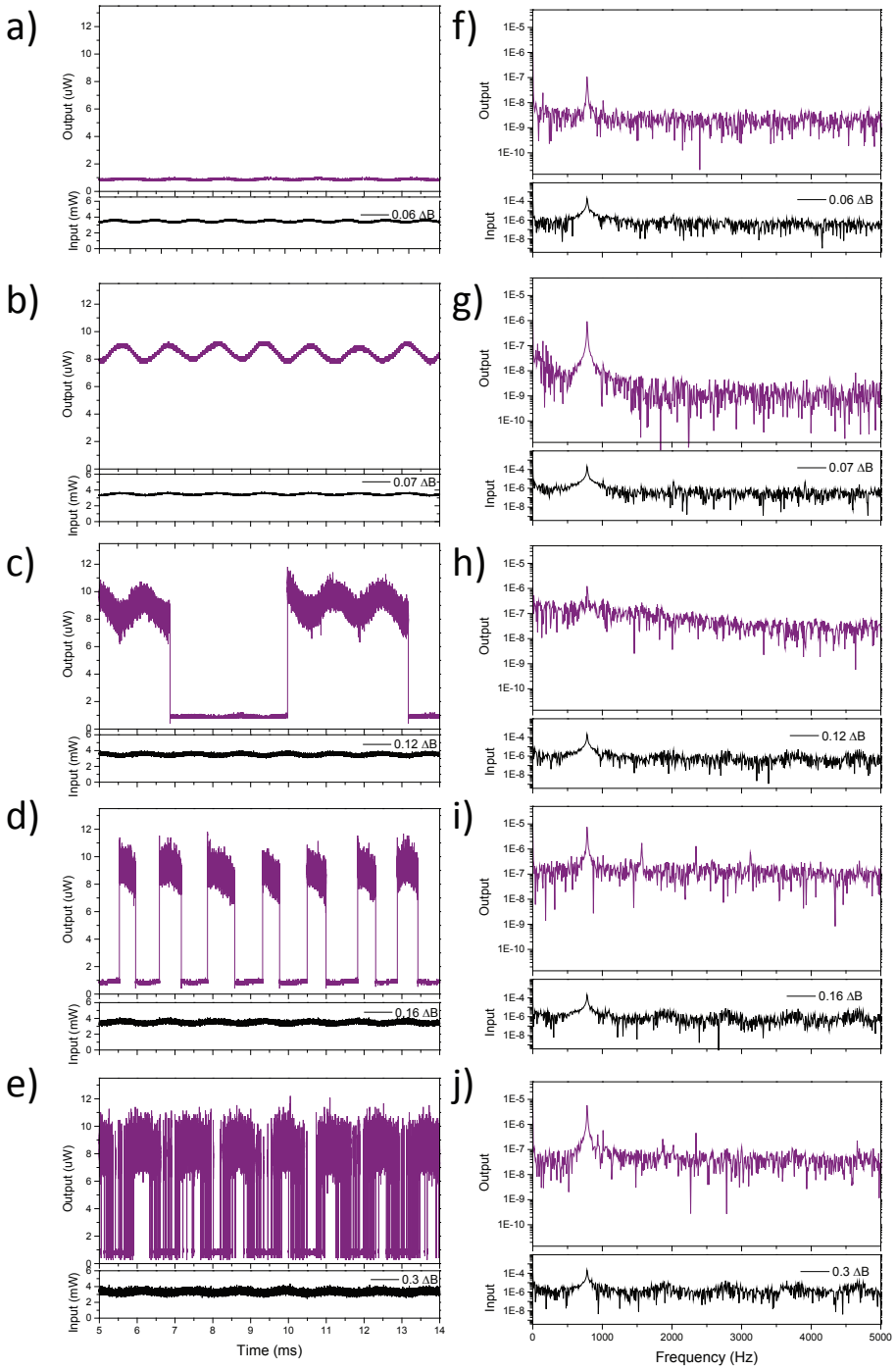

Figure 5.9: **Demonstration of stochastic resonance in 2D polariton bistability. a-d** The input (black) and the output (purple) signal in time domain whereas noise intensity is continuously increased: 49 μW (0.06ΔB), 57 μW (0.07ΔB), 97 μW (0.12ΔB), 130 μW (0.16ΔB), 243 μW (0.3ΔB). **e-h** Frequency spectra. The frequency and the amplitude of modulation are ν_0=780 Hz and $A_0 = 230\mu$W (0.28ΔB) respectively.

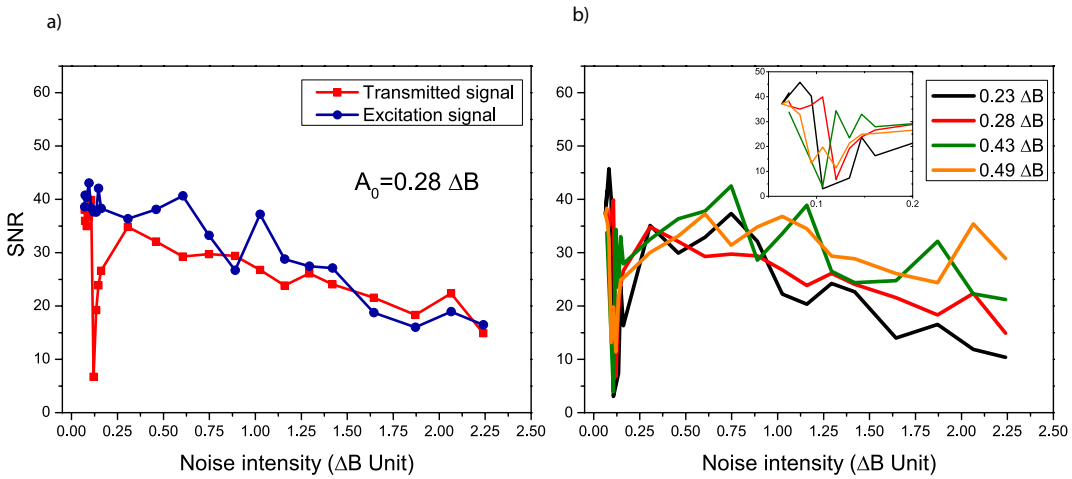

Figure 5.10: **Signal-to-noise ratio for 2D intensity stochastic resonance. a** SNR of the input and output signal for $A_0 = 230\mu$W (0.28ΔB). **b** SNR for different amplitudes of input modulation $A_0 = 0.23\Delta$B, 0.28ΔB, 0.43ΔB and 0.49ΔB.

2D stochastic resonance quantifiers

Signal-to-noise ratio To quantify 2D stochastic resonance, we present experimental signal-to-noise ratio for excitation and transmitted signal for the amplitude of modulation equal to 230 μW (0.28ΔB) (Fig. 5. 10 **a**). The background noise is averaged between 640.4 Hz to 725.3 Hz. Obviously for minimum noise contribution a relatively large SNR is measured which corresponds to the linear transmission of the polaritons through the bistability. As the noise is increased, due to the polariton random jumps between the two bistable states, the SNR decreased considerably. For the optimum noise value (D_{SR}) output SNR recovers the input SNR value. Since the amplitude of modulation of the input signal is about twice weaker than in the 0D case (Fig. 5. 5 **a**), the SNR values observed here in the 2D system (Fig. 5. 10 **a**) are around twice smaller. Similar to the 0D case, for a range of input noise intensity the polariton nonlinearity recovers the input SNR of the system. We study the SNR for different amplitudes of input modulation from 0.19 mW (0.23 ΔB) to 0.4 mW (0.49 ΔB) (Fig. 5. 10 **b**). Comparing this result with Figure 5. 5 b, we clearly find that in 2D system for these modulation amplitudes the resonance behaviour is not so pronounced. Since the 2D bistability width is smaller than 0D hysteresis, applying small enough modulation amplitude, which would give clear resonance, goes beyond the limits of our experimental possibilities.

Magnification factor We also study the spectral magnification factor for the same range of the modulation amplitudes (Fig. 5. 11). As in the 0D case, we normalize spectral peak intensity for different noise amplitudes $I_{out}(\nu_0, D)$ with respect to the transmitted signal intensity for minimum external fluctuations $I_{out}(\nu_0, D_0)$. For small amplitude of sinusoidal signal, we observe the typical resonance behaviour, and for the largest ones we observe a

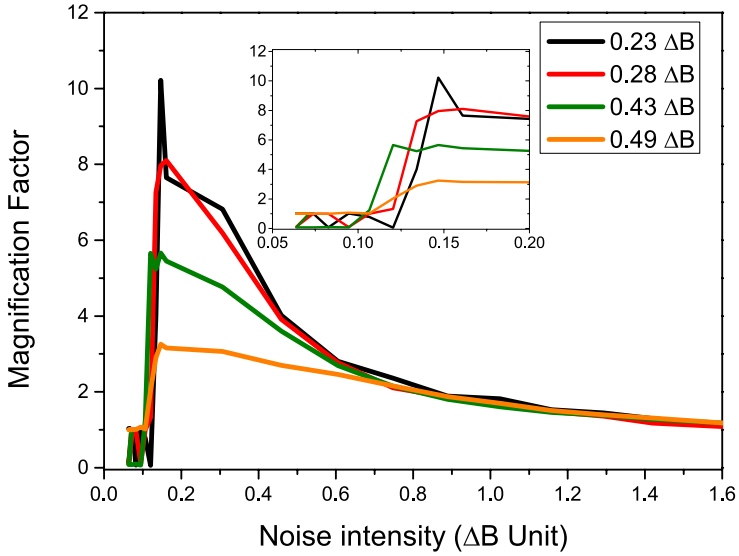

Figure 5.11: **Spectral magnification factor for 2D intensity stochastic resonance.** Spectral magnification factor for amplitude of modulations $A_0 = 0.23\Delta B$, $0.28\Delta B$, $0.43\Delta B$ and $0.49\Delta B$. The amplification factor for noise intensity between 0 and 0.2 ΔB is shown as an inset.

plateau which demonstrates the deterministic jumps between the two branches. For a low noise intensity, because of random jumps of the output signal between the upper and lower states, the polariton transmission through 2D bistability changes randomly. This is evidenced by the fluctuations of the magnification factor between 1 and 0.08 (inset of Fig. 5. 11).

To conclude, we have demonstrated intensity stochastic resonance in 2D polariton bistability. We discussed about the effect of two stable states gradients on stochastic resonance phenomenon and its main quantifiers.

5.4 Spinor stochastic resonance

5.4.1 Introduction

Nowadays, frequency and intensity modulation are two common ways of encoding the information in optical communication technology. Although spin property of light could increase the degree of freedom for data transformation, the light polarization modulation is rarely used mainly because of the loss of polarization through optical fiber transmission. During the last decade, this idea motivated plenty of experimental and theoretical works on optical devices which their operation is based on light polarization [99, 100]. Spintronics and, more recently, spinoptronics [11, 56] are research fields demonstrating innovative devices that take advantage of the spin properties of the charge carriers. Furthermore, a number of studies

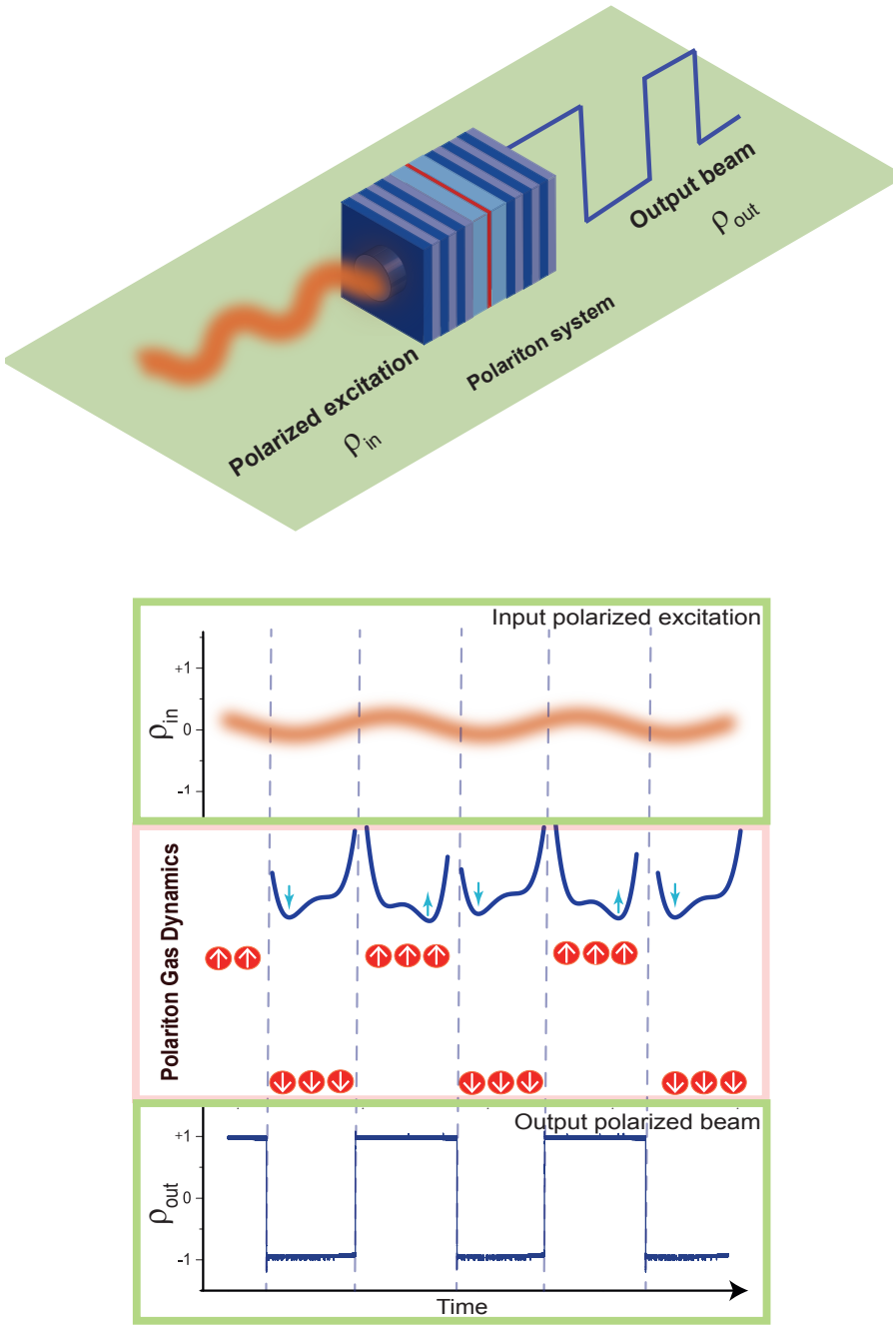

Figure 5.12: **Principle of spinor stochastic resonance.** A noisy polarization modulated signal around linear polarization state controls the polariton population between two well-defined spin states ±1. The spin-trigger regime can be simply modeled as a double well potential in two spin states ↑ and ↓. Altering the input polarization ρ_{in}, favors one of these wells compared to the other one. This induces polarization ordering of polariton population in time with a defined spin either up or down. As a result, the emitted light possesses full circular polarization which alternates between $\sigma+$ and $\sigma-$.

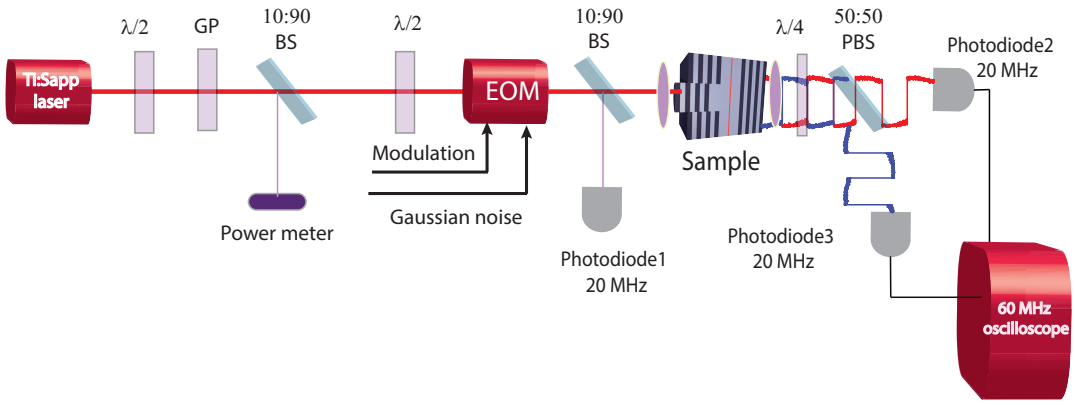

Figure 5.13: **Spinor stochastic resonance setup** The cw single mode laser excites resonantly a microcavity polariton gas. By means of a half wave plate ($\lambda/2$), mounted on motorized rotation stage, and a Glan polarizer (GP) excitation laser power is tuned with high precision. Polarization modulation and polarization Gaussian noise are imprinted on laser light using EOM. Using a quarter wave plate ($\lambda/4$) emitted light is converted in linear polarization. Polarizing beam splitter (PBS) separates horizontal and vertical components of the polarized emission. Spin-up and Spin-down polaritons are detected simultaneously using two fast photodiodes.

have focused on optical devices based on the polariton non-linearities [11, 10, 101, 54, 55]. In this framework, noise intrinsically affects the overall dynamics of system and should be studied carefully. Consequently, we investigate the effect of polarization modulation and also of polarization noise on polariton dynamics. Some works on stochastic resonance, based on spin control, have been reported in magnetic materials [102, 103, 104]. In particular, stochastic resonance has been demonstrated in a nanoscale spin-valve driven by spin-polarized current [102]. Nevertheless to the best of our knowledge only the populations of the bistable states are driven and the demonstration of a spin ordering induced by fluctuations was still missing.

In this section, we take advantage of the particular spin properties of exciton-polaritons to open a novel field of stochastic resonance. We name this phenomenon "*spinor stochastic resonance*", which is based on fluctuation-induced spin-ordering in collective exciton-polariton excitations. Spinor stochastic resonance (SSR) is evidenced by the spin amplification of the noisy modulated input signal.

We consider a spin-trigger regime (see chapter 3) that simply originates from a double well potential featuring two spin states: spin-down ($\downarrow$) and spin-up ($\uparrow$). Then, by imprinting polarization noise and modulation we study the dynamical response of both spin up ($I_{\sigma+}$) and spin down ($I_{\sigma-}$) polaritons (Fig. 5. 12).

5.4.2 Experimental setup

The experimental setup is shown in Figure 5. 13 which is almost same as Fig. 3. 2 path number 2. As in the previous case of intensity stochastic resonance we excite the sample at normal incidence (k=0) using cw single mode Ti:Sapphire laser with 20 μm diameter. A half-wave plate mounted on a motorized rotation stage accompanied with a Glan polarizer is used in order to tune the excitation power with high precision. Using a non-polarizing beam splitter 10 percent of the laser light is sent to power meter to monitor the excitation power. The laser then passes through the second half-wave plate to make sure the input light polarization of EOM is prepared along the vertical direction. By means of EOM, we apply external modulation and noise on the polarization of laser beam. The excitation polarization is accurately controllable and allows tuning fully the laser polarization from left circular to linear and then to right circular polarization state. The transmitted signal is projected into the circular polarization basis using a quarter-wave plate, which converts spin-up and spin-down populations into cross-linear polarizations. We then separate the two linear polarizations using a polarizing beam splitter. We record two spin populations simultaneously with two 20 MHz bandwidth photodiodes connected to a 60 MHz bandwidth oscilloscope. We present the results based on excitation (ρ_{in}) and emission (ρ_{out}) circular polarization degree defined as:

$$\rho_{in,out} = \frac{I_{\sigma+} - I_{\sigma-}}{I_{\sigma+} + I_{\sigma-}} \tag{5.7}$$

5.4.3 Noise-induced-spin-ordering

Spin-trigger

We perform the experiments with a confined 3 μm mesa at exciton-cavity detuning of $\delta = 2.55$ meV. The laser energy is blue detuned from the polariton ground state ($\Delta = 0.8$ meV), and the sample is cooled down to 4K. Scanning the input laser intensity for a fixed input polarization we measure simultaneously the transmitted intensities of both spin up ($I_{\sigma+}$) and spin down ($I_{\sigma-}$) polaritons. Figure 5. 14 shows the two spin populations versus excitation power for four different laser polarizations. For the laser polarization close to linear state, we observe a double hysteresis curve (Fig. 5. 14 **b-d**); The two upper thresholds coincide, while the lower thresholds are decoupled. As discussed before, in the presence of both spin populations, biexciton formation results in nonlinear loss in the system. When the minority spin population falls down to the lower sate, biexciton creation mechanism decrease accordingly and the majority spin intensity increases. Figure 5. 14 **a** shows the behaviour of the two polariton spin populations for laser polarization close to left circular state (-1). We observe a usual polariton bistability for majority polariton population ($I_{\sigma-}$).

We fix the laser power between the lower thresholds of the two spin populations, at 7.8 mW, where polaritons are either on the spin-up or spin-down state of the hysteresis (Fig. 5. 14). Then for this fixed laser intensity, using the EOM, we tune the polarization degree (ρ_{in}) from

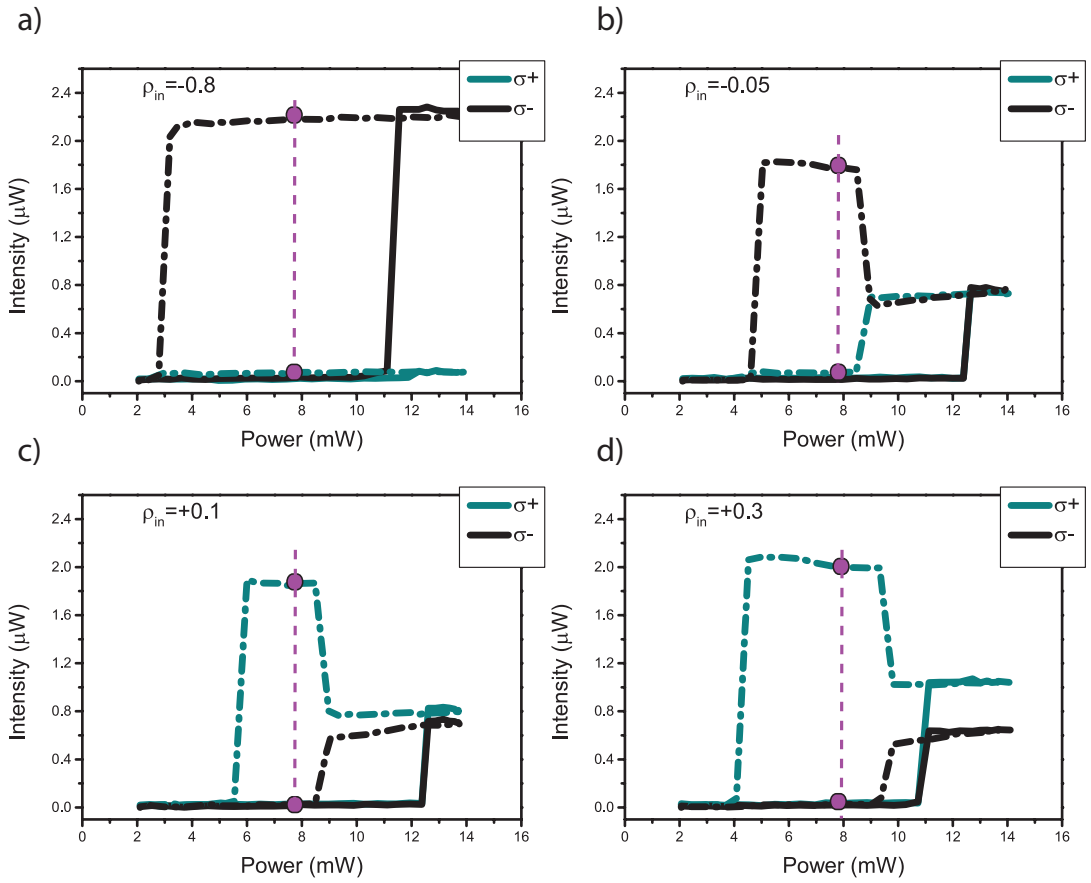

Figure 5.14: **Spinor bistability measurement** The excitation power is scanned from 2 mW to 14 mW forward and backward for four fixed polarization degrees ρ_{in}=-0.8, -0.05, +0.1 and +0.3. The exciton-cavity detuning is δ = 2.55 meV and the laser is blue detuned from the polariton ground state by Δ = 0.8 meV. **a** At large circular polarization degree (ρ_{in}=-0.8), the system shows a conventional polariton bistability. **b-d** Biexciton formation results in a nonlinear loss in the system. This gives rise to the middle stable branch around 10 mW. When the minority spin population jumps back to its lower state, biexciton creation mechanism decrease and all the majority spin population remain in resonance with the laser. Consequently majority polariton intensity jumps up. For the following experiments laser power is fixed at 7.8 mW(dash line).

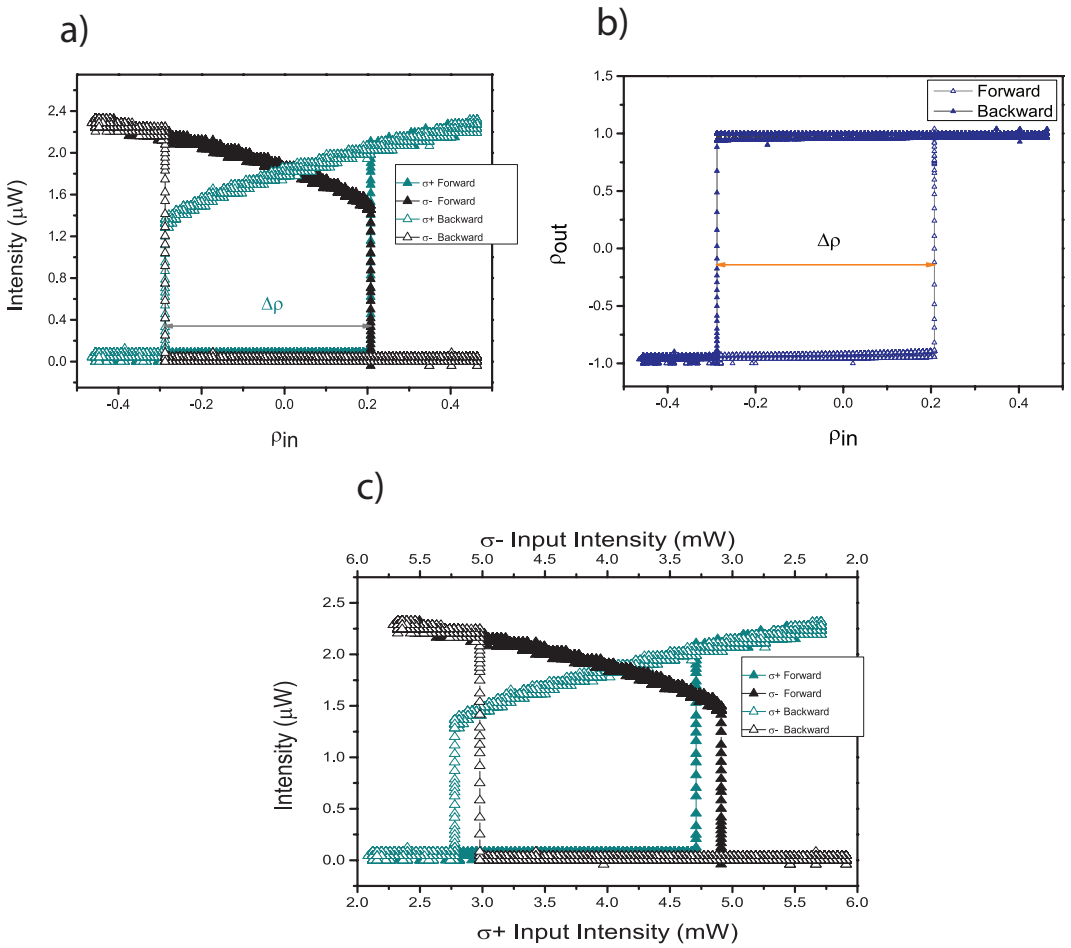

Figure 5.15: **Spin-trigger regime** For the excitation power of 7.8 mW (see Fig 5. 14), the laser polarization degree is scanned between -0.45 and 0.45 forward and backward. **a** Spin-up and spin-down polariton emission intensities versus excitation polarization degree show two overlapping bistabilities. **b** The polariton polarization degree versus input polarization shows the hysteresis behaviour called spin-trigger regime ($\Delta\rho$=0.5). **c** Both polariton spin populations as a function of effective laser power for each spin-up (lower axis) and spin-down (upper axis) polaritons. The curves evidence two polariton bistability loops with the same width (ΔB=1.93 mW).

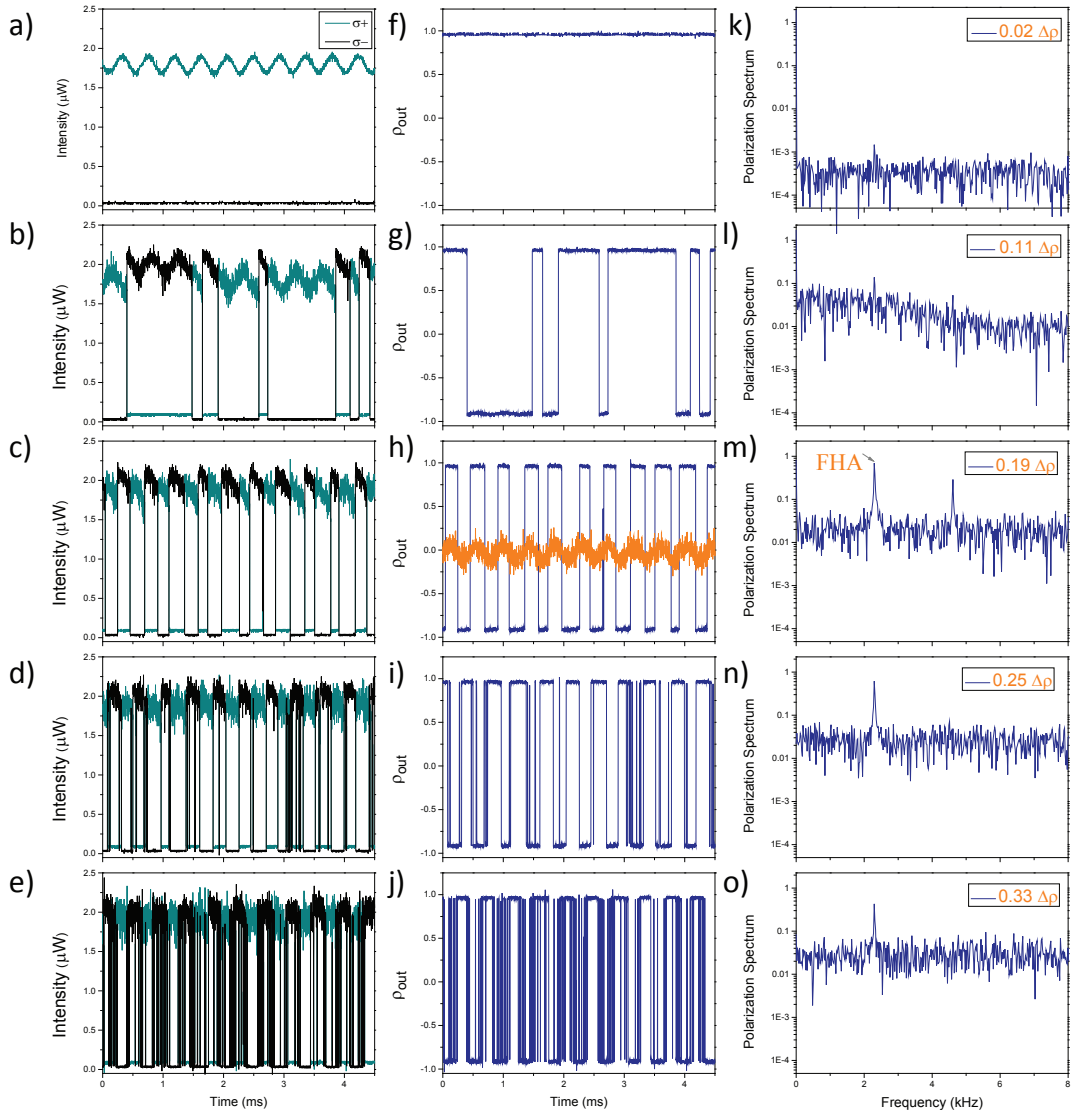

Figure 5.16: **Demonstration of spinor stochastic resonance. a-e** Spin-up (green) and spin-down (black) polariton population in time domain whereas noise intensity is continuously increased: 39 μW (0.02ΔB), 212 μW (0.11ΔB), 367 μW (0.19ΔB), 482 μW (0.25ΔB), 637 μW (0.33ΔB). **f-j** Polariton spinor state in time domain (corresponding to (a-e)) for different polarization noise: 0.02$\Delta\rho$, 0.11$\Delta\rho$, 0.19$\Delta\rho$, 0.25$\Delta\rho$, 0.33$\Delta\rho$. **k-o** Frequency spectra corresponding to (f-j). The frequency and the amplitude of modulation are ν = 2.33 kHz and A_0 =0.17$\Delta\rho$ respectively. FHA is the first harmonic amplitude.

circular-left (-1) to circular-right (+1) favoring respectively the creation of spin-down or spin-up polaritons. We show in Figure 5. 15 **a** the spin up and spin down polariton populations obtained when scanning the laser polarization degree (ρ_{in}) between -0.45 and +0.45 forward and backward. We obtain this graph with the X-Y method (See section 3. 5). For ρ_{in}=-0.45, spin down polaritons are majority populations within the microcavity, and consequently the spin up polariton intensity is near zero. Upon varying the excitation polarization in the circular-right direction, at ρ_{in}=0.21, $\sigma-$ polaritons fall back to the lower state and reversely $\sigma+$ polaritons are in the upper state. Then by sweeping the ellipticity in the backward direction, we observe the second threshold at ρ_{in}=-0.29 and polaritons turn back to the spin-down state. Using equation (5. 7), we determine polariton polarization state (Fig. 5. 15 **b**). The detected spin orientation of the polariton population displays clear hysteresis behaviour, directly imaging the bistability of the spin state of polaritons. Under such conditions we reach the polariton spin-trigger regime, in which it is possible to switch between the two well-defined polarization states: spin-up ↑ and spin-down ↓ with a large hysteresis width $\Delta\rho$=0.5. The excitation polarization degree determines the effective laser intensity which drives each spin population ($F_{\pm}$), even though their addition would be constant at fixed laser power (7.8 mW). In Figure 5. 15. **c** we show the intensity of spin up ($I_{\sigma+}$) and spin down ($I_{\sigma-}$) polaritons versus their corresponding laser intensities. We start with (F_+=2.15 mW) spin up and (F_-=5.65 mW) spin down excitation laser that is equivalent to ρ_{in}=-0.45. Clearly in such conditions, the majority polariton population ($I_{\sigma-}$) which are in the resonance with the laser are located on the upper state. When increasing the $\sigma+$ contribution of the laser, for a certain amount of laser polarization (F_+=3.09 mW), spin down polaritons jump back to the lower state and reversely spin up polaritons are in resonance with the laser. Then by changing the input polarization in the backward direction, we observe the second threshold at (F_-=2.77 mW). Finally we have two polariton bistabilities for two different spin populations with the same width of (ΔB=1.93 mW).

Two synchronized spin populations

At this point, in order to study the interplay between external fluctuations and periodic signal in polarization, we fix the laser polarization in the middle of double hysteresis (F_+=3.74 mW, F_-=4.05 mW) (Fig. 5. 15 **c**), which corresponds to ρ_{in}=-0.04 the middle of spin-trigger hysteresis (Fig. 5. 15 **b**). Then, using the EOM, we imprint a weak sinusoidal signal together with a 500 KHz white noise on the laser polarization. The modulated force and external noise in spin can be interpreted as two different anticorrelated signals affecting spin up and down polaritons separately. Furthermore, each signal centered on linear polarization and both bistability having exactly same size, this leads to an equal amount of external force, noise and modulation for both polariton spin populations. Then, we sweep the polarization of the excitation with a small sinusoidal modulation amplitude $A_0 < 0.5\Delta\rho$. Adding a proper amount of Gaussian noise in polarization to the modulation signal permits polaritons to overcome nonlinear thresholds and to switch between well-defined spin states. In the following, we will not iterate that sinusoidal modulation and noise are applied on the polarization and not on

the intensity.

We did the experiment for modulated signal amplitude of $A_0 = 0.17\Delta\rho$. The modulated signal frequency is $\nu_0 = 2.33$ kHz. While increasing the polarization noise standard deviation ($D_{\rho_{in}}$), we record simultaneously the polariton emission intensities in the circular basis $I_{\sigma+}$ and $I_{\sigma-}$ as a function of the time (Fig. 5. 16 **a-e**). Then using Eq. (5. 7), we compute circular polarization degree of the polariton population ρ_{out} (Fig. 5. 16 **f-j**). We Fourier transform polariton polarization time streams recorded for a 50 ms period to obtain polarization spectra with a spectral resolution of 21 Hz (Fig. 5. 16 **k-o**). The noise $D_{\rho_{in}}$ is changed from 0.02 to 0.33 $\Delta\rho$. Practically, the polarization noise ($D_{\rho_{in}}$) which is imprinted on laser DC power, can be measured through intensity noise (D_σ) of both spin population. Since the two intensity fluctuations are anticorrelated, the effective noise is equivalent for spin-up and spin-down noise. Then, using equation (5. 7) we calculate spin noise in the system .We normalize the intensity noise for spin-up and spin-down laser intensity by the bistability width (ΔB) in Figure 5. 15 **c**. Spin noise values are also normalized by spin-trigger width ($\Delta\rho$) (Fig. 5. 15 **b**). The same scenario holds for the applied modulation amplitude. The system is initialized in the upper state, spin up (↑), of the spin-trigger. For low noise intensity ($D_{\rho_{in}}$=0.02 $\Delta\rho$, D_σ=0.02 ΔB), the modulated force is not large enough to reach the polarization thresholds and the system stays in the spin up state (Fig. 5. 15 **b**). The periodic signal imprinted on laser polarization is transmitted through coherent spin ensemble of spin up polaritons, while the spin down polariton population is locked on the lower state (Fig. 5. 16 **a, f**). Because of flatness of the lower state in hysteresis (Fig. 5. 15 **c**), the spin down population cannot transmit input modulated signal properly. In Figure 5. 16 **f** we show the circular polarization degree of polariton population. Note that, the transmission of the input modulation through spinor response of the system is negligible (Fig. 5. 16 **k**). In Figure 5. 16 **b, g**, by increasing the noise intensity to ($D_{\rho_{in}}$=0.11 $\Delta\rho$, D_σ=0.11 ΔB), the superposition of periodic signal and external fluctuations starts to induce erratic jumps between two spin populations , and accordingly we see a large amount of background noise at low frequency (Fig. 5. 16 **l**). For an optimized amount of external fluctuations ($D_{\rho_{in}}$=0.19 $\Delta\rho$, D_σ=0.19 ΔB), we observe synchronization between two polariton populations while they jump in resonance with the external laser periodically. Therefore, fluctuations authorize controlling a spinor polariton ensemble inside the microcavity (Fig. 5. 16 **c, h**). To confirm the frequency locking between input and output signal, which is a characteristic of the stochastic resonance, we superimpose the sinusoidal input on Figure 5. 16 **h**. Here we observe experimentally the spinor stochastic resonance behaviour. A noisy modulated polarized input signal coherently controls polariton spin population between two well-defined spin states. Certainly the stronger the fluctuations, the less transmitted signal is measurable from background noise (Fig. 5. 16 **e, j, o**).

Spinor stochastic resonance quantifiers

First harmonic amplitude and spin amplification To reveal the spinor stochastic resonance, by tuning the polarization noise ($D_{\rho_{in}}$) between 0.02 $\Delta\rho$ and 0.6 $\Delta\rho$, we study the

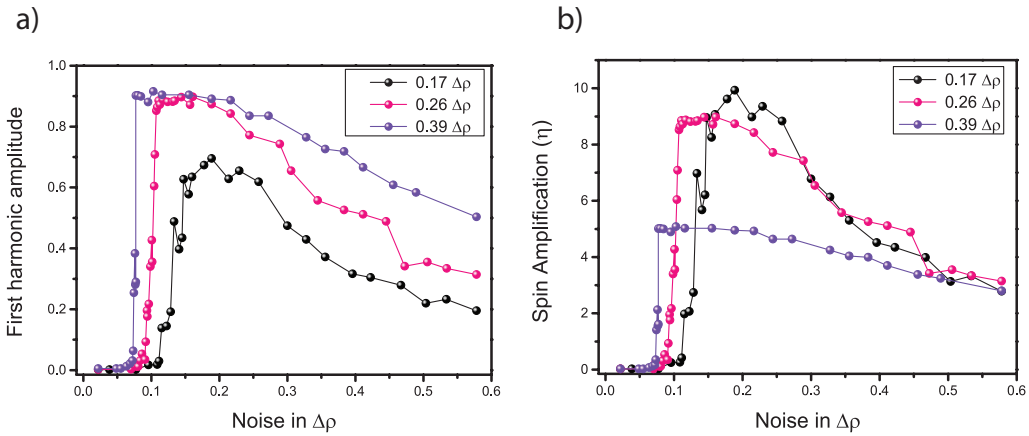

Figure 5.17: **First harmonic amplitude and spin amplification for spinor stochastic resonance. a** First harmonic amplitude for polarization modulation $A_0 = 0.17\Delta\rho$, $0.26\Delta\rho$, $0.39\Delta\rho$. **b** Stochastic resonance spin amplification for same amplitudes of spin modulations. Polarization noise normalized in $\Delta\rho$ unit.

polariton polarization spectra as a function of the input polarization noise for three different amplitude of the modulated signal.

In Figure 5. 17 **a** we present the first harmonic amplitude (FHA) of polariton polarization spectrum at frequency ν_0 = 2.33 kHz for polarization modulation amplitude (A_0) of 0.17 $\Delta\rho$, 0.26 $\Delta\rho$ and 0.39 $\Delta\rho$. For minimum polarization amplitude (A_0=0.17 $\Delta\rho$), we note that the FHA first increases by increasing the noise intensity, and then reaching a maximum, it decreases again. This is the well-known stochastic resonance effect. By increasing A_0, we evidence the enhancement of the FHA. The larger is the polarization modulation amplitude, the easier it is to achieve deterministic jumps of polariton populations between two spin states. Besides, a reduced amount of noise assisted jumps between states leads to less breathing of the pulse width and consequently to larger FHA.

For the same experimental conditions we investigate the polariton spin amplification. The spin amplification is defined as the ratio between the first harmonic amplitude of the output signal (FHA) to the corresponding value for minimum noise input signal (FHA_{in}):

$$\eta = \frac{FHA}{FHA_{in}} \tag{5.8}$$

In Figure 5. 17 **b** we plot the spin amplification as a function of the polarization noise for three amplitudes of input modulation. The extracted FHA_{in} for the amplitudes of A_0=0.17 $\Delta\rho$, 0.26 $\Delta\rho$ and 0.39 $\Delta\rho$ are 0.07, 0.1 and 0.18 degree of polarization, respectively. For $A_0 = 0.17\Delta\rho$, we observe a large spin amplification, reaching the stochastic resonance condition at $D_{\rho_{in}}$=0.19 $\Delta\rho$. This behaviour clearly indicates the critical role played by the spin fluctuations on the transmission of the carried input signal at the input frequency (ν_0). Eventually, synergic inter-

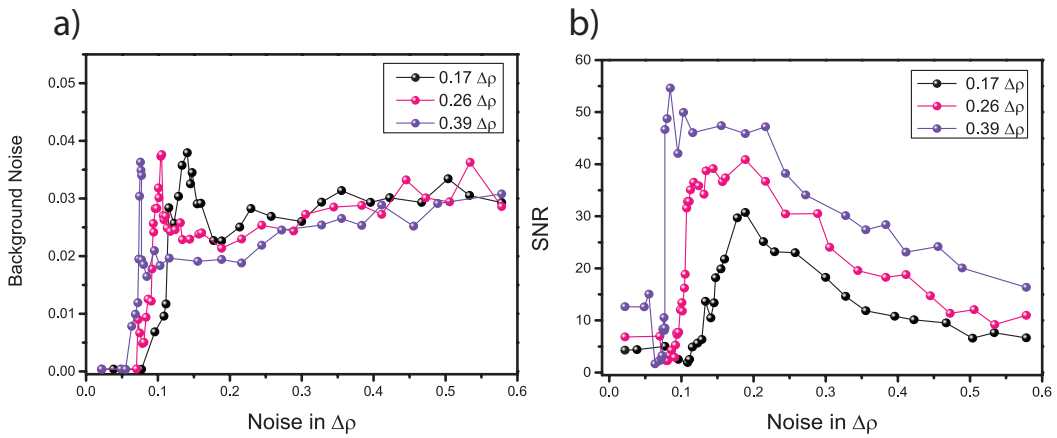

Figure 5.18: **Background noise and SNR for spinor stochastic resonance.** **a** Background noise averaged between 2.42 kHz and 3.83 kHz for polarization modulation $A_0 = 0.17\Delta\rho$, $0.26\Delta\rho$, $0.39\Delta\rho$. **b** Signal-to-noise ratio for the same amplitudes of spin modulations.

play between noise and modulation in spin domain promotes the system to amplify the input polarization through the microcavity. Upon increasing the modulation amplitude, the amplification decreases accordingly and the resonance shape is less pronounced. Consequently the amount of noise allowing the observation of stochastic resonance decreases and the system tends to show a flat response for different noise amplitudes.

Background noise and signal-to-noise ratio To evaluate the role of the spin noise, we study the spin spectrum noise background ($N(\nu, D)$) averaged between 2.42 kHz and 3.83 kHz. By increasing noise intensity, because of random jumps of polaritons between spin-trigger lower and upper states, background noise increases drastically. Achieving the spinor stochastic resonance, for optimum noise intensity, background noise reduces and then increases with a small slope (Fig. 5. 18 **a**).

For the same modulated-signal-polarization amplitudes, we study the signal-to-noise ratio (SNR) defined as:

$$SNR = \frac{FHA}{N(\nu, D)} \tag{5.9}$$

Similar to the polariton spin amplification, we notice the expected stochastic resonance behaviour as a function of the noise (Fig. 5. 18 **b**). For minimum polarization amplitude $A_0 = 0.17\Delta\rho$, the resonance shape is more obvious compared to $0.26\,\Delta\rho$ and $0.39\,\Delta\rho$. In fact, for larger A_0, deterministic jumps of polaritons between the two spin states are preferred. This indicates an increase of the SNR complemented by a decreasing of the $D_{\rho_{in}}$ value needed to reach the stochastic resonance. Finally, comparing Figures 5. 17 and 5. 18, one can notice that the spin amplification at the stochastic resonance always goes together with a recovering of the SNR.

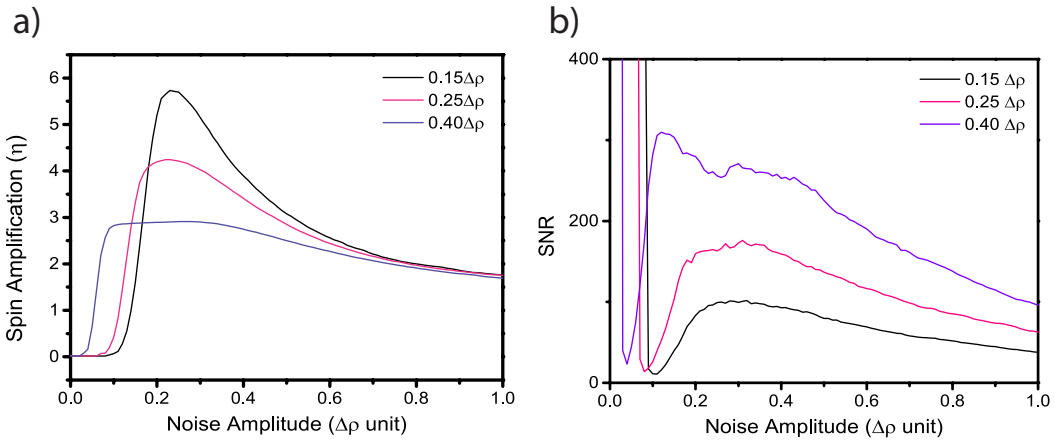

Figure 5.19: **Numerical spin amplification and SNR for spinor stochastic resonance. a** Numerical spin amplification and **b** Numerical SNR for spin modulation amplitude of $A_0 = 0.15\Delta\rho, 0.25\Delta\rho, 0.40\Delta\rho$. The noise standard deviation varies from 0 to 1 $\Delta\rho$.

Theoretical model

Similarly to the intensity stochastic resonance case, we study the two spin mode polariton wave functions ($\Psi\downarrow,\uparrow$) using spinor Gross-Pitaevskii equation obtained in the circular basis ($\sigma+,\sigma-$):

$$i\frac{d\Psi_{\uparrow,\downarrow}}{dt} = [-\Delta - i(\gamma_p + \beta|\Psi_{\downarrow,\uparrow}|^2) + \alpha_1|\Psi_{\uparrow,\downarrow}|^2 + \alpha_2|\Psi_{\downarrow,\uparrow}|^2]\Psi_{\uparrow,\downarrow} + \frac{\epsilon_{lin}}{2}\Psi_{\downarrow,\uparrow} + F_{\uparrow,\downarrow} \tag{5.10}$$

where ϵ_{lin}, β, and γ_p represent linear polarization splitting, biexciton nonlinear loss, and polariton linewidth, respectively. Δ is the energy detuning between the laser energy and the polariton ground state. We consider anisotropic spin interactions between co-polarized (α_1) and cross-polarized (α_2) polaritons. Randomly polarized driving fields $F_{\uparrow,\downarrow} = \sqrt{I_{\uparrow,\downarrow}}$ for the two polariton polarizations, are writen as

$$I_{\uparrow,\downarrow}(t') = \frac{I_0}{2} \times |\rho_{in} \pm 1 + A_0\cos(2\pi\nu_0 t' + \phi) + D(t')| \tag{5.11}$$

where D, the polarization noise amplitude, follows a normal distribution with standard deviation $D_{\rho_{in}}$ and $|\rho_{in}| < 0.25$ is the DC polarization component of the laser excitation. I_0 is the fixed laser intensity expressed as $I_0 = I_{\sigma+} + I_{\sigma-}$. Since the intrinsic polariton dynamics (few GHz) is orders of magnitude faster than the modulation frequency, we can apply the adiabatic approximation and consider $F_{\uparrow,\downarrow}$ as constant driving term in equation (5. 10). $_{F\uparrow,\downarrow}(t')$ is an input time sequence of 1 second with time steps of 2 μs, corresponding to the noise correlation time. Here the polarization noise can be approximated as a white noise since the modulation frequency is only 2.3 kHz. The spin-trigger width ($\Delta\rho$) is obtained with the

following set of parameters: $\alpha_1 = 0.01$ meV, $\alpha_2 = 2.8$ μeV, Δ =0.6 meV, ϵ_{lin} =0.06 meV, β =1.98 μeV and $\gamma = \hbar/13$ ps with $\hbar$ the reduced Planck constant. The results of numerical simulation for spin amplification and SNR are presented in Figure 5. 19 **a, b**, respectively. All the experimental features described above are qualitatively well reproduced by our model. Numerical SNR diverges for minimum polarization noise, while residual experimental noise prevents experimental SNR to display large values.

Modulation frequency and activation noise

As mentioned before, by applying an optimal amount of noise to the particles in double-well potential, synchronization between the Kramers rate and the frequency of applied modulated

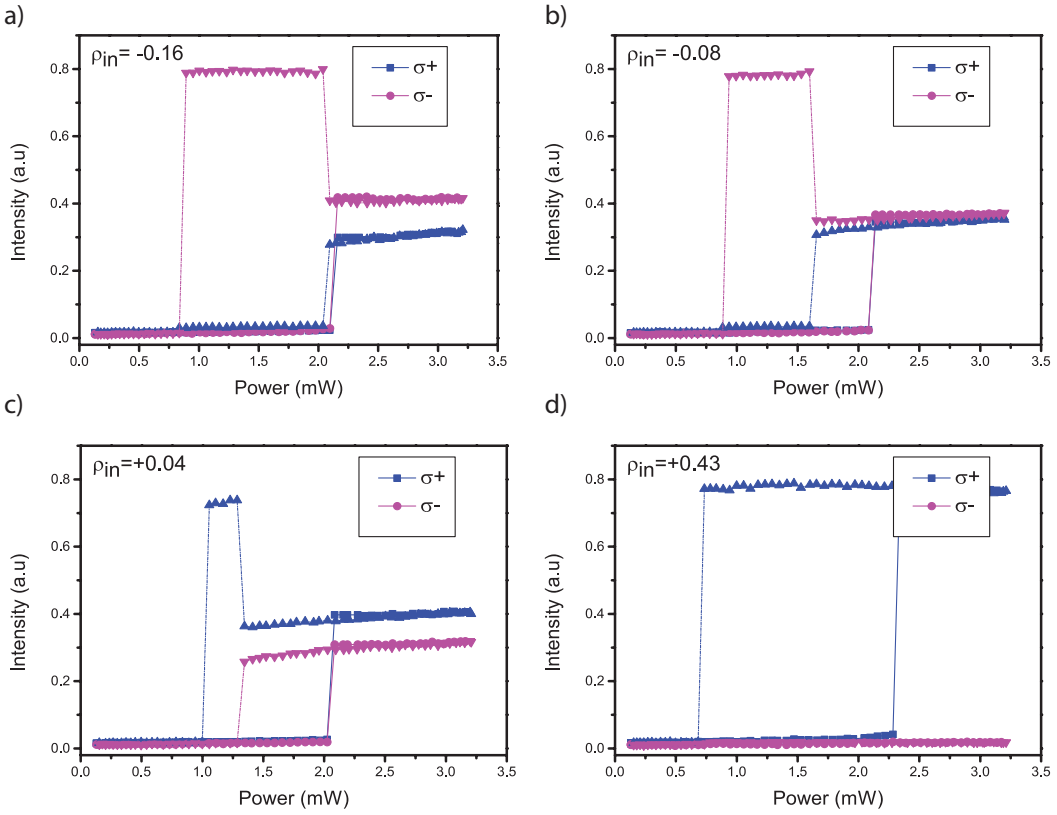

Figure 5.20: **Spinor bistability measurement** The excitation power is scanned from 0.1 mW to 3.2 mW forward and backward for four fixed polarization degrees ρ_{in}=-0.16, -0.08, +0.04 and +0.43. The exciton-cavity detuning is δ = 1.32 meV and the laser is blue detuned from the polariton ground state by Δ = 0.7 meV. **a** Due to the biexciton resonance, the formation of the middle stable branch is observed around 2.5 mW. **b** By changing the excitation polarization degree towards ρ_{in}=0, the minority lower threshold shifts to smaller laser power. **d** At the polarization degree of ρ_{in}=+0.43, the system shows a conventional polariton bistability. For the following experiments, the laser power is fixed at 1.1 mW.

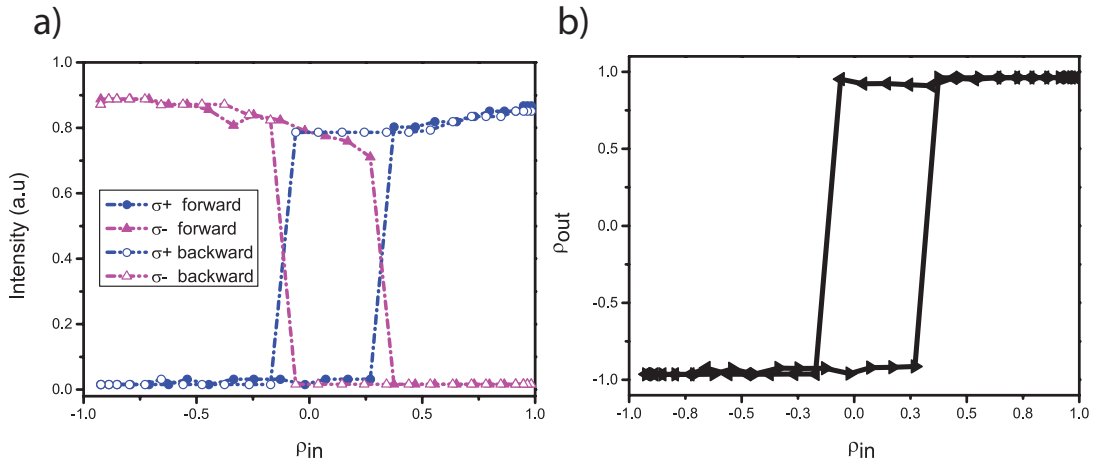

Figure 5.21: **Spin-trigger regime.** For the excitation power of 1.1 mW (see Fig 5. 20), the laser polarization degree is scanned between -1 and+1 forward and backward. **a** Spin-up and spin-down polariton emission intensities versus excitation polarization degree show two overlapping bistabilities. **b** The polariton polarization degree versus input polarization shows the characteristic hysteresis behaviour called spin-trigger regime with $\Delta\rho$=0.44.

signal occurs. In order to study the effect of modulation frequency we prepared the experiment in a 3μm mesa structure with exciton-cavity detuning of δ=1.32 meV. The continuous wave laser is blue detuned by Δ=0.7 meV respect to the polariton ground state. The system shows the typical double bistability for two polariton spin populations as shown in Figure 5. 20. For a fixed laser power (1.1 mW) between the lower thresholds of the spin-up and spin-down polariton populations, we tune the laser polarization degree from left-circular (-1) to right-circular (+1) and vice versa (Fig. 5. 21 **a**). We obtain a polariton spin-trigger with a width $\Delta\rho$=0.44 (Fig. 5. 21 **b**). We fix the laser polarization at ρ_{in}=+0.05 in the middle of the spin-trigger regime. For a modulation amplitude of A_0=0.3 $\Delta\rho$, we investigate the system response for two modulation frequencies of ν_0=1 kHz and 4.8 kHz.

In Figures 5. 22 and 5. 23 we show the effect of polarization noise on spin property of exciton-polariton populations for two different modulation frequencies of 1 kHz and 4.8 kHz, respectively. For the minimum polarization noise ($D_{\rho_{in}}$=0.01 $\Delta\rho$) the polariton population is stable in one spinor state (+1) (Fig. 5. 22 **a**, Fig. 5. 23 **a**). By increasing the noise power, polariton spinor state starts to switch randomly between two well-defined stable branches ($\pm$ 1). For ν_0=1 kHz, the critical polarization fluctuations needed for noise –induced hopping is $D_{\rho_{in}}$=0.14 $\Delta\rho$ (Fig. 5. 22 **b**), while for ν_0=4.8 kHz this value increases to $D_{\rho_{in}}$=0.16 $\Delta\rho$ (Fig. 5. 23 **b**). At such noise amplitudes we measure a large amount of background noise, which comes from low frequency random jumps between the two stable states (Fig. 5. 22 **f**, Fig. 5. 23 **f**). For larger amounts of polarization noise, $D_{\rho_{in}}$=0.25 $\Delta\rho$ at ν_0 =1 kHz and $D_{\rho_{in}}$=0.27 $\Delta\rho$ at ν_0 =4.8 kHz, we clearly demonstrate spinor stochastic resonance in time and frequency domains (Fig. 5. 22 **c, g**, 5. 23 **c, g**). For larger noise amplitudes the polariton spinor state starts

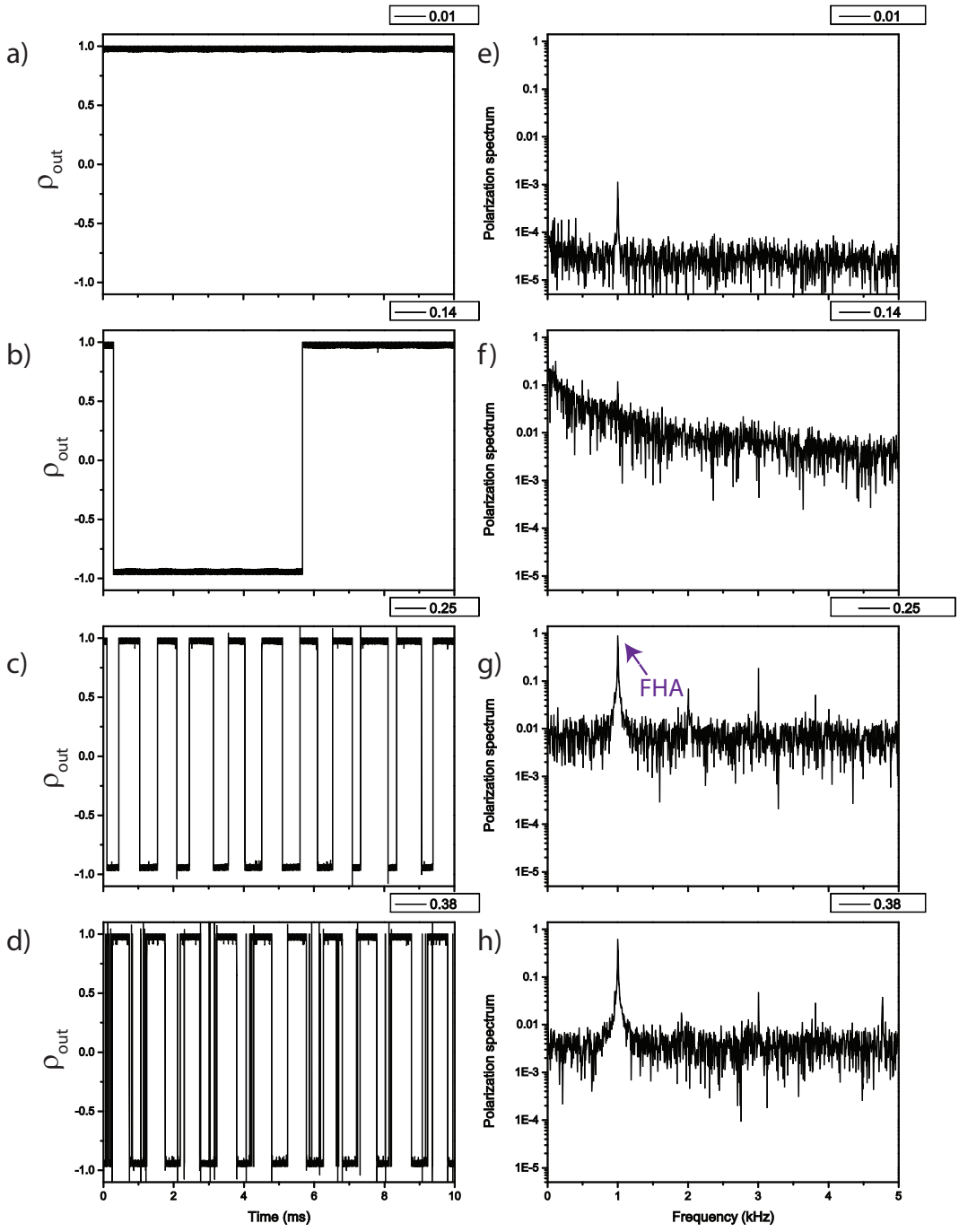

Figure 5.22: **Demonstration of spinor stochastic resonance at 1 kHz. a-d** Time domain traces of the polariton spinor state upon continuous increasing of the noise intensity: 0.01$\Delta\rho$, 0.14 $\Delta\rho$, 0.25 $\Delta\rho$ and 0.38$\Delta\rho$. **e-h** Frequency spectra corresponding to (a-d). The frequency and the amplitude of modulation are ν_0 = 1 kHz and A_0 =0.3 $\Delta\rho$ respectively. FHA is the first harmonic amplitude.

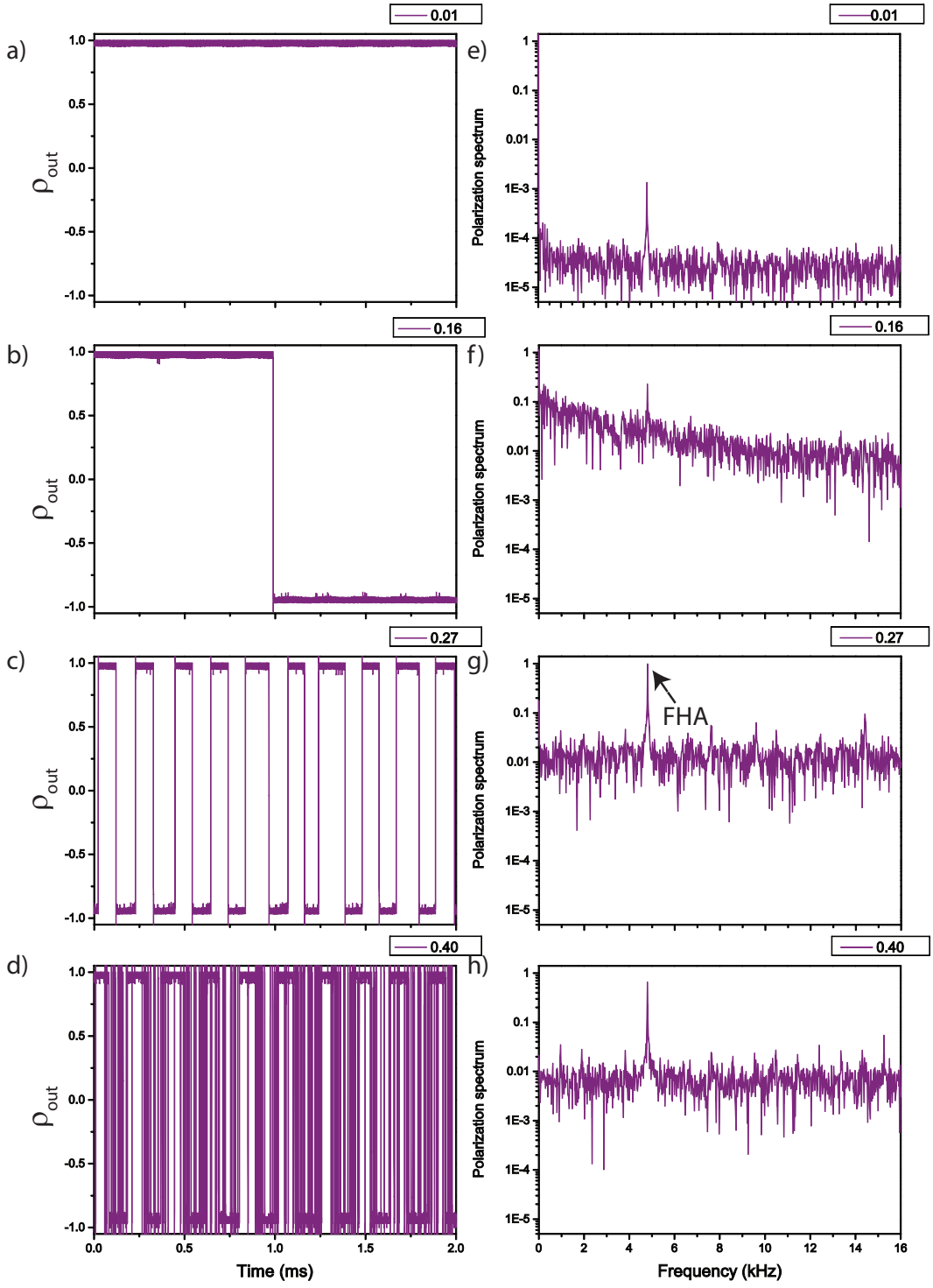

Figure 5.23: **Demonstration of spinor stochastic resonance at 4.8 kHz. a-d** Time domain traces of polariton spinor state upon continuous increasing of the noise intensity: $0.01\Delta\rho$, $0.16\ \Delta\rho$, $0.27\ \Delta\rho$ and $0.4\Delta\rho$. **e-h** Frequency spectra corresponding to (a-d). The frequency and the amplitude of modulation are $\nu_0 = 4.8$ kHz and $A_0 = 0.3\ \Delta\rho$ respectively. FHA is the first harmonic amplitude.

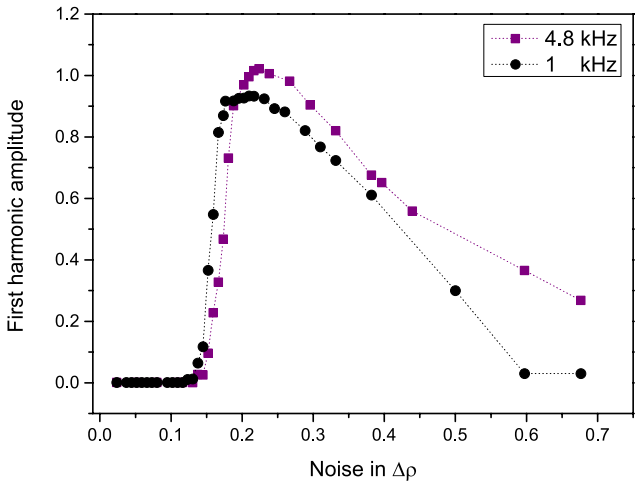

Figure 5.24: **The effect of applied modulation frequency on first harmonic amplitude.** First harmonic amplitude (FHA) versus polarization noise for polarization modulation of $A_0 = 0.3\Delta\rho$. $D_{\rho_{in}}$ tuned from 0.01 $\Delta\rho$ to 0.7 $\Delta\rho$.

to be buried in the noise (Fig. 5. 22 **d**, Fig. 5. 23 **d**).

We tune the polarization noise between 0.02 $\Delta\rho$ to 0.7 $\Delta\rho$. In Figure 5. 24 the first harmonic amplitude (FHA) versus polarization noise is shown. We observe that, for larger modulation frequencies, the optimum spin noise required for stochastic synchronization increases. Indeed the Kramers rate increases with noise power and for higher modulation frequencies the synchronization occurs for larger amounts of noise.

We studied the effect of modulation amplitude and frequency on the spinor stochastic resonance. Concomitant with its intrinsic interest, spinor stochastic resonance might get into broad investigations on the effect of noise on spinoptronic devices and permit to propose schemes taking advantage of intrinsic noise contributions.

5.5 Conclusion

We have reported observation of "*intensity stochastic resonance*" in zero-dimensional and two-dimensional microcavity polaritons under bistable condition. The experimental observations are well reproduced by a model based on the Gross-Pitaevskii equation. The observed behaviour shows the potential of using stochastic resonance as a technique to progress the coherent processing of a signal buried in the noise. This work can opens appealing perspectives for using stochastic resonance as a tool to drive coherent polariton fluids either for fundamental aspects as spontaneous phase transition driven by fluctuation or application in all-optical processing.

We have also demonstrated a new kind of stochastic resonance, in spin-trigger regime, named

"*spinor stochastic resonance*". A noisy polarization modulated signal around a linear polarization state enforces spin ordering of the polariton population, in which the spinor state of the collective polariton excitation alternates periodically between spin-up and spin-down. Consequently, the emitted light with full circular polarization respectively alternates between $\sigma+$ and $\sigma-$. We reproduce theoretically the experimental results using spinor Gross-Pitaevskii equation. Spinor stochastic resonance might be a practical method to amplify the input polarization of telecommunication system working based on spinor state. It can be also an applied technique to improve signal to noise ratio of a spintronic network.

6 Intensity fluctuations of exciton-polaritons

6.1 Introduction

In this chapter, we present the initiation of our study on the degree of coherence of polariton emission intensity fluctuations. Time-dependent intensity fluctuations are a crucial feature for describing a light source, and for defining its possible exploitations and applications. This effect was first investigated in detail by Hanbury Brown and Twiss in 1950s. They discovered photon bunching in light emitted by chaotic source [105]. The Hanbury Brown and Twiss (HBT) experiment is concerned with the concept of second-order correlation function ($g^2(t)$). This quantity authorizes a new classification of light depending whether photon streams are bunched, coherent or antibunched.

Nowadays, correlation functions are used nearly in all branches of modern physics. A coherent source of light can be characterized with $g^2(t) = 1$. Typically, a standard source of incoherent light is characterized via an enhanced probability of emitting photons in bunches. This leads to a zero-delay second-order correlation function $g^2(0) = 2$ [106, 107]. On the other hand, due to the quantum nature of light, photon intensity fluctuations can also provide $g^2(0) < 1$ which is called as photon antibunching.

During the last years, intensive research efforts have been spent on the investigation of light sources with super bunched photon statistics ($g^2(0) > 2$). Superbunching has been experimentally perceived in several environments like near-equispaced multiparticle systems [108], nonlinear crystal superlattices [109], multi-atom entangled Rydberg states [110], and also thermal cavity in the ultrastrong coupling regime [111]. Light sources with large photon correlations are great candidates for a number of practical applications such as many-body phenomenon with strongly interacting photons [112] or photonic quantum information processing [113, 114].

In this chapter we study polariton statistics in a zero-dimensional polariton system in two different regimes: polariton bistability and polariton discriminator regime. We investigate the polariton intensity fluctuations via second-order correlation function using a Hanbury

Brown and Twiss setup. We will investigate the effect of excitation laser power on $g^2(0)$. In the following, the concept of second-order correlation function in multilevel systems will be explained. Then, in section 6. 3 the experimental setup (HBT) will be described. Finally at the end of this chapter, our experimental results will be presented. We will show how random transitions of polariton population between lower and upper stable states of optical bistability can effectively modify polariton second order correlation function characteristics.

6.2 Second-order correlation function

A perfectly coherent light beam with a constant intensity, which is one of the most stable types of light, has Poissonian photon statistics. It is a well-known result that, in this case, the mean value of the photon number ($\bar{n}$) is equal to the photon variance (Δn). Within a general classification of light, there are three possibilities:

Poissonian Statistics ($\Delta n = \sqrt{\bar{n}}$)

Super-Poissonian statistics ($\Delta n > \sqrt{\bar{n}}$)

Sub-Poissonian statistics ($\Delta n < \sqrt{\bar{n}}$)

Generally, for classical chaotic light beams, time-varying light intensity will show super-Poissonian photon number distribution, while the sub-Poissonian light statistics has no classical counterpart. Figure 6. 1 **a** shows the difference between these three regimes. We notice that the photon distribution can be broader (narrower) than the Poisson distribution for super (sub)-poissonian statistics.

Following the Hanbury Brown and Twiss experiment, a new classification of the light is given using the second-order correlation function ($g^2(\tau)$) defined as [31]:

$$g^2(\tau) = \frac{< I(t)I(t+\tau) >}{< I(t) >< I(t+\tau) >} \tag{6.1}$$

where I(t) is the intensity of the light beam at time t. The <...> symbols indicate the time average calculated over a long time period. In the following, we suppose that the spatially coherent light from a small area of the source will be studied.

The correlation degree between the emission of two photons at zero time delay ($g^2(\tau = 0)$), discriminates different types of light: coherent light $g^2(0) = 1$, classical thermal light source with a bunched statistics $g^2(0) > 1$, and finally, a nonclassical light with an antibunched statistics $g^2(0) < 1$. Figure 6. 1 **b** illustrates simply the three different types of light in terms of the photon streams.

The second-order correlation function for a classical source of light satisfies several relations.

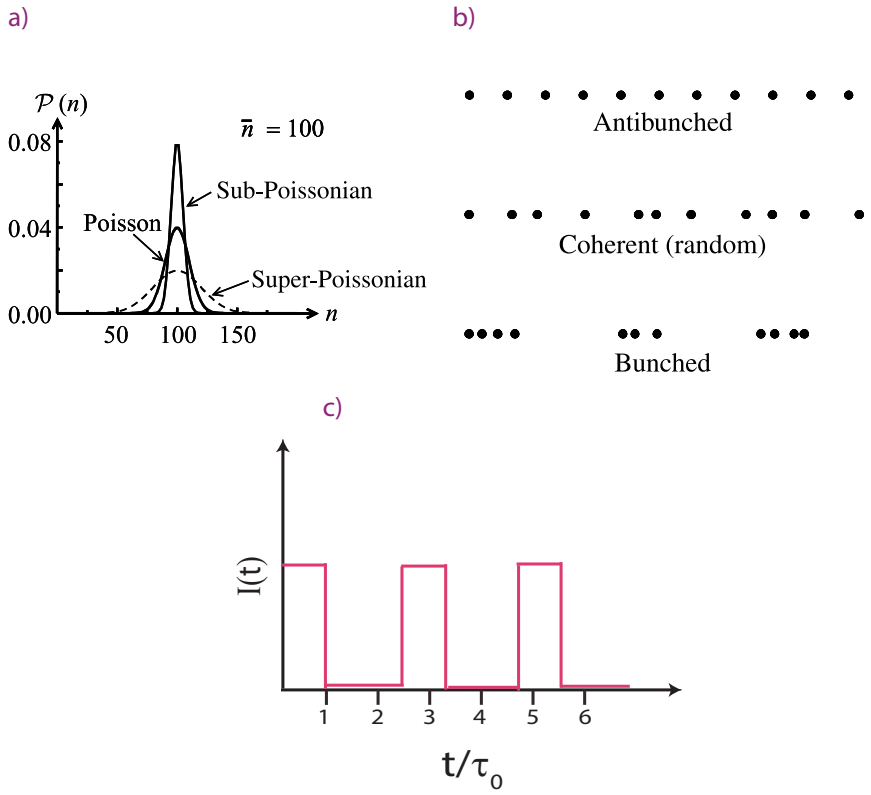

Figure 6.1: **Different categorization of light source. a** From [31]. Photon statistics for light with Poissonian, sub-Poissonian and super-Poissonian distributions. The distributions have the same mean photon number $\bar{n}$=100. **b** Photon streams for antibunched, coherent and bunched light. For a coherent light source, Poissonian distribution resembles the random time intervals between photons. **c** A series of pulse waves with on and off states for τ_0 and 1.5 τ_0 respectively.

According to Cauchy's inequality, for a general case of intensity measurements on two beams

$$< I_1^2 >< I_2^2 > \geq < I_1 I_2 >^2 \tag{6.2}$$

This equation is valid for correlation measurements performed at any random time with a fixed time delay between two beams, and results in:

$$g_{11}^2(0) g_{22}^2(0) \geq [g_{12}^2(\tau)]^2 \tag{6.3}$$

where g_{xx} and g_{xy} represent the correlation function for a single beam or between two different beams, respectively.

For a large enough time delay, much longer than any correlation time between or within the

light beams, the measured intensities are uncorrelated and basically it follows as:

$$g_{11}^2(\infty) = g_{12}^2(\infty) = 1 \tag{6.4}$$

In order to study the degree of second-order coherence in an optical bistable system, we consider a simple example: a train of rectangular pulses (Fig. 6. 1 **c**). We illustrate a series of square waves with pulse duration of τ_0 as 'on' state and 1.5 τ_0 as 'off' state. It can be shown that [115]:

$$g_{11}^2(0) = \frac{1}{n} \tag{6.5}$$

where n represents the number of pulses per unit time multiplied by τ_0. In our example n=0.4 which leads to a superbunched value of $g_{11}^2(0) = 2.5$ at zero time delay. In a more general case of the same rectangular pulses distributed with random times of initiation, one can finds that the degree of second-order coherence is given by:

$$\begin{aligned} g_{11}^2(t) = 1 + (1 + \frac{t}{\tau_0})\frac{1}{\bar{n}} \quad & \text{for } t < \tau_0 \\ 1 \quad & \text{for } t > \tau_0 \end{aligned} \tag{6.6}$$

Where $\bar{n}$ denotes the average number of pulses present simultaneously. The unit term comes from the correlation between different pulses, and the additional term originates from the correlation within individual pulses. For case of $\bar{n} \ll 1$, the latter term would be dominant, while for crowded, multiply-overlapping pulse $\bar{n} \gg 1$, the last term would be negligible. The two terms are called as the 'background' term and 'anomalous' term, respectively [115].

As we have already shown in chapter 4, in a polariton bistable system, small laser fluctuations induce noise-assisted transitions between two stable states with random distribution of pulse durations as residence time. In the next part, we investigate the second-order correlation function of these trains of random pulse waves in polariton bistability.

6.3 Experimental setup

We have measured intensity fluctuations of microcavity polaritons in a 3 μm mesa structure. The setup is shown in Figure 6. 2. The light source is a single-mode tunable cw Ti: sapphire laser with a linewidth in the order of a few MHz. The laser spot diameter onto the sample is 20 μm. In our experiment, the lower polariton branch is excited close to resonance at normal incidence angle with circular polarized laser. Using a noise eater, the laser noise intensity is reduced to 0.1%. The excitation power is precisely controlled through a half-wave plate mounted on a motorized rotation stage in addition to a Glan polarizer. We detect the light in the transmission configuration. In detection, using a 25 μm pinhole, the central part of the polariton light from the 3 μm mesa is incident on a 50:50 beam splitter, and is equally divided between the two silicon avalanche photo diodes (APDs). Their outputs are fed to the

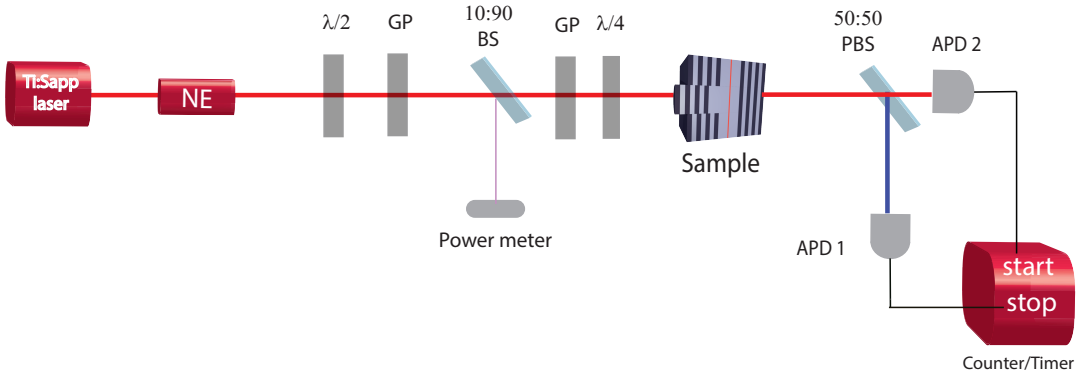

Figure 6.2: **Hanbury Brown and Twiss (HBT) experiment.** The pulses from two avalanche photo diodes (APDs) are fed into the start and stop inputs of a time-correlated single photon counter. The counter/timer records the time between several pulses at the start-stop inputs, and also counts the number of pulses from each detector. Using noise eater (NE) laser noise intensity is reduced to 0.1 percent. The laser power is tuned via a rotating half-wave plate ($\lambda/2$) and a Glan polarizer (GP).

start and stop inputs of a time-correlated single photon counting system. We have used the Time-Tagged-Time-Resolved (TTTR) mode of a PicoHarp controller system, which allows one to record each photon event with its corresponding arrival time and provides off-line data analysis with resolution of 40 picosecond. The average number of counts recorded by each APD in a counting time (T) is given by:

$$N(T) = \frac{\eta P T}{\hbar\omega} \tag{6.7}$$

where $\hbar\omega$, η and P represent photon energy, detector quantum efficiency and light power, respectively. The experiments has been performed with high efficiency APD ($\eta \approx 0.8$) with active area diameter of 20 μm.

The experimental results are presented in two different ways. One is the photon stream for each of the APDs, and the second is the second order correlation function. Since the number of counts registered on a photon counting detector is proportional to the photon intensity, the classical definition of $g^2(t)$ is:

$$g^2(t) = \frac{< n_1(t) n_2(t+\tau) >}{< n_1(t) >< n_2(t+\tau) >} \tag{6.8}$$

where $n_i(t)$ is the number of photon counts registered on APD_i at time t. This means that $g^2(t)$ depends on the simultaneous probability of counting photons at time t on APD_1 and at time t+τ on APD_2 [31].

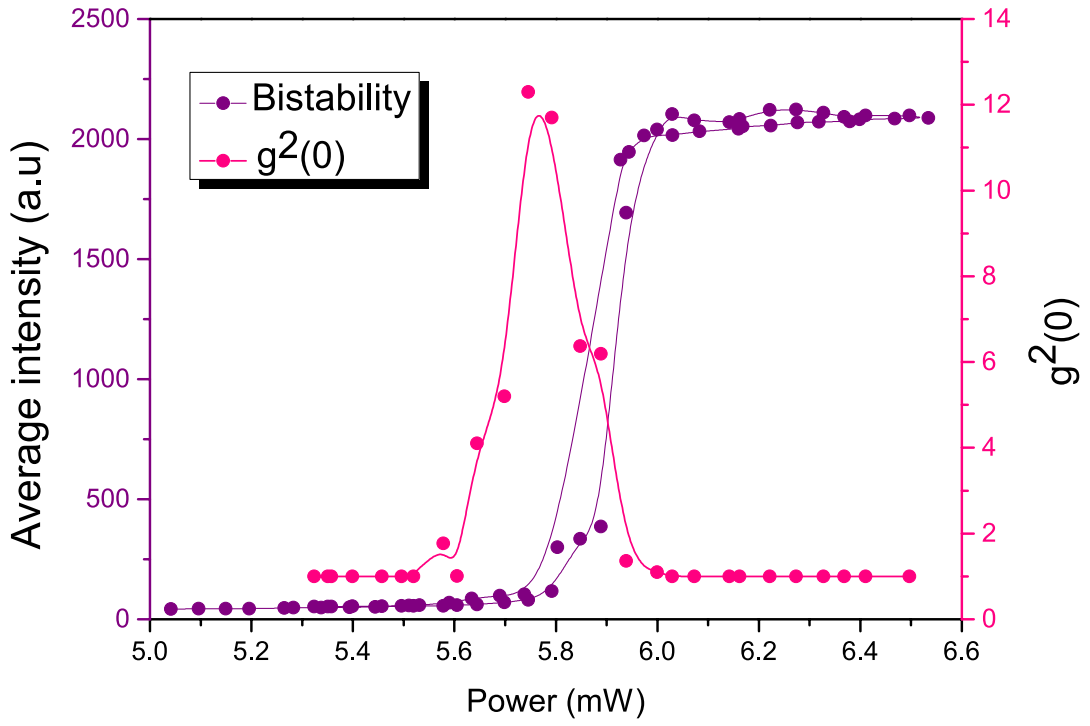

Figure 6.3: **Polariton average intensity and zero-delay second-order correlation function.** Averaged polariton intensity as a function of the excitation power (left axis), and $g^2(0)$ (right axis). For the low and high excitation power coherent light with ($g^2(0) = 1$) is detected, while around nonlinear threshold, due to the bistable behaviour polariton superbunching is observed.

6.4 Results

In order to study polariton intensity fluctuations around nonlinear thresholds, we performed the experiment in two specific cases: optical bistability and optical discriminator in a 3μm mesa structure.

6.4.1 The degree of coherence in optical bistability

This experiment is performed at positive exciton-cavity detuning ($\delta = 1.62$ meV) for which the continuous wave laser is blue detuned ($\Delta = 0.16$meV) with respect to the polariton ground state. By tuning the excitation power in the forward and backward directions, the polariton time streams and accordingly the average intensity of polariton emission have been acquired. In Figure 6. 3 the averaged polariton intensity in both forward and backward directions (purple) in addition to the zero-delay second-order correlation function (pink) are shown. Far below and far above the nonlinear threshold, the polariton light is coherent and the degree of coherence is one. We observe a clear modification of polariton intensity fluctuations around the nonlinear threshold. By increasing the power, $g^2(0)$ increases gradually to a superbunched

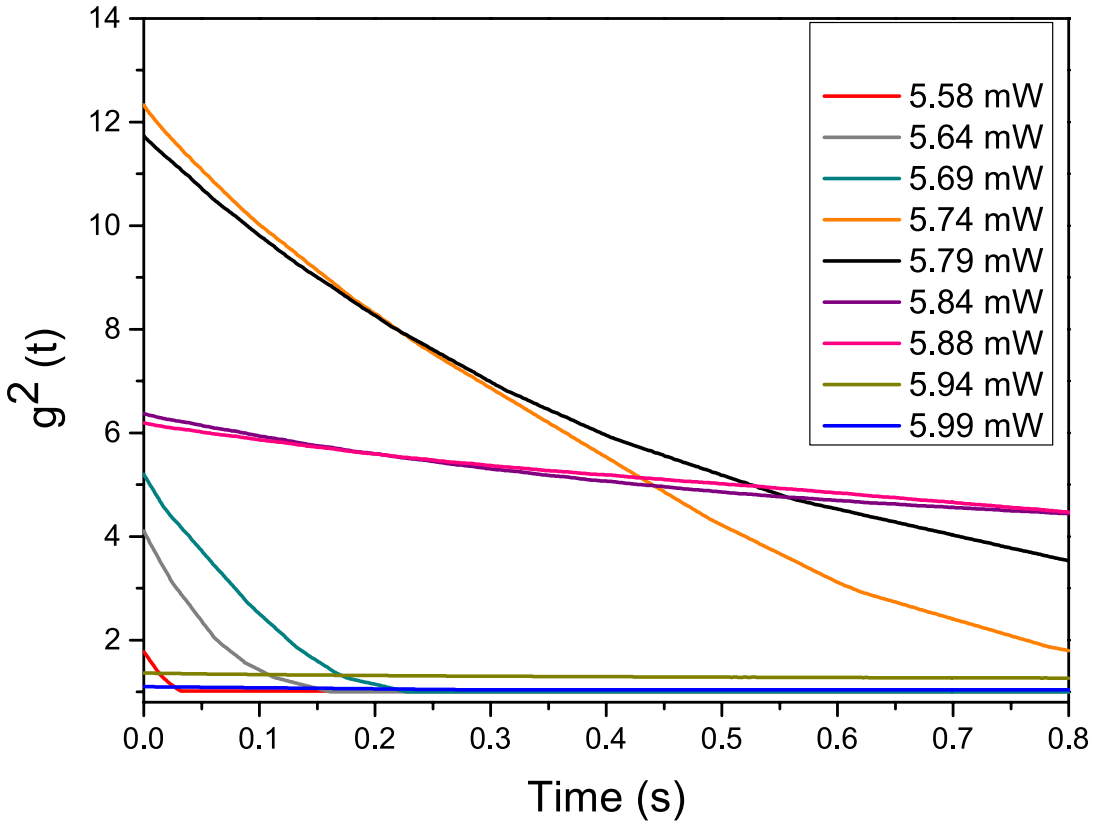

Figure 6.4: **Second-order correlation function.** **a** $g^2(t)$ versus time for several excitation powers below, around and above the bistability threshold. By increasing the power from 5.58 mW to 5.74 mW $g^2(0)$ increase gradually. For further increasing of excitation power, this quantity reduces to 1.

value of 12.3, and then a further rise of excitation power leads to the reduction of this quantity to 1.

In Figure 6. 4 we show a series of $g^2(t)$ measurements for different excitation powers. At P=5.58 mW, we detect a bunch of photons with a short characteristic coherence time (τ_c). By increasing the excitation power up to 5.74 mW, $g^2(0)$ and τ_c boost gradually. For further increase of power the reduction of $g^2(0)$ is concomitant with additional increase in τ_c.

In Figure 6. 5 we have summarized the degree of coherence at zero time delay and the corresponding characteristic times for several excitation powers. By looking at this figure, the main question that arises is to understand which parameters in the polariton bistable system can modify the characteristics of the second-order correlation function? To answer this question, we investigate the polariton time streams for six different excitation powers (Figure 6. 6). From **a** to **d** we show the polariton time streams at P= 5.58 mW, 5.69 mW, 5.74 mW and 5.94 mW which correspond respectively to $g^2(0)$=1.77, 5.2, 12.3 and 1.36 and τ_c=0.013, 0.08, 0.35 and 9.33 second. As presented in the fourth chapter, considering the polariton

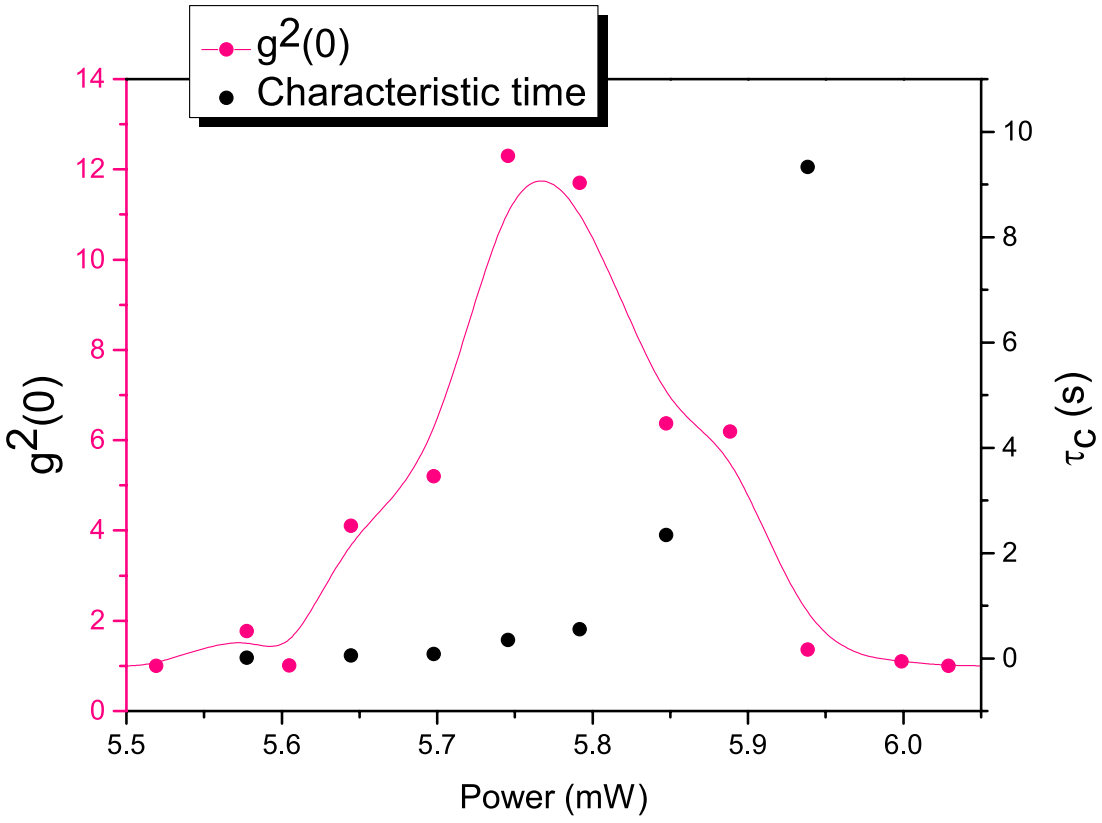

Figure 6.5: **Second-order correlation function characteristics in optical bistability.** The second order correlation function at zero time delay (left axis), in addition to their corresponding characteristic times (right axis) (τ_c).

population initiated on the lower stable state, for fixed laser noise intensity, increasing the excitation power leads to more probable transitions of polaritons to the upper state. According to Eq. 6. 6, the average number of pulses and their corresponding duration play an important role on the zero-delay amplitude and on the characteristic coherence time of the bunched second-order correlation function. Depending on the pulse distribution in the polariton time stream, it is possible to measure several values of $g^2(0)$ with bunching to superbunching. We observe that, by increasing the noise assisted transitions, to an optimal excitation power, $g^2(0)$ gradually increases. Nevertheless, at P=5.94 mW, where double well potential is nearly symmetric and the polariton time stream demonstrates multiple transitions between lower and upper branches, $g^2(0)$ is not any more superbunched and is equal to 1.15 (Figure 6. 6 **d**). It is worth mentioning that $g^2(0)$ is extremely sensitive to the statistics of the photon stream.

Looking at all four polariton streams and comparing with summarized values in Figure 6. 5, one finds that in optical bistable system, the characteristic time of the second-order correlation function (τ_c) represents the statistical time period when polaritons are located on the upper state. For example for P=5.74 mW and P=5.94 mW (Figure 6. 6 **c**, **d**) the characteristic time is

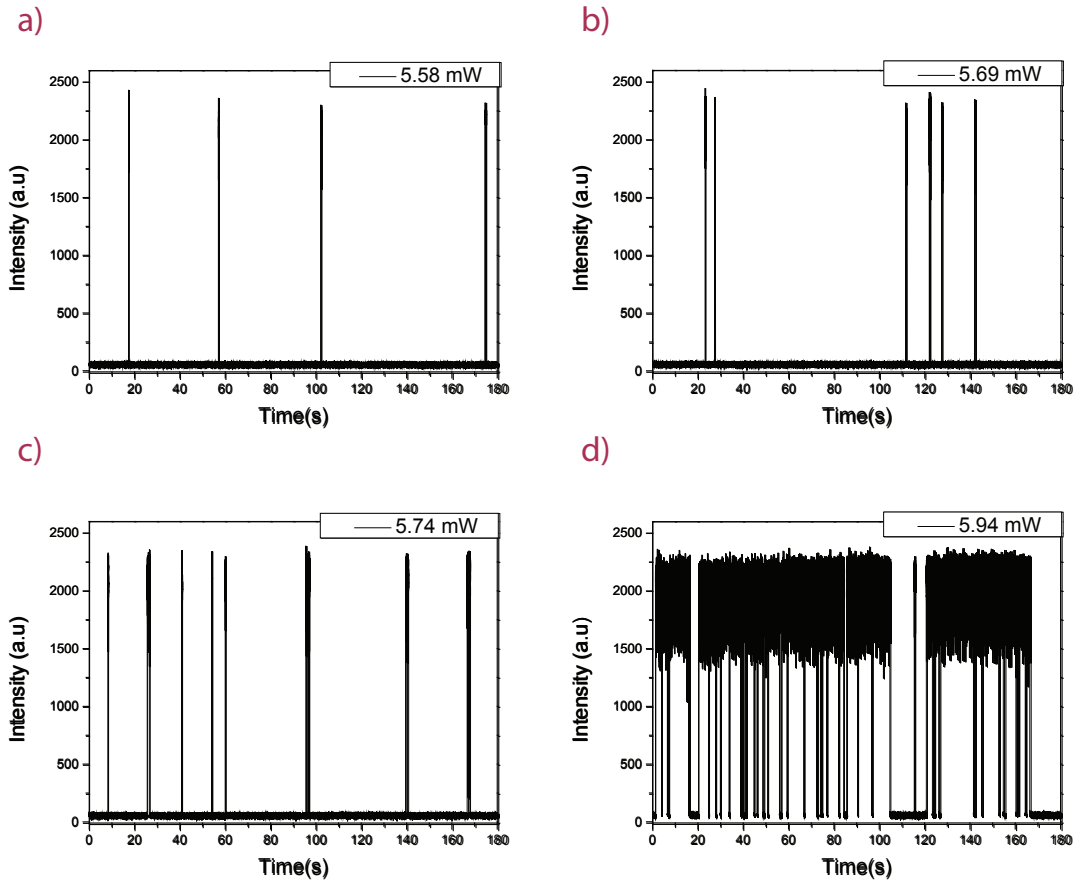

Figure 6.6: **Polariton time streams. a-d** Polariton intensity versus time for 4 different excitation powers: P=5.58 mW, 5.69 mW, 5.74mW and 5.94 mW. For larger excitation powers, noise-assisted transitions of polariton population between two stable states are modified, while the residence time of exciton-polaritons on the upper state is increased.

respectively 0.35 and 9.33 second.

In conclusion, For nearly fixed fluctuations of driving laser in an optical bistable system, by tuning the excitation power we can modify both the polariton stable state and the system transition between the two stable states. Such modifications can strongly change the degree of coherence. In this experiment we choose a small bistable system in which a small amount of laser noise can more easily switch polaritons between two states.

6.4.2 The degree of coherence in optical discriminator regime

We performed the same experiment as section 6. 4. 1 for a smaller detuning between cw laser and polariton ground state of Δ=0.12 meV. In such an experimental condition, the discriminator regime shows a nonlinear jump which is not as sharp as within a standard optical bistability loop.

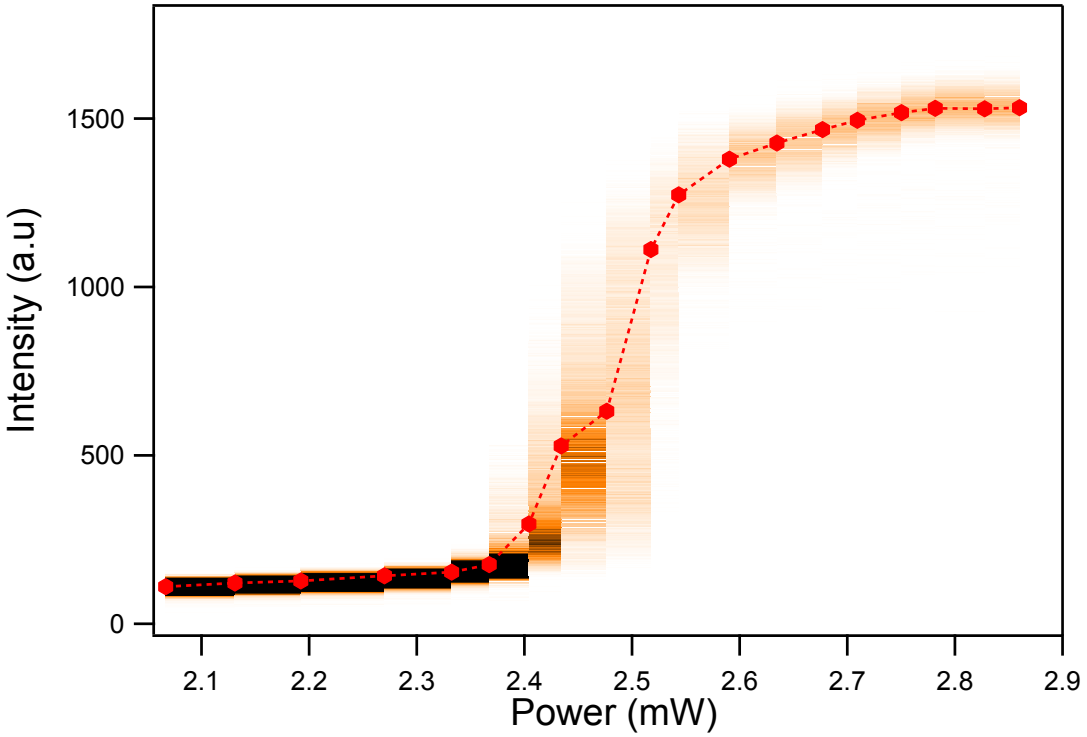

Figure 6.7: **Discriminator regime.** The polariton intensity versus laser power. The continuous wave laser is blue detuned ($\Delta = 0.12$meV) respect to the polariton ground state of a 3 μm mesa with positive exciton-cavity detuning of δ=1.62 meV. For each excitation power, the polariton time stream is acquired using one of the two APDs. Polariton intensity fluctuates around an average value (red hexagonal). These fluctuations are shown around each averaged value. The maximum and minimum numbers of counts are shown as black and white color respectively.

By increasing and then decreasing the laser power (P) from 2 mW to 2.9 mW, we measure the polariton time streams through one of the APDs. In order to understand the relation between the polariton intensity fluctuations and the second-order correlation function, we show the photon statistics around each of the averaged polariton intensities (red hexagonal) as a function of the laser power (Fig. 6. 7). Around the nonlinear jump, due to the internal fluctuations and also small laser intensity noise (0.1 percent), polariton population fluctuates strongly. The maximum and minimum numbers of counts are shown as black and white color respectively. In Figure 6. 8 we present polariton probability distribution for several excitation powers. At P=2.19 mW, far from nonlinear threshold, polariton population shows no fluctuations in intensity and the distribution is one peaked. Around the turning point of polariton discriminator (P=2.36 mW) it develops a long tail and subsequently starts to become double peaked. For higher excitation powers (P=2.47 mW) the polariton population shows even triple peaked probability distribution. Above the upper turning point of polariton discriminator (P>2.58 mW), the distribution approaches the one peaked configuration. In a way, these probability distributions represent the shape of double-well potential in polariton system. We are dealing with a potential with a very small barrier between the two stable

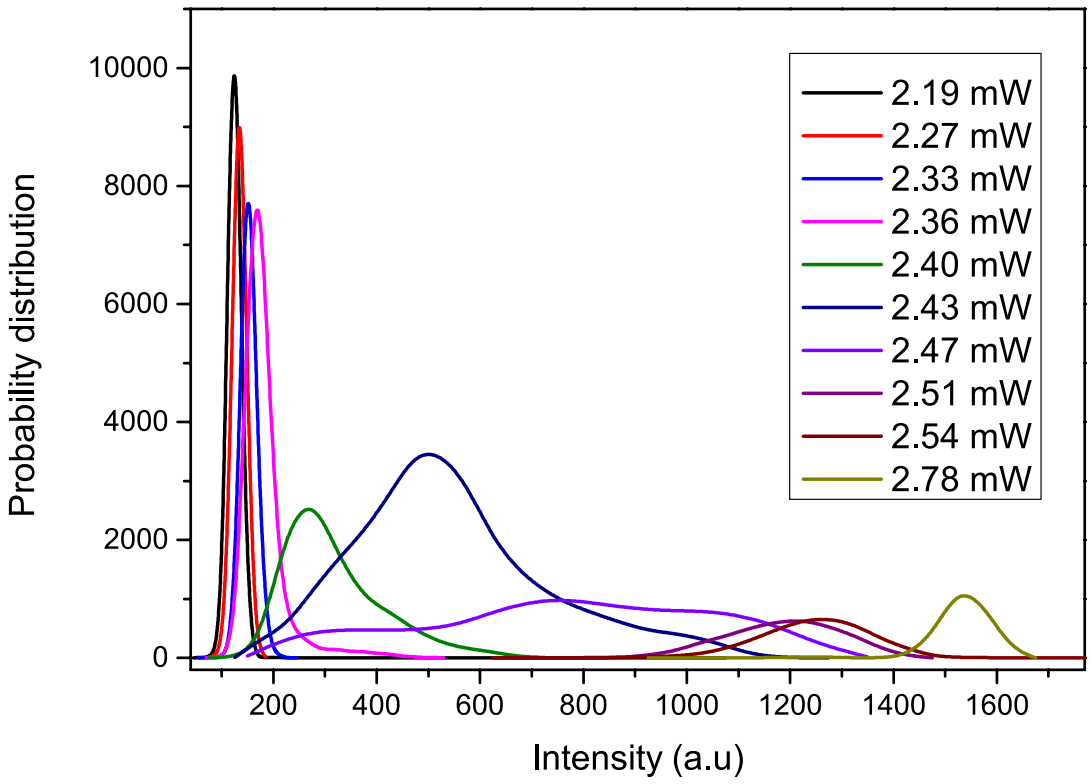

Figure 6.8: **Polariton probability distribution.** One, double and even three peaks probability distribution of exciton-polaritons in optical discriminator regime for laser power increasing from 2.19 mW to 2.78 mW.

states. First, polaritons are stable on the lower branch. By increasing the excitation power the potential is more and more symmetrical and the polariton populations can pass the potential barrier from one to the other state. This transition mechanism is slightly different from noise-induced transitions in bistable system. Here for some powers (P=2.47 mW) we demonstrate a broad probability distribution instead of the usual double-peaked probability distribution in polariton bistability (see Figure 4. 7).

In order to investigate the polariton-coincidence counting statistics we measured second-order correlation function $g^2(t)$ for each excitation power (Fig. 6. 9). We evidence the same behaviour as observed for the case of optical bistability. In Figure 6. 10 **a**, $g^2(0)$ and the polariton intensity versus excitation power are shown. Far below the threshold (P=2 mW), in the linear region, $g^2(0)$ is equal to 1, which demonstrates a coherent polariton state. By increasing the laser power, the second-order correlation function at zero delay increases gradually and reaches a maximum value of $g^2(0)$=2.7 at P=2.4 mW. Then, by further increasing of the excitation power, the second-order correlation function at zero delay reduces to 1. For each laser power, the second-order correlation time has been extracted (Fig. 6. 10 **b**). Similarly to the case of optical bistability, we observe that, when increasing laser intensity τ_c

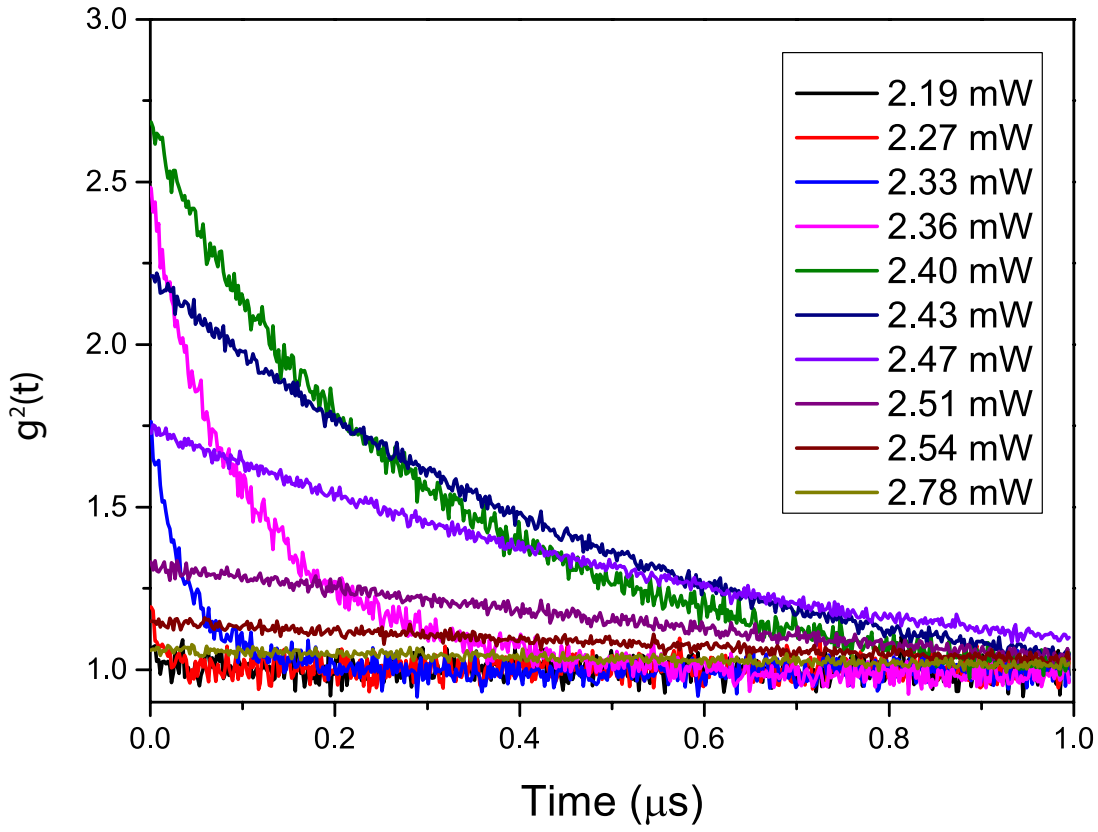

Figure 6.9: **Second-order correlation function.** g^2(t) as a function of the time for laser power increasing from 2.19 mW to 2.78 mW. For 2.36 mW, 2.4 mW and 2.43 mW a clear superbunching is observed.

increases gradually. Although for P< 2.27 mW and P> 2.54 mW we measure a coherent light, and τ_c measurement is meaningless. All experimental results are fully connected with our explanations in the framework of polariton bistability. However, in the discriminator regime, the modelling of the second-order correlation function is not as straightforward as within the bistability regime, and further theoretical studies are needed.

6.5 Conclusion

We find that depending on the excitation power, photons escaping from the microcavity can display very diverse statistical behaviour, characterized by $g^2(0)$ approaching one or exceeding two. We demonstrate of an amplification of polariton fluctuations close to nonlinear thresholds in optical bistability and discriminator. Depending on the polariton dynamics and fluctuations in intensity and time domain second-order correlation function characteristics can be effectually changed.

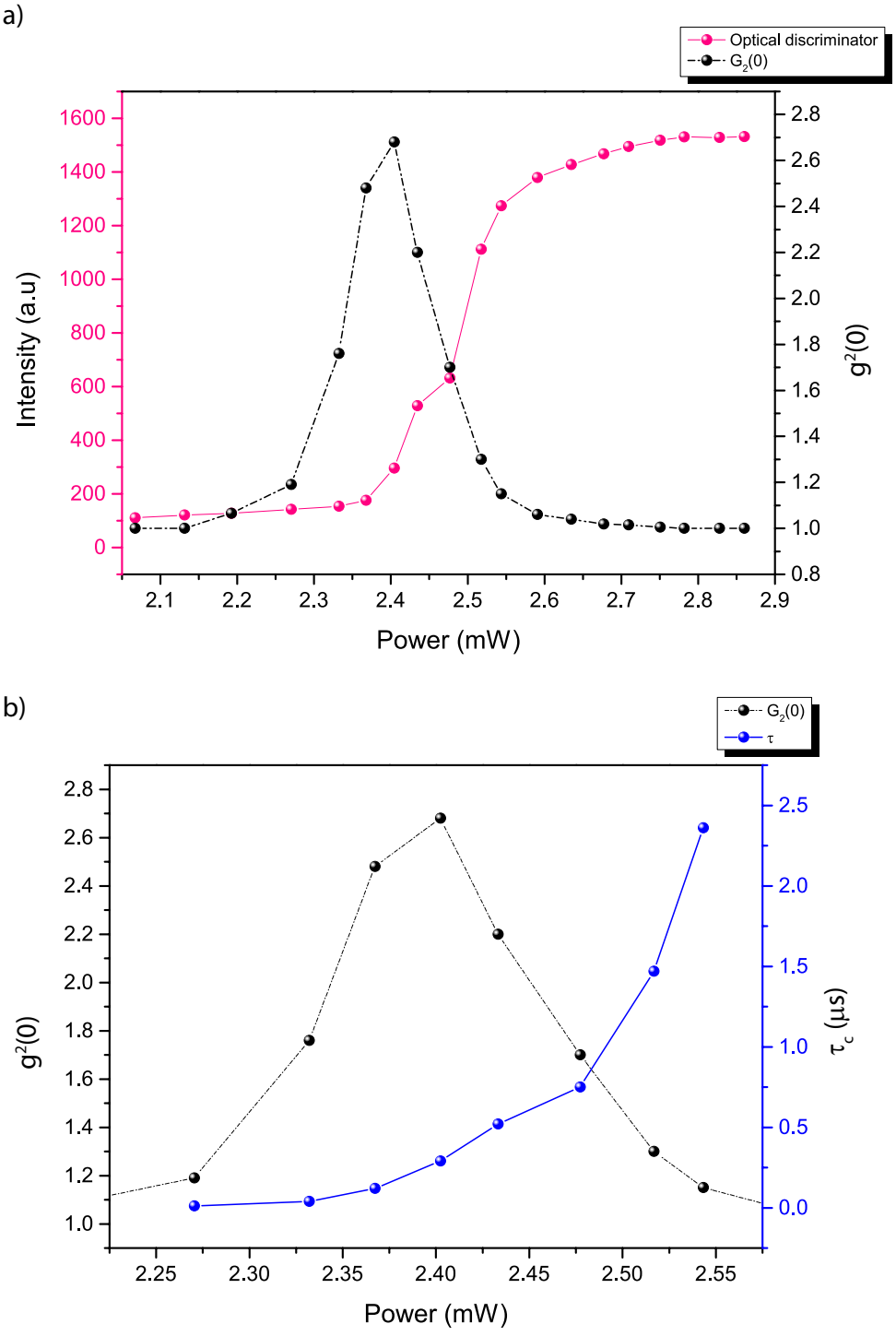

Figure 6.10: **Second-order correlation function characteristics around discriminator regime. a** zero-delay second-order correlation function ($g^2(0)$) (right axis), and polariton intensity (left axis) versus laser power. **b** Second-order correlation function characteristic time (τ_c) (right axis), and $g^2(0)$ (left axis) as a function of the laser power.

7 Conclusion

Within the frame of this thesis, the knowledge about noise assisted phenomena in microcavity exciton-polariton gas has been extended by investigating intensity and spinor stochastic resonance, and examining the influence of nonlinear interaction on polariton intensity fluctuations. Different optical spectroscopy techniques such as Fourier-space photoluminescence and time-resolved measurement in addition to Hanbury Brown and Twiss (HBT) setup, served as experimental basis. For modelling and interpreting a part of the experimental results the Gross-Pitaevskii equation with stochastic driving field has been developed.

7.1 Summary

Following a brief introduction about the two-dimensional excitons and photons and also exciton-polaritons in microcavity, the third chapter focused on the effect of polariton-polariton interactions and the biexciton reservoir on polariton bistability and multistability in the studied sample. For a large negative exciton-cavity detuning, far from the biexciton resonance, the ratio between two spin polarized populations of polariton follows the polarization degree of excitation laser. However, when the biexciton resonance comes into play, due to the competition between biexciton formation and polariton nonlinear interactions, the situation becomes complex. Depending on the excitation power and polarization, two or three stable states for polariton intensity in steady state regime have been demonstrated. The effect of polariton-laser energy detuning on the multistability and spin-trigger regimes have been investigated.

In the next two chapters, the effect of an external Gaussian noise on the polariton dynamics has been studied. Polariton bistability is mainly based on nonlinearities and feedback mechanism through a cw laser blue detuned with respect to the polariton ground state. By introducing a Gaussian noise on the DC component of the laser, fluctuations are induced on the polariton population and consequently the polariton energy. This effect induces noise-induced transitions of polariton population between lower and upper states of polariton bistability. Polariton Kramers time and residence time on two stable states influenced by noise intensity

and bandwidth have been presented. The driving field intensity fluctuations, which can be unavoidable in many practical systems, can modify the bistable behaviour depending on the bistability acquisition time compared to the polariton residence time in the lower and upper states. In order to optimize the influence of external noise, we have started a complete study on the observation of polariton stochastic resonance. We have shown how the synchronization between an external modulation signal with Gaussian noise can affect the signal-to noise ratio of a nonlinear system like exciton-polariton microcavity. Depending on the amplitude of the modulated signal the synchronization mechanism would be more deterministic or noise-assisted. Then, we have introduced a novel type of stochastic resonance in the spin-trigger regime. Thanks to the polariton complex treatment in presence of the biexciton state, we are dealing with a bistable regime in polarization domain. We have shown how the superposition of spin fluctuations and modulation can induce a spin-ordering in the system. We believe that this mechanism can improve the signal-to-noise ratio of a network of spintronic systems working based on polaritons. At the end, the effect of the amplitude and the frequency of the external modulated signal on spinor stochastic resonance has been investigated.

The last part of this thesis, the polariton-coincidence counting statistics in both polariton bistability and discriminator regimes have been investigated. In both cases, tuning the excitation power can effectively modify the coherence time, and the intensity of the second-order correlation function. It is shown that there is a direct link between noise-induced polariton fluctuations and characteristics of $g^2(t)$.

7.2 Perspectives

Up to now, the effect of the biexciton resonance on the polariton bistability has modelled by two types of equations: first, spinor Gross-Pitaevskii equation and second exciton photon basis considering the biexciton population via corresponding rate equation [57]. Our experimental observations demonstrate that, depending on the detuning between the lower polariton ground state and the biexciton energy, different types of spinor bistabilities would be possible. This type of examination requires a complete model in exciton photon basis including the biexciton field amplitude.

Although in all optical systems the external noise fluctuations are hazardous and unpredictable effects, but internal fluctuations can also play an important role in any system like polaritons. In future studies, the external laser noise intensity can be replaced by different sources of internal or external noise such as relaxation mechanism, spontaneous emission and thermal fluctuations. From fundamental point of view, one can profit stochastic resonance phenomenon for characterizing the internal noise in polariton system. Furthermore, Josephson oscillation in polariton system can be a promising playground for observation of quantum stochastic resonance [116, 117].

In addition, the observation of polariton superbunching can be a starting point for all related noise studies in polariton system. Using a local oscillator in HBT setup, a comprehensive

investigation of polariton phase diagram can be achieved. The same study can be performed in multistability regime. Due to the biexciton formation in polariton system noise properties of two spin populations close to the nonlinear thresholds of optical bistability have also a great interest.

Bibliography

[1] R. Hall, G. Fenner, J. Kingsley, T. Soltys, and R. Carlson, "Coherent Light Emission from GaAs Junctions," *Phys. Rev. Lett*, vol. 9, p. 366, 1962.

[2] H. Soda, K.-i. Iga, C. Kitahara, and Y. Suematsu, "GaInAsP/InP surface emitting injection lasers," *Japanese Journal of Applied Physics*, vol. 18, no. 12, p. 2329, 1979.

[3] C. Weisbuch, M. Nishioka, A. Ishikawa, and Y. Arakawa, "Observation of the coupled exciton-photon mode splitting in a semiconductor quantum microcavity," *Phys. Rev. Lett.*, vol. 69, no. 23, p. 3314, 1992.

[4] J. Kasprzak, M. Richard, S. Kundermann, A. Baas, P. Jeambrun, J. Keeling, F. Marchetti, M. Szymańska, R. Andre, J. Staehli, *et al.*, "Bose–Einstein condensation of exciton polaritons," *Nature*, vol. 443, no. 7110, pp. 409–414, 2006.

[5] A. Amo, J. Lefrère, S. Pigeon, C. Adrados, C. Ciuti, I. Carusotto, R. Houdré, E. Giacobino, and A. Bramati, "Superfluidity of polaritons in semiconductor microcavities," *Nature Physics*, vol. 5, no. 11, pp. 805–810, 2009.

[6] G. Grosso, G. Nardin, F. Morier-Genoud, Y. Léger, and B. Deveaud-Plédran, "Soliton instabilities and vortex street formation in a polariton quantum fluid," *Physical Review Letters*, vol. 107, no. 24, p. 245301, 2011.

[7] V. Kohnle, Y. Léger, M. Wouters, M. Richard, M. T. Portella-Oberli, and B. Deveaud-Plédran, "From single particle to superfluid excitations in a dissipative polariton gas," *Physical review letters*, vol. 106, no. 25, p. 255302, 2011.

[8] V. Kohnle, *Nonlinear Spectroscopy of a Dissipative Polariton Quantum Fluid.* PhD thesis, EPFL, 2011.

[9] V. Kohnle, Y. Léger, M. Wouters, M. Richard, M. Portella-Oberli, and B. Deveaud, "Four-wave mixing excitations in a dissipative polariton quantum fluid," *Physical Review B*, vol. 86, no. 6, p. 064508, 2012.

[10] R. Cerna, Y. Léger, T. K. Paraïso, M. Wouters, F. Morier-Genoud, M. T. Portella-Oberli, and B. Deveaud, "Ultrafast tristable spin memory of a coherent polariton gas," *Nature Comm.*, vol. 4, 2013.

[11] A. Amo, T. Liew, C. Adrados, R. Houdré, E. Giacobino, A. Kavokin, and A. Bramati, "Exciton–polariton spin switches," *Nature Phot.*, vol. 4, no. 6, pp. 361–366, 2010.

[12] T. Gao, P. Eldridge, T. C. H. Liew, S. Tsintzos, G. Stavrinidis, G. Deligeorgis, Z. Hatzopoulos, and P. Savvidis, "Polariton condensate transistor switch," *Physical Review B*, vol. 85, no. 23, p. 235102, 2012.

[13] A. Baas, J. P. Karr, H. Eleuch, and E. Giacobino, "Optical bistability in semiconductor microcavities," *Phys. Rev. A*, vol. 69, p. 023809, Feb 2004.

[14] T. Paraiso, M. Wouters, Y. Léger, F. Morier-Genoud, and B. Deveaud-Plédran, "Multistability of a coherent spin ensemble in a semiconductor microcavity," *Nature Mat*, vol. 9, no. 8, p. 655, 2010.

[15] M. Albiez, R. Gati, J. Fölling, S. Hunsmann, M. Cristiani, and M. K. Oberthaler, "Direct observation of tunneling and nonlinear self-trapping in a single bosonic Josephson junction," *Physical Review Letters*, vol. 95, no. 1, p. 010402, 2005.

[16] F. Cataliotti, S. Burger, C. Fort, P. Maddaloni, F. Minardi, A. Trombettoni, A. Smerzi, and M. Inguscio, "Josephson junction arrays with Bose-Einstein condensates," *Science*, vol. 293, no. 5531, pp. 843–846, 2001.

[17] S. Cecchi, G. Giusfredi, E. Petriella, and P. Salieri, "Observation of optical tristability in sodium vapors," *Physical Review Letters*, vol. 49, no. 26, p. 1928, 1982.

[18] E. Giacobino, "Tristability and bifurcations in sodium vapor," *Optics Communications*, vol. 56, no. 4, pp. 249–254, 1985.

[19] H. Gibbs, S. McCall, and T. Venkatesan, "Differential gain and bistability using a sodium-filled fabry-perot interferometer," *Physical Review Letters*, vol. 36, no. 19, p. 1135, 1976.

[20] B. McNamara, K. Wiesenfeld, and R. Roy, "Observation of stochastic resonance in a ring laser," *Physical Review Letters*, vol. 60, no. 25, p. 2626, 1988.

[21] H. A. Kramers, "Brownian motion in a field of force and the diffusion model of chemical reactions," *Physica*, vol. 7, no. 4, pp. 284–304, 1940.

[22] L. Gammaitoni, P. Hänggi, P. Jung, and F. Marchesoni, "Stochastic resonance," *Rev. Mod. Phys.*, vol. 70, no. 1, p. 223, 1998.

[23] T. Wellens, V. Shatokhin, and A. Buchleitner, "Stochastic resonance," *Reports on Progress in Physics*, vol. 67, no. 1, p. 45, 2004.

[24] S. Fauve and F. Heslot, "Stochastic resonance in a bistable system," *Phys. Lett. A*, vol. 97, no. 1, 1983.

[25] A. Guderian, G. Dechert, K.-P. Zeyer, and F. Schneider, "Stochastic resonance in chemistry. 1. the belousov-zhabotinsky reaction," *The Journal of Physical Chemistry*, vol. 100, no. 11, pp. 4437–4441, 1996.

[26] A. Förster, M. Merget, and F. Schneider, "Stochastic resonance in chemistry. 2. the peroxidase-oxidase reaction," *The Journal of Physical Chemistry*, vol. 100, no. 11, pp. 4442–4447, 1996.

[27] W. Hohmann, J. Müller, and F. Schneider, "Stochastic resonance in chemistry. 3. the minimal-bromate reaction," *The Journal of Physical Chemistry*, vol. 100, no. 13, pp. 5388–5392, 1996.

[28] S. Barbay, G. Giacomelli, and F. Marin, "Stochastic resonance in vertical cavity surface emitting lasers," *Physical Review E*, vol. 61, no. 1, p. 157, 2000.

[29] J. Collins, C. C. Chow, and T. T. Imhoff, "Aperiodic stochastic resonance in excitable systems," *Physical Review E*, vol. 52, no. 4, p. R3321, 1995.

[30] F. Moss, L. M. Ward, and W. G. Sannita, "Stochastic resonance and sensory information processing: a tutorial and review of application," *Clinical Neurophysiology*, vol. 115, no. 2, pp. 267–281, 2004.

[31] M. Fox, *Quantum Optics: An Introduction: An Introduction*, vol. 6. Oxford University Press, 2006.

[32] J. Hopfield, "Theory of the contribution of excitons to the complex dielectric constant of crystals," *Physical Review*, vol. 112, no. 5, p. 1555, 1958.

[33] C. B. a la Guillaume, A. Bonnot, and J. Debever, "Luminescence from polaritons," *Physical Review Letters*, vol. 24, no. 22, p. 1235, 1970.

[34] C. Weisbuch and R. G. Ulbrich, "Resonant polariton fluorescence in gallium arsenide," *Physical Review Letters*, vol. 39, no. 10, p. 654, 1977.

[35] D. Sell, R. Dingle, S. Stokowski, and J. DiLorenzo, "Observation of polaritons in GaAs: A new interpretation of the free-exciton reflectance and luminescence," *Physical Review Letters*, vol. 27, no. 24, p. 1644, 1971.

[36] S. T. Pantelides, "The electronic structure of impurities and other point defects in semiconductors," *Reviews of Modern Physics*, vol. 50, no. 4, p. 797, 1978.

[37] G. H. Wannier, "The structure of electronic excitation levels in insulating crystals," *Physical Review*, vol. 52, no. 3, p. 191, 1937.

[38] P. Y. Yu and M. Cardona, *Fundamentals of semiconductors*. Springer, 1996.

[39] V. Agranovich and O. Dubovskii, "Effect of retarded interaction on the exciton spectrum in one-dimensional and two-dimensional crystals," *JETP Lett*, vol. 3, pp. 223–226, 1966.

[40] K. Lagoudakis, *On the physics of Exciton-Polariton condensates*. PhD thesis, EPFL, 2010.

[41] M. Maialle, E. d. A. e Silva, and L. Sham, "Exciton spin dynamics in quantum wells," *Physical Review B*, vol. 47, no. 23, p. 15776, 1993.

[42] H. Benisty, H. De Neve, and C. Weisbuch, "Impact of planar microcavity effects on light extraction-part i: Basic concepts and analytical trends," *Quantum Electronics, IEEE Journal of*, vol. 34, no. 9, pp. 1612–1631, 1998.

[43] B. Deveaud, F. Clerot, N. Roy, K. Satzke, B. Sermage, and D. Katzer, "Enhanced radiative recombination of free excitons in GaAs quantum wells," *Physical Review L*, vol. 67, no. 17, p. 2355, 1991.

[44] V. Savona, L. Andreani, P. Schwendimann, and A. Quattropani, "Quantum well excitons in semiconductor microcavities: Unified treatment of weak and strong coupling regimes," *Solid State Communications*, vol. 93, no. 9, pp. 733–739, 1995.

[45] G. Rossbach, *High-Density Excitonic Effects in GaN: Mott-Transition and Polariton Lasing*. PhD thesis, EPFL, 2014.

[46] S. Hoogland, J. Baumberg, S. Coyle, J. Baggett, M. Coles, and H. Coles, "Self-organized patterns and spatial solitons in liquid-crystal microcavities," *Physical Review A*, vol. 66, no. 5, p. 055801, 2002.

[47] H. Gibbs, S. McCall, T. Venkatesan, A. Gossard, A. Passner, and W. Wiegmann, "Optical bistability in semiconductors," *Applied Physics Letters*, vol. 35, no. 6, pp. 451–453, 1979.

[48] A. Szöke, V. Daneu, J. Goldhar, and N. Kurnit, "Bistable optical element and its applications," *Applied Physics Letters*, vol. 15, no. 11, pp. 376–379, 1969.

[49] R. Bonifacio and L. Lugiato, "Optical bistability and cooperative effects in resonance fluorescence," *Physical Review A*, vol. 18, no. 3, p. 1129, 1978.

[50] E. Abraham and S. Smith, "Optical bistability and related devices," *Reports on Progress in Physics*, vol. 45, no. 8, p. 815, 1982.

[51] D. Miller, D. Chemla, T. Damen, A. Gossard, W. Wiegmann, T. Wood, and C. Burrus, "Novel hybrid optically bistable switch: The quantum well self-electro-optic effect device," *Applied Physics Letters*, vol. 45, no. 1, pp. 13–15, 1984.

[52] H. Gibbs, *Optical bistability: controlling light with light*. Elsevier, 1985.

[53] Y. Takase, P. T. Thanh, R. Fujimura, and K. Kajikawa, "A low-power all-optical bistable device based on a liquid crystal layer embedded in thin gold films," *Applied Physics Express*, vol. 7, no. 4, p. 042202, 2014.

[54] D. Ballarini, M. De Giorgi, E. Cancellieri, R. Houdré, E. Giacobino, R. Cingolani, A. Bramati, G. Gigli, and S. D., "All-optical polariton transistor," *Nature Comm.*, vol. 4, p. 1778, 2013.

[55] G. Grosso, S. Trebaol, M. Wouters, F. Morier-Genoud, M. Portella-Oberli, and B. Deveaud, "Nonlinear relaxation and selective polychromatic lasing of confined polaritons," *Physical Review B*, vol. 90, no. 4, p. 045307, 2014.

[56] T. Liew, A. Kavokin, and I. Shelykh, "Optical circuits based on polariton neurons in semiconductor microcavities," *Physical review letters*, vol. 101, no. 1, p. 016402, 2008.

[57] M. Wouters, T. K. Paraiso, Y. Léger, R. Cerna, F. Morier-Genoud, M. T. Portella-Oberli, and B. Deveaud-Plédran, "Influence of a nonradiative reservoir on polariton spin multistability," *Phys. Rev. B*, vol. 87, p. 045303, Jan 2013.

[58] S. Gavrilov, A. Sekretenko, S. Novikov, C. Schneider, S. Höfling, M. Kamp, A. Forchel, and V. Kulakovskii, "Polariton multistability and fast linear-to-circular polarization conversion in planar microcavities with lowered symmetry," *Applied Physics Letters*, vol. 102, no. 1, p. 011104, 2013.

[59] S. Gavrilov, N. Gippius, S. Tikhodeev, and V. Kulakovskii, "Multistability of the optical response in a system of quasi-two-dimensional exciton polaritons," *Journal of Experimental and Theoretical Physics*, vol. 110, no. 5, pp. 825–836, 2010.

[60] D. Vishnevsky, D. Solnyshkov, N. Gippius, and G. Malpuech, "Multistability of cavity exciton polaritons affected by the thermally generated exciton reservoir," *Physical Review B*, vol. 85, no. 15, p. 155328, 2012.

[61] O. E. Daif, *0D microcavity polaritons : trapping light-matter quasiparticles*. PhD thesis, EPFL, 2007.

[62] R. I. Kaitouni, O. El Daïf, A. Baas, M. Richard, T. Paraiso, P. Lugan, T. Guillet, F. Morier-Genoud, J. Ganiere, J. Staehli, *et al.*, "Engineering the spatial confinement of exciton polaritons in semiconductors," *Physical Review B*, vol. 74, no. 15, p. 155311, 2006.

[63] O. El Daïf, A. Baas, T. Guillet, J.-P. Brantut, R. I. Kaitouni, J.-L. Staehli, F. Morier-Genoud, and B. Deveaud, "Polariton quantum boxes in semiconductor microcavities," *Applied Physics Letters*, vol. 88, no. 6, p. 061105, 2006.

[64] R. Houdré, R. Stanley, and M. Ilegems, "Vacuum-field rabi splitting in the presence of inhomogeneous broadening: Resolution of a homogeneous linewidth in an inhomogeneously broadened system," *Physical Review A*, vol. 53, no. 4, p. 2711, 1996.

[65] C. Ciuti, P. Schwendimann, B. Deveaud, and A. Quattropani, "Theory of the angle-resonant polariton amplifier," *Physical Review B*, vol. 62, no. 8, p. R4825, 2000.

[66] C. Ciuti, V. Savona, C. Piermarocchi, A. Quattropani, and P. Schwendimann, "Role of the exchange of carriers in elastic exciton-exciton scattering in quantum wells," *Physical Review B*, vol. 58, no. 12, p. 7926, 1998.

[67] T. Paraiso, *Dynamics of Interactions of Confined Microcavity Polaritons*. PhD thesis, EPFL, 2010.

[68] M. Saba, F. Quochi, C. Ciuti, U. Oesterle, J. Staehli, B. Deveaud, G. Bongiovanni, and A. Mura, "Crossover from exciton to biexciton polaritons in semiconductor microcavities," *Physical review letters*, vol. 85, no. 2, p. 385, 2000.

[69] T. Baars, G. Dasbach, M. Bayer, and A. Forchel, "Biexciton states in semiconductor microcavities," *Physical Review B*, vol. 63, no. 16, p. 165311, 2001.

[70] P. Borri, W. Langbein, U. Woggon, J. R. Jensen, and J. M. Hvam, "Biexcitons or bipolaritons in a semiconductor microcavity," *Physical Review B*, vol. 62, no. 12, p. R7763, 2000.

[71] N. Kwong, R. Takayama, I. Rumyantsev, M. Kuwata-Gonokami, and R. Binder, "Third-order exciton-correlation and nonlinear cavity-polariton effects in semiconductor microcavities," *Physical Review B*, vol. 64, no. 4, p. 045316, 2001.

[72] P. Smith and E. Turner, "A bistable fabry-perot resonator," *Applied Physics Letters*, vol. 30, no. 6, pp. 280–281, 1977.

[73] N. Takemura, S. Trebaol, M. Wouters, M. T. Portella-Oberli, and B. Deveaud, "Polaritonic feshbach resonance," *Nature Physics*, 2014.

[74] N. Takemura, S. Trebaol, M. Wouters, M. T. Portella-Oberli, and B. Deveaud, "Heterodyne spectroscopy of polariton spinor interactions," *Physical Review B*, vol. 90, no. 19, p. 195307, 2014.

[75] A. Simon and A. Libchaber, "Escape and synchronization of a brownian particle," *Physical Review Letters*, vol. 68, no. 23, p. 3375, 1992.

[76] M. Dykman, G. Golubev, D. Luchinsky, A. Velikovich, and S. Tsuprikov, "Fluctuational transitions and related phenomena in a passive all-optical bistable system," *Physical Review A*, vol. 44, no. 4, p. 2439, 1991.

[77] L. I. McCann, M. Dykman, and B. Golding, "Thermally activated transitions in a bistable three-dimensional optical trap," *Nature*, vol. 402, no. 6763, pp. 785–787, 1999.

[78] R. Johne, N. S. Maslova, and N. A. Gippius, "Fluctuation-induced transitions of a bistable driven polariton system in the presence of damping," *Solid State Communications*, vol. 149, no. 11, pp. 496–500, 2009.

[79] M. Dykman, D. Luchinsky, R. Mannella, P. V. McClintock, N. Stein, and N. Stocks, "Supernarrow spectral peaks and high-frequency stochastic resonance in systems with coexisting periodic attractors," *Physical Review E*, vol. 49, no. 2, p. 1198, 1994.

[80] M. Dykman and M. Krivoglaz, "Theory of fluctuational transitions between the stable states of a non-linear oscillator," *Sov. Phys. JETP*, vol. 77, pp. 60–73, 1979.

[81] W. Coffey, Y. P. Kalmykov, and J. T. Waldron, *The Langevin equation: with applications to stochastic problems in physics, chemistry, and electrical engineering*, vol. 14. World Scientific, 2004.

[82] R. L. Badzey and P. Mohanty, "Coherent signal amplification in bistable nanomechanical oscillators by stochastic resonance," *Nature*, vol. 437, no. 7061, pp. 995–998, 2005.

[83] R. Benzi, A. Sutera, and A. Vulpiani, "The mechanism of stochastic resonance," *Journal of Physics A*, vol. 14, no. 11, 1981.

[84] P. Hänggi, "Stochastic resonance in biology how noise can enhance detection of weak signals and help improve biological information processing," *ChemPhysChem*, vol. 3, no. 3, pp. 285–290, 2002.

[85] G. Giacomelli, F. Marin, and I. Rabbiosi, "Stochastic and bona fide resonance: an experimental investigation," *Physical Review Letters*, vol. 82, no. 4, p. 675, 1999.

[86] A. Joshi and M. Xiao, "Stochastic resonance in atomic optical bistability," *Physical Review A*, vol. 74, no. 1, p. 013817, 2006.

[87] R. Bartussek, P. Hänggi, and P. Jung, "Stochastic resonance in optical bistable systems," *Physical Review E*, vol. 49, no. 5, p. 3930, 1994.

[88] F. Marino, M. Giudici, S. Barland, and S. Balle, "Experimental evidence of stochastic resonance in an excitable optical system," *Physical Review Letters*, vol. 88, no. 4, p. 040601, 2002.

[89] S. M. Bezrukov and I. Vodyanoy, "Stochastic resonance in non-dynamical systems without response thresholds," *Nature*, vol. 385, p. 319, 1997.

[90] R. Löfstedt and S. Coppersmith, "Quantum stochastic resonance," *Physical Review Letters*, vol. 72, no. 13, p. 1947, 1994.

[91] J. K. Douglass, L. Wilkens, E. Pantazelou, and F. Moss, "Noise enhancement of information transfer in crayfish mechanoreceptors by stochastic resonance," *Nature*, vol. 365, no. 6444, pp. 337–340, 1993.

[92] D. V. Dylov and J. W. Fleischer, "Nonlinear self-filtering of noisy images via dynamical stochastic resonance," *Nature Photonics*, vol. 4, no. 5, pp. 323–328, 2010.

[93] K. Nishiguchi and A. Fujiwara, "Detecting signals buried in noise via nanowire transistors using stochastic resonance," *Applied Physics Letters*, vol. 101, no. 19, p. 193108, 2012.

[94] Abbaspour, H. and Trebaol, S. and Morier-Genoud, F. and Portella-Oberli, M. T. and Deveaud, B., "Stochastic resonance in collective exciton-polariton excitations inside a gaas microcavity," *Phys. Rev. Lett.*, vol. 113, p. 057401, Jul 2014.

[95] T. Zhou, F. Moss, and P. Jung, "Escape-time distributions of a periodically modulated bistable system with noise," *Physical Review A*, vol. 42, no. 6, p. 3161, 1990.

[96] C. Sturm, D. Tanese, H. Nguyen, H. Flayac, E. Galopin, A. Lemaître, I. Sagnes, D. Solnyshkov, A. Amo, G. Malpuech, *et al.*, "All-optical phase modulation in a cavity-polariton mach–zehnder interferometer," *Nature Comm.*, vol. 5, 2014.

[97] C. Antón, T. Liew, J. Cuadra, M. Martín, P. Eldridge, Z. Hatzopoulos, G. Stavrinidis, P. Savvidis, and L. Viña, "Quantum reflections and shunting of polariton condensate wave trains: Implementation of a logic and gate," *Physical Review B*, vol. 88, no. 24, p. 245307, 2013.

[98] M. De Giorgi, D. Ballarini, E. Cancellieri, F. Marchetti, M. H. Szymanska, C. Tejedor, R. Cingolani, E. Giacobino, A. Bramati, G. Gigli, *et al.*, "Control and ultrafast dynamics of a two-fluid polariton switch," *Physical Review Letters*, vol. 109, no. 26, p. 266407, 2012.

[99] I. Shelykh, A. Kavokin, Y. G. Rubo, T. Liew, and G. Malpuech, "Polariton polarization-sensitive phenomena in planar semiconductor microcavities," *Semiconductor Science and Technology*, vol. 25, no. 1, p. 013001, 2010.

[100] I. A. Shelykh, A. V. Kavokin, and G. Malpuech, "Spin dynamics of exciton polaritons in microcavities," *physica Status Solidi (b)*, vol. 242, no. 11, pp. 2271–2289, 2005.

[101] S. Tsintzos, N. Pelekanos, G. Konstantinidis, Z. Hatzopoulos, and P. Savvidis, "A GaAs polariton light-emitting diode operating near room temperature," *Nature*, vol. 453, no. 7193, pp. 372–375, 2008.

[102] X. Cheng, C. T. Boone, J. Zhu, and I. N. Krivorotov, "Nonadiabatic stochastic resonance of a nanomagnet excited by spin torque," *Physical Review Letters*, vol. 105, no. 4, p. 047202, 2010.

[103] G. Finocchio, I. Krivorotov, X. Cheng, L. Torres, and B. Azzerboni, "Micromagnetic understanding of stochastic resonance driven by spin-transfer-torque," *Physical Review B*, vol. 83, no. 13, p. 134402, 2011.

[104] D. Gourier and D. Gerbault, "Stochastic resonance in an electron-spin–nuclear-spin system," *Physical Review B*, vol. 57, no. 5, p. 2679, 1998.

[105] R. H. Brown and R. Twiss, "Correlation between photons in two coherent beams of light," *Nature*, vol. 177, no. 4497, pp. 27–29, 1956.

[106] R. J. Glauber, "The quantum theory of optical coherence," *Physical Review*, vol. 130, no. 6, p. 2529, 1963.

[107] R. J. Glauber, "Nobel lecture: One hundred years of light quanta," *Reviews of Modern Physics*, vol. 78, no. 4, pp. 1267–1278, 2006.

[108] M. Macovei and C. H. Keitel, "Superbunched photons via a strongly pumped near-equispaced multiparticle system," *Physical Review B*, vol. 75, no. 24, p. 245325, 2007.

[109] D. A. Antonosyan, T. V. Gevorgyan, and G. Y. Kryuchkyan, "Three-photon states in nonlinear crystal superlattices," *Physical Review A*, vol. 83, no. 4, p. 043807, 2011.

[110] J. Pritchard, C. Adams, and K. Mølmer, "Correlated photon emission from multiatom Rydberg dark states," *Physical Review Let*, vol. 108, no. 4, p. 043601, 2012.

[111] A. Ridolfo, S. Savasta, and M. J. Hartmann, "Nonclassical radiation from thermal cavities in the ultrastrong coupling regime," *Physical Review Letters*, vol. 110, no. 16, p. 163601, 2013.

[112] D. Chang, V. Gritsev, G. Morigi, V. Vuletić, M. Lukin, and E. Demler, "Crystallization of strongly interacting photons in a nonlinear optical fibre," *Nature Physics*, vol. 4, no. 11, pp. 884–889, 2008.

[113] A. V. Gorshkov, J. Otterbach, M. Fleischhauer, T. Pohl, and M. D. Lukin, "Photon-photon interactions via Rydberg blockade," *Physical Review Lett*, vol. 107, no. 13, p. 133602, 2011.

[114] A. I. Lvovsky, B. C. Sanders, and W. Tittel, "Optical quantum memory," *Nature Photonics*, vol. 3, no. 12, pp. 706–714, 2009.

[115] R. Loudon, "Non-classical effects in the statistical properties of light," *Reports on Progress in Physics*, vol. 43, no. 7, p. 913, 1980.

[116] B. J. Kim, P. Minnhagen, H. J. Kim, M. Choi, and G. S. Jeon, "Double stochastic resonance peaks in systems with dynamic phase transitions," *EPL (Europhysics Letters)*, vol. 56, no. 3, p. 333, 2001.

[117] G. S. Jeon and M. Choi, "Autonomous stochastic resonance in fully frustrated josephson-junction ladders," *Physical Review B*, vol. 66, no. 6, p. 064514, 2002.

Hadis Abbaspour

Personal details

Birth	July 20, 1986
Address	Rue de Verdeaux 17, 1020 Renens, Switzerland
Phone	+41 21 693 76 25, +41 78 705 06 97
Email	hadis.abbaspour@epfl.ch
Nationality	Iranian
Gender	Female

Education

2011-March 2015

PhD in Photonics, Ecole Polytechnique Fédérale de Lausanne (**EPFL**), Switzerland

Focused on noise-induced phenomena in collective spinor polariton excitations

- Nonlinear phenomena in exciton-polaritons (optical bistability and multistability)
- Investigation of second order correlation function using the Haundry Brown and Twiss (HBT) setup
- Using synergic interplay of Gaussian noise and modulated signal in order to improve signal-to-noise ratio (SNR) in polariton system (Stochastic Resonance)

Supervisors: Prof. B. Deveaud
Dr. M. T. Portella-Oberli

2008-2011

MS in Electrical Engineering, Tarbiat Modares University (**TMU**), Iran

Simulation of semiconductor lasers using finite difference methods in MATLAB

- Thermal effects in quantum dot vertical cavity surface emitting laser (QD-VCSEL)
- Lasing behavior, gain properties and frequency response of QD-VCSEL

Supervisor: Prof. V. Ahmadi

2004-2008

BS in Electrical Engineering, University of Tehran (**UT**), Iran

Focused on clean room skills

- Manufacturing metal oxide semiconductor field effect transistor (MOSFET)

Supervisor: Prof. S. Mohajerzadeh

Awards

Ranked **1st** among graduate electrical engineering students at Tarbiat Modares University (2011).
Ranked **83th** among more than 400,000 participants in under-graduate nationwide university entrance exam (2004).

Skills and abilities

Optics

Lasers and optoelectronic devices, cryogenics, vacuum techniques, design and realization of setup for optical measurement, spectroscopy, Streak camera, interferometry, noise measurement, imaging

Software

Matlab, Labview, Hspice, Pspice, Modelsim, Quartus, Zemax, LEdit, Verilog- VHDL
Knowledge in C++ and Assembly language (8088, 8086)
Adobe Illustrator, AutoCAD

Clean room

Experienced in thin film deposition, lithography, etching

Problem solving and analytical approach
Scientific writing and fluent oral presentation

Experiences

2011-2013

Teaching activities: Numerical Analysis, Analysis III (multiple integrals), Analysis IV (complex analysis), Practical work (thermodynamics) to 1st year and 2nd year physics students

2010-2011

Teaching activities: Linear control systems, Electromagnetic, Electronic circuits to electrical engineering students

2009-2010

In the frame of a student project, computer simulation of tunnel injection quantum well laser and heterojunction bipolar transistor

2006

In the frame of a student project, programing the Atmel AVR

2005

In the frame of a student project, design of an 8*8 bit booth multiplier

Publications

- H. Abbaspour, *et al*., Analysis of QD VCSEL Dynamics Characteristics Considering Homogeneous and Inhomogeneous Broadening. *IEEE J. Sel. Topics Quant. Electron.* **17**, 1327 (2011).
- H. Abbaspour, *et al*., Stochastic Resonance in Collective Exciton-Polariton Excitations Inside a GaAs Microcavity. *Phys. Rev. Lett.* **113,** 057401 (2014).
- H. Abbaspour, *et al*., Spinor Stochastic Resonance, accepted in Physical Review B.

Conference contributions and presentations

- Optics of Excitons in Confined Systems 12 (OECS12), Paris, France 2011.
- The 31ST International Conference on the Physics of Semiconductors (ICPS), Zurich, Switzerland, 2012.
- Polatom Network, Toledo, Spain, May 2012.

- The 6th International Conference on Spontaneous Coherence in Exciton systems (ICSCE), Stanford, California, 2012.
- Polatom Network, Cambridge, September 2012.
- Photonics day, EPFL, Lausanne, Switzerland, 2012. "Polariton Squeezing in Semiconductor Microcavities" (poster)
- The 14th Conference on Physics of Light-Matter Coupling in Nanostructures (PLMCN), Crete, Greece, 2013. "Polariton Statistics Dynamics in a Zero-Dimensional Microcavity" (poster)
- Optics of Excitons in Confined Systems 13 (OECS13), Rome, Italy, 2013. "Stochastic Resonance in a Bistable Driven Polariton System" (poster)
- The 7th International Conference on Spontaneous Coherence in Exciton systems (ICSCE), Japan, 2012. "Polariton Stochastic Resonance" (poster)
- The 15th Conference on Physics of Light-Matter Coupling in Nanostructures (PLMCN), Montpellier, France, 2014. "Spinor Stochastic Resonance in Zero Dimensional Polaritons" (Oral)
- The 32ST International Conference on the Physics of Semiconductors (ICPS), Austin, USA, 2014. "Intensity and Spinor Stochastic Resonance in Zero Dimensional Polaritons" (Oral)

Languages

Persian (mother tongue)
English (full proficiency)
French (B1)
German (A0)
Arabic (A1)

References

Prof. B. Deveaud
Institute of Condensed Matter Physics,
EPFL, LOEQ, Switzerland,
benoit.deveaud@epfl.ch
+41 21 69 35496

Prof. V. Ahmadi
School of Electrical and Computer Engineering,
Tarbiat Modares University, Tehran, Iran,
v_ahmadi@modares.ac.ir
+98 21 82883368

Dr. M. T. Portella-Oberli
Institute of Condensed Matter Physics,
EPFL, LOEQ, Switzerland,
marcia.portellaoberli@epfl.ch
+41 21 69 34497

Dr. S. Trebaol
Fonctions Optiques pour les Technologies
de l'information, CNRS UMR 6082, France,
stephane.trebaol@enssat.fr
+33 2 96 46 90 07

Activities and interests

Horse riding, hiking, playing Setar, cooking, literature and poetry.